Journal of Print and Media Technology Research

Scientific contributions

Journal of Print and Media Technology Research

A PEER-REVIEWED QUARTERLY

A mission statement

To meet the need for a high quality scientific publishing platform in its field, the International Association of Research Organizations for the Information, Media and Graphic Arts Industries is publishing a quarterly peer-reviewed research journal.

The journal is fostering multidisciplinary research and scholarly discussion on scientific and technical issues in the field of graphic arts and media communication, thereby advancing scientific research, knowledge creation, and industry development. Its aim is to be the leading international scientific journal in the field, offering publishing opportunities and serving as a forum for knowledge exchange between all those interested in contributing to or learning from research in this field.

By regularly publishing peer-reviewed, high quality research articles, position papers, surveys, and case studies as well as review articles and topical communications, the journal is promoting original research, international collaboration, and the exchange of ideas and know-how. It also provides a multidisciplinary discussion on research issues within the field and on the effects of new scientific and technical developments on society, industry, and the individual. Thus, it intends to serve the entire research community as well as the global graphic arts and media industry.

The journal is covering fundamental and applied aspects of at least, but not limited to, the following topics:

Printing technology and related processes

- Conventional and special printing
- Packaging
- Fuel cells and other printed functionality
- Printing on biomaterials
- Textile and fabric printing
- Printed decorations
- Materials science
- Process control

Premedia technology and processes

- Colour reproduction and colour management
- Image and reproduction quality
- Image carriers (physical and virtual)
- Workflow and management

Emerging media and future trends

- Media industry developments
- Developing media communications value systems
- Online and mobile media development
- Cross-media publishing

Social impact

- Media in a sustainable society
- Environmental issues and sustainability
- Consumer perception and media use
- Social trends and their impact on media

Submissions to the Journal

Submissions are invited at any time and, if meeting the criteria for publication, will be rapidly submitted to peer-review and carefully evaluated, selected and edited. Once accepted and edited, the papers will be published as soon as possible.

✉ Contact the Editorial office: journal@iarigai.org

Journal of
Print and Media Technology
Research

2-2024

November 2024

Contents

A letter from the Editor

Daniel Bohn
Editor-in-Chief
E-mail: danielbohn@jpmtr.org
journal@iarigai.org

Dear Readers,

As we present this latest issue of the Journal of Print and Media Technology Research, we continue to witness the rapid evolution of print and media technologies, driven by both cutting-edge research and practical innovations. This issue showcases three research papers that delve into advanced applications of neural networks, organizational resilience, and the mechanics of ink transfer – topics that highlight the diverse directions of research in our field.

The article by Sven Ritzmann and Peter Urban from the University of Wuppertal explores the use of neural networks to predict the spectral reflectance of prints. This research addresses the need within the printing industry and beyond: accurate color reproduction on a pixel level using RGB cameras. By training a neural network with a dataset of over 10 000 color patches, they demonstrate how different numbers of light source and the number of color patches influence the network's performance. Their findings emphasize the potential of multispectral color measurement using relatively cheap RGB-cameras.

Turning to the business side of the print and media industry, the work by Nalinda Nuwan and colleagues investigates how dynamic capability and strategic orientation can foster organizational resilience, particularly in Sri Lanka's print and media enterprises. This study's insights into how older enterprises must adapt to evolving market conditions, while maintaining resilience through strategic alignment, are especially relevant in today's volatile global business environment.

Another technical exploration comes from Svitlana Havenko and her team, who present a mathematical model of ink transfer in gravure printing. Their research reveals the complex interactions between substrate, ink, and printing mechanics, emphasizing how variables such as pressure and speed impact print quality. This study contributes to the growing body of work focused on improving the precision and efficiency of printing processes.

In our Topicalities section, curated by Markéta Držková, we provide an overview of news, publications and events. Among recent trends and innovations shaping the future of print and media technology, notable mentions include the European Union's Horizon-funded projects, such as GrapheneCore3, which builds on previous efforts in graphene technologies, and RealNano, which advances in-line digital nano-characterization technologies for flexible electronics. Moreover, we feature impressions from drupa 2024, the premier event in the print industry, which showcased a positive outlook with new partnerships, technological advancements, and a strong emphasis on automation and sustainability.

This issue also highlights a range of recently published books and dissertations relevant to our field. New books include include 'Transfer Printing Technologies and Applications', edited by Changhong Cao and Yu Sun, which explores the fun-

damentals and applications of transfer printing for micro- and nanofabrication. Additionally, 'Robotics, Vision and Control' by Peter Corke, provides an in-depth discussion on robotics and machine vision using Python.

Several academic dissertations are also featured, including Hossein Golzar's dissertation titled 'Development of 3D Printable, Hydrophilic, and Rapidly Curing Silicone-Based Ink Formulations for Various Biomedical Applications'. This work facilitated progress in the 3D printing of elastic biomimetic structures, addressing challenges such as slow curing, low viscosity, and hydrophobicity by developing UV-curable, hydrophilic ink formulations with tunable mechanical and rheological features. Golzar's research also enabled the creation of biocompatible human articular cartilage substitutes with controlled stiffness, and demonstrated in-situ surgical applications as well as efficient fabrication of flexible microfluidic devices.

Another dissertation from David Tilve Martínez is titled '3D Printing and Electromagnetic Properties of Conductive Nanocarbon Based Composites'. This research focused on electrically conductive carbon nanocomposites with low mass fractions of conductive components, exploring their production using digital light processing and their potential as electromagnetic wave absorbing materials. Martínez's work involved developing novel transparent conductive acrylic resins based on graphene oxide and carbon nanotubes, optimizing the formulations and 3D printing processes, and presenting key findings on electrical anisotropy and dielectric properties.

Finally, Pauline Rothmann-Brumm's dissertation, which focuses on the visualization, analysis, and modeling of fluid dynamic pattern formation phenomena in the cylinder gap using machine learning, is an important contribution to the understanding of fluid dynamics in gravure printing. The work offers an exploration of how fluid dynamic patterns form during the printing process, and it is framed around improving process control for industrial applications. Her research bridges the gap between laboratory settings and industrial-scale printing, shedding light on key elements such as fluid splitting modes, pattern formation, and machine learning in predicting these phenomena.

As always, we express our deepest gratitude to the authors, reviewers, and editorial team for their dedication and invaluable contributions of great value. We also extend our thanks to our readers and the broader community for their continued engagement and support. Together, we advance the boundaries of print and media technology, fostering innovation and excellence.

Daniel Bohn

Editor-in-Chief

Wuppertal, November 2024

S. Ritzmann, P. Urban – J. Print Media Technol. Res. – Vol. 13 No. 2 (2024), 63–79

63

A neural network to predict the spectral reflectance of prints

Sven Ritzmann, Peter Urban

University of Wuppertal,
School of Electrical, Information and Media Engineering,
42119 Wuppertal, Germany

ritzmann@uni-wuppertal.de
purban@uni-wuppertal.de

Abstract

The reconstruction of spectral reflectance from RGB triplets created by digital cameras is a topic of great interest. Different approaches dealing with this topic have been published. In the recent years, most approaches utilize neural networks. These approaches mainly differ in the chosen network architecture, the way of obtaining the dataset and the used hardware. While the most approaches aim for generalized applicability on a wide range of spectra, this paper aims for applicability on a limited set of spectra given by a typical use case of the printing industry. In this paper a neural network was trained to predict the spectral reflectance of prints. Therefore, 10 800 color patches were printed, measured by a spectrophotometer and captured by an RGB camera under different light sources generated with a DLP projector. The performance of the trained network was tested by determining the CIEDE2000 color difference as well as the mean squared error between the predicted and the measured spectral reflectance. The dataset was systematically reduced to examine how the number of color patches and light sources used for training influences the performance of a network. This paper shows that a network performed best when confronted with prints printed on the same substrate using the same color management settings as the dataset used for training. Training a network with multiple datasets on different substrates increased the generalization of a network, but decreased the performance compared to a network trained with a single combination of substrate and color management settings. Reducing the number of color patches as well as reducing the number of light sources influenced the performance of a network negatively, but still leads to decent results.

Keywords: spectral reflectance reconstruction, neural networks, RGB to multispectral, light source, color patches

1. Introduction and context

This article is part of a project that aims to digitize cultural heritage items. The digitization system used implements the 3D scanning method of structured light. During a structured light scan, a projector projects a series of light patterns onto the scene while a camera captures these patterns. This series of patterns results in a unique code for each pixel of the projector. As the camera captures the patterns, each of its pixels corresponds to a pixel of the projector. A 3D point of the scene is triangulated based on these correspondents and the known position and orientation of the camera and the projector (Drouin and Beraldin, 2020). To obtain a colorized 3D scan each 3D point is assigned to an RGB triplet captured by the used camera.

The main idea of the mentioned project is to use a neural network and specific hardware (a camera and

a projector) to reconstruct the spectral reflectance of a scene point based on RGB triplets captured under different light sources. As a colorized 3D scan processes the same RGB triplets, the reconstruction of the spectral reflectance leads to a multispectral 3D scan. This article represents the first step to realize this concept. As a 3D scene adds complexity to the problem, e.g. interreflections, this research reduces the problem to a 2D space and uses a typical scenario from the printing industry. It centers on the reconstruction of the spectral reflectance of color patches printed by a UV-curing digital printer. The neuronal network will be able to predict the spectral reflectance for each pixel of an RGB image of a print. This opens new ways to proof the accuracy of a print or a specific part of a print, e.g. during production.

The idea to use neural networks to reconstruct the spectral reflectance of a scene is not new. In the past years, three competitions on spectral reconstruc-

tion from RGB images have been conducted (Arad, et al., 2018; 2020; 2022). The datasets used for training consist of hyper spectral images showing a diverse set of scenes captured with a mobile hyperspectral camera in several (not specified) environments. A simulated camera pipeline transforms the multispectral images to RGB images. The pipeline implements the spectral response of a real camera, automated exposure determination, noise, image signal processing and image compression for the JPEG format. Arad, et al. (2018; 2020; 2022) briefly describe the best performing approaches for each year. Zhang, et al. (2022) offer a detailed insight and categorization of several approaches based on the same or similar datasets. Simplified, due to the used datasets, most of the approaches presented are based on convolutional neural networks (CNN) or generative adversarial networks (GAN), that process the image as a whole. Therefore, the resulting networks perform well reconstructing the spectral reflectance of a whole scene, including interreflections. Due to interreflections and the diverse dataset, a network trained based on printed color patches with no interreflections should perform better in the specific scenario of this research.

Lazar, Javoršek and Hladnik (2020) follow a contrary approach. They use 1 031 Munsell matte patches as the foundation of their dataset. Each is measured by a spectrophotometer at five different points. The average of the five measurements equals the spectral reflectance of the patch. To obtain the corresponding RGB triplets a digital camera captures each patch under constant lighting conditions (3 019 K). The median RGB triplet of the inner 50 % of the pixels represent the RGB triplet of the corresponding patch. A densely connected feed forward network with one hidden layer is trained using the dataset. As such networks tend to find a local minimum of the cost function instead of the global minimum, each training is repeated 41 times. Lazar, Javoršek, and Hladnik (2020) suggest that the performance of the best network (with 96.2 % of the predicted reflectance resulting in a $\Delta E_{00} < 3.0$) could be enhanced by increasing the number of hidden layers and the number of RGB triplets per patch, using multiple cameras with different spectral responses. Lazar and Hladnik (2023) proof this assumption to be correct.

The described approach is close to the approach of this research. However, the first difference is the use of printed color patches instead of Munsell patches. While Munsell patches are predefined, printing gives freedom to define a dataset regarding the used halftone values and the number of patches. The disadvantage is, that the range of spectra is limited by the gamut of the used printer. The second difference is the use of multiple light sources instead of multiple cameras to enhance the number of RGB triplets. Both approaches follow

the same principal. In this article the light source is changed due to the given hardware. Furthermore, using multiple cameras will lead to registering issues when predicting the spectral reflectance for a whole image.

2. Methods

2.1 Mathematical background and main research workflow

A camera captures the light reflected from a point in a scene and converts it into a triplet of red, green, and blue color values. The resulting triplets depend on the spectral distribution of the light source, the spectral reflectance of the material of the scene point, and the characteristics of the RGB filters used in the camera (Park, et al., 2007) (Equation 1).

$$\mathrm{px}_K = \int_{380nm}^{730nm} \mathrm{LS}(\lambda)\beta(\lambda)C_K(\lambda)\mathrm{d}\lambda \qquad [1]$$

where $\mathrm{LS}(\lambda)$ is the spectral power distribution of the light source, px_K is the k-th color channel of a pixel, $\beta(\lambda)$ is the spectral reflectance of a scene point, and C_K is the spectral response of the camera for k-th color channel.

Assuming the spectral distribution of the light source $\mathrm{LS}(\lambda)$ and the spectral response of the camera C are measured in discrete steps and the unknown spectral reflectance $\beta(\lambda)$ is discrete as well, the integral in Equation 1 reduces to a summation as shown in Equation 2. The use of multiple light sources leads to a linear equation system as shown in Equation 3. Equation 4 shows Equation 3 in matrix notation. To compute the spectral reflectance, the inverse of the matrix LSC is multiplied to both sides of Equation 4 leading to Equation 5. Solving Equation 5 leads to the unknown spectral reflectance.

In general, the use of multiple light sources ensures that the LSC is a square matrix and therefore invertible. In the optimal case, a monochromatic grayscale camera K = [gray] captures the patches, and the number of light sources n equals the number of measurement points in the discrete spectra *m*. The discrete spectral distribution of each light source is 1 at one measurement point (or wavelength) and 0 at the others and has no overlap with the other light sources. Consequently, the spectral distribution of $\mathrm{LS}_{j=1}$ is [1, 0, ..., 0] and the spectral distribution of $\mathrm{LS}_{j=m}$ is [0, 0, ..., 1]. This means that LSC is a diagonal matrix and easy to invert. Using a camera with multiple color channels (e.g. K = [R, G, B]) would reduce the number of necessary light sources n according to Equation 6.

$$\text{px}_{jK} = \sum_{i=1}^{m} \text{LS}_{ij}\, \beta_i\, C_{Ki} \qquad [2]$$

$$\begin{bmatrix} \text{px}_{1K} \\ \vdots \\ \text{px}_{nK} \end{bmatrix} = \begin{bmatrix} LS_{11}\,C_{K1} & \cdots & LS_{m1}\,C_{Km} \\ \vdots & \ddots & \vdots \\ LS_{1n}\,C_{K1} & \cdots & LS_{mn}\,C_{Km} \end{bmatrix} \begin{bmatrix} \beta_1 \\ \vdots \\ \beta_m \end{bmatrix} \qquad [3]$$

$$\overrightarrow{\text{px}_K} = \text{LSC}_K\ \vec{\beta} \qquad [4]$$

$$\vec{\beta} = \text{LSC}_K^{-1}\ \overrightarrow{\text{px}_K} \qquad [5]$$

$$n = \frac{m}{n_{\text{channels}}} \qquad [6]$$

Where i is the i-th point in the discrete spectrum $[1\,;m]$, j is the j-th light source $[1\,;n]$, K is the color channel [R,G,B] or monochromatic [gray], n_{channels} represents the number of color channels, β is the discrete spectral reflectance of the patch, C is the discrete spectral response of the camera, LS is the discrete spectral distribution of the light source, and px is a pixel vector.

In practice, using these equations has disadvantages. All variables, except the spectral reflectance, has to be known. While measuring the spectral distribution of each light source would be relatively easy, measuring the spectral response of a camera would be more complex. Furthermore, Equation 1 neglects the camera pipeline processing of the captured data to an RGB image. For most consumer cameras these pipelines are black boxes, but have to be known to reproduce the spectral reflectance.

A neural network can be trained to approximate these equations including the spectral distributions of the light sources and the spectral response of the camera. Furthermore, a neural network can approximate those equations with less light sources than determined by Equation 6. A set of RGB triplets captured under different light sources and the corresponding spectral reflectance would be sufficient. Therefore, obtaining these datasets is the main task alongside training and evaluating the neural network. Figure 1 shows the main research workflow and the performed processes.

Each process is assigned to one of the main fields namely the datasets, the capturing device and the neural network. The datasets field deals with building the sets of RGB triplets and corresponding spectral reflectance used to train, validate and test the neural network. The first processes are to define the halftone values of the color patches (Section 2.4.1) and to print these patches on charts using different parameters (Section 2.4.2). The results are four printed datasets. For each printed dataset each color patch is measured by a spectrophotometer to obtain its spectral reflectance (Section 2.4.2). The obtained data is reorganized in an array for further processing (Section 2.4.3). Parallel, the color charts are placed into the capturing device (Section 2.4.4) for being captured (Section
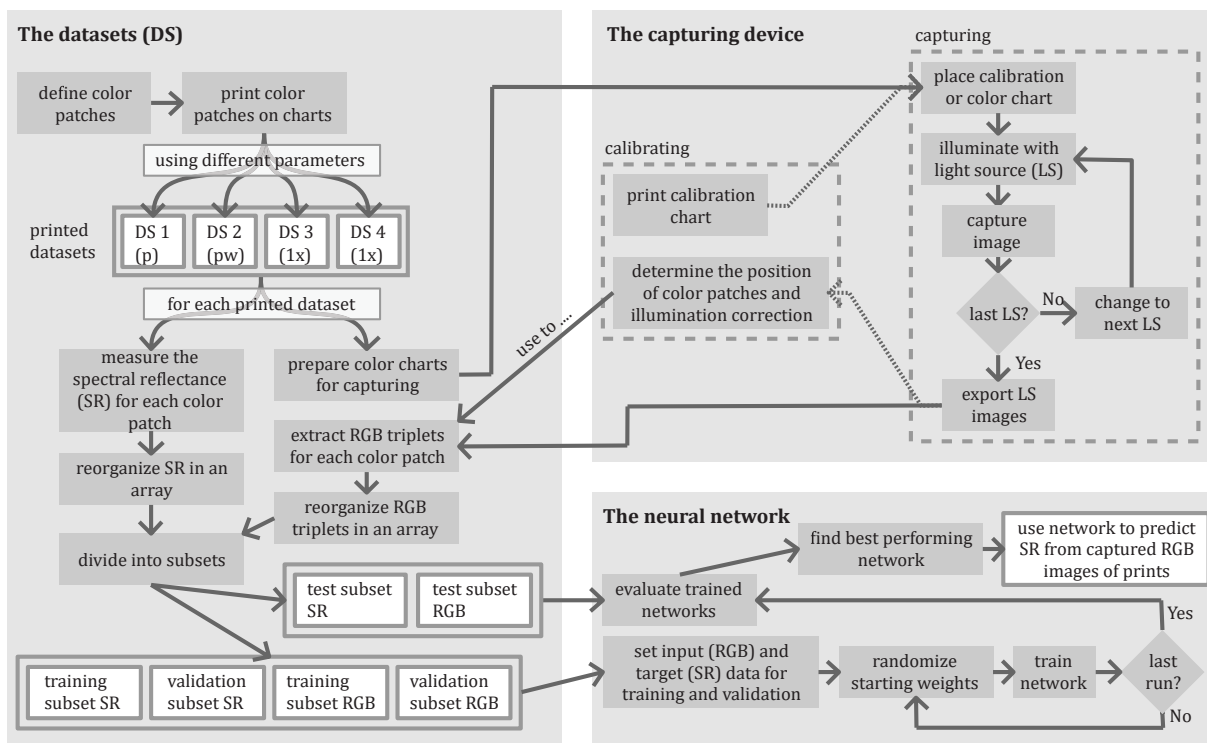

Figure 1: The main research workflow

2.4.5) The capturing device field has two main processes that interacts with each other. The calibration process starts with printing a calibration chart (Section 2.4.6). The calibration chart is given to the capturing process. During capturing the calibration chart is illuminated by a light source emitted by a projector and an RGB camera captures an image of the illuminated chart. As long as the current light source is not the last one it is changed to the next one. At the end, an RGB image of the calibration chart is captured for each light source. The capturing process, returns these images to the calibration process which determines the position and dimension of each patch in the image (Section 2.4.6) and computes a factor for each patch to correct uneven illumination (Section 2.4.8). The calibration result is stored for later use.

The prepared color charts run through the same capturing process as the calibration chart. The resulting images are returned to the extract RGB triplets process in the dataset field. This process extracts an RGB triplet for each color patch and light source (Section 2.4.7) using the information gathered during calibration. The results are reorganized into an array following the same order as the corresponding spectral reflectance array.

The two arrays represent the RGB triplets and the corresponding spectral reflectance of one dataset. In the next process each dataset is divided into a training, validation and test subset (Section 2.5). The training and validation subsets are set as input (RGB) and target (spectral reflectance) data for the first process concerning the neural network. The starting weights of the network are randomized followed by the actual training of the network. As the starting weights highly influence the training outcome, the randomization and training are repeated several times (Section 2.6). When the last training run is finished, the test subset is used to evaluate the trained networks (Section 2.7). Based on the results, the best performing network is chosen. This network can be used to predict the spectral reflectance for each pixel of an RGB image of a sample printed and captured with the same parameters as the dataset used for training.

By varying parameters of this workflow, this article examines the performance of a neural network depending on the use of different datasets (Section 3.1), regarding its generalization capabilities (Section 3.2), depending on the size of the dataset (Section 3.3) and the number and combination of the light sources used (Section 3.4).

2.2 Software and frameworks

Adobe InDesign (Adobe Inc., 2023) version 18.1 was used to create the printing files for the datasets. The raster image processor software VersaWorks (Roland Digital Group Corporation, 2023) version 6.18.1.1 was used to prepare the datasets for printing especially in terms of color management. The framework gPhoto2 version 2.5.28 (gPhoto, 2022) was used on a Raspberry PI 4b to programmatically trigger the camera to capture the color charts and to control camera parameters like ISO, shutter speed and aperture. OpenCV for Python version 4.51.48 (Bradski, 2000) was used to open, save and convert images. It was also used to detect the position and dimension of color patches in images. The framework will be referred as cv2 in the following. Numpy version 1.21.4 (Harris, et al., 2020) was used to prepare, store, and process the created data. The framework will be referred as np in the following. Keras version 2.10 as part of TensorFlow version 2.10.1 (TensorFlow, 2023) was used to build, train and evaluate the neural networks in this paper. The framework colour-science version 0.4.1 (Mansencal, et al., 2022) was used to transform spectra to CIEXYZ (ISO, 2020b), RGB and CIELAB (ISO, 2020c). Each color transformation in this paper used the color matching functions of the CIE 1931 2° Standard Observer (ISO, 2020a) and D50 (ISO, 2022a) as illuminant. In addition, transformations from spectra to RGB use Aces2065 as color space. Furthermore, colour-science was used to visualize the CIE 1976 UCS (ISO, 2023) chromaticity diagrams and to compute the CIE ΔE_{00} (ISO, 2022b) color difference between predicted and measured spectral reflectance.

2.3 Hardware

The flatbed printer RolandDG VersaUV LEF-300 (firmware 2.80) was used to print the datasets. The printer was equipped with ECO-UV-4 UV-curing inks. Besides cyan, magenta, yellow and black the printer is able to print white. It will be referred as LEF300 printer in the following. A Konica Minolta Auto Scan Spectrophotometer FD9 was used to obtain the spectral reflectance of the printed color charts. It will be referred as FD9 spectrophotometer in the following. A Canon EOS M50 MK2 (firmware 1.0.3) digital camera equipped with a Canon EF-M 28MM F/3.5 MACRO IS STM lens and a polarizing filter was used to capture the color charts. It will be referred as M50 camera in the following. During capturing the Texas Instruments DLP LightCrafter Display 230NP EVM projector served as adjustable light source. Its relevant components are an Osram KR CSLNM1.23_EN red LED, an Osram KP CSLNM1.F1_EN green LED and an Osram KB CSLNM1.14_EN blue LED, that define the spectral distribution of the emitted light. A polarizing filter was installed in front of its lens. The projector will be referred as DLP projector in the following. A RaspberryPI 4b was used to programmatically control the M50 camera and the DLP projector.

2.4 Obtaining the datasets

2.4.1 Defining the color patches

A total of 10 800 color patches were defined, whereby 400 were combined into one color chart. To reach a sufficient variance of colors chart 27 represents primary colors (cyan, magenta, yellow) as well as black with opacities from 1 % to 100 % ascending 1 % per step. Charts 1 to 3 represent secondary colors (red, green, and blue) where opacity of one primary color ascends in 5 % steps from 5 % to 100 % per row while opacity of the other primary color ascends per column. Charts 24 to 26 each combine one primary color with black following the same principle. The remaining charts (4 to 23) represent tertiary colors. Therefore, opacity of magenta ascends per row and opacity of cyan ascends per column while opacity of yellow ascends per chart in 5 % steps from 5 % to 100 % (Figure 2). The background of each chart was set to 4C black (cyan, magenta, yellow, black) with an opacity of 100 %. The export function in InDesign creates the printable pdf. During creation any color transformation processes were deactivated and no color profile was embedded.

2.4.2 Printing the color patches and obtaining their spectral reflectance

The datasets were printed by the LEF300 printer on Clairfontaine DCP 1849C paper. To obtain four different datasets each chart was printed four times with different parameters. In the RIP software VersaWorks LEF300EcoUV4_Generic_v720x720.icc delivered by Roland DG was set as device color profile for all datasets. The CMYK simulation target profile and the matching method was set to PSOCoated_v3.icc and colorimetric for the first three datasets. The first dataset was directly printed on the substrate. From here on this dataset will be referred as 'p' (for paper). As the substrate includes optical brighteners the second dataset aims to eliminate their influences. Therefore, one layer of 100% 4c black (cyan, magenta, yellow and black) is printed to block these influences. Three layers of white were printed on top followed by the actual color charts. This dataset will be referred as '1x' (1 = one layer of color, x = blocked substrate). Printing the third dataset followed the same procedure except that the color charts were printed with 200% instead of

100% opacity (setting) by setting the overprint parameter in VersaWorks to 2. This dataset will be referred as '2x'. The fourth dataset was also directly printed on DCP 1849C paper but with the CMYK simulation target profile set to RolandWideGamut2_CMYK.icc. This dataset will be referred as 'pw' (for paper wide gamut). Figure 3 shows the mentioned profiles in comparison. While the LEF300 profile represents the printable gamut of the printer, the simulation target profile PSOcoated_v3 limits its gamut. RolandWideGamut2_CMYK includes the complete gamut of the LEF300-printer and, therefore, does not limit the printable gamut.
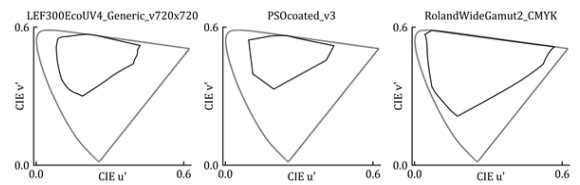
Figure 3: CIE 1976 UCS chromaticity diagrams of the ICC profiles used for printing

The spectral reflectance of each patch was measured by the FD9 spectrophotometer using the measurement modes M0, M1 and M2. The spectral reflectance was measured from 380 nm to 730 nm in 10 nm steps. Figure 4 visualizes the datasets in the CIE 1976 UCS chromaticity diagram. For an analytical comparison Figure 5 shows the ΔE_{00} differences between every pair of datasets.
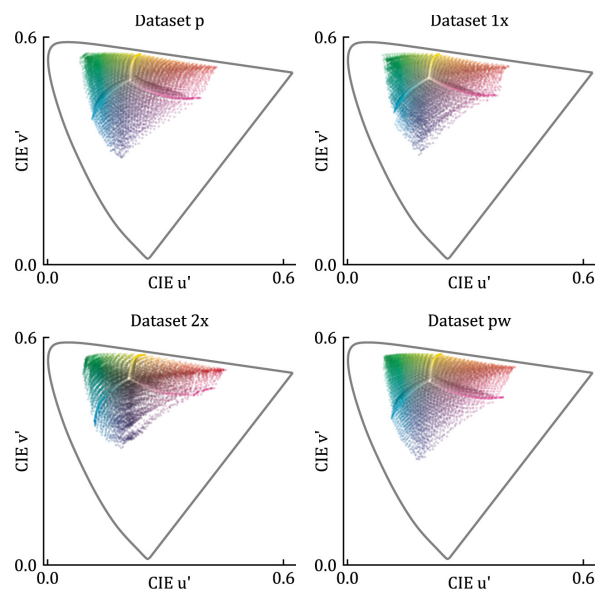
Figure 4: CIE 1976 UCS chromaticity diagrams of the datasets

Figure 2: The 10 800 color patches on 27 charts
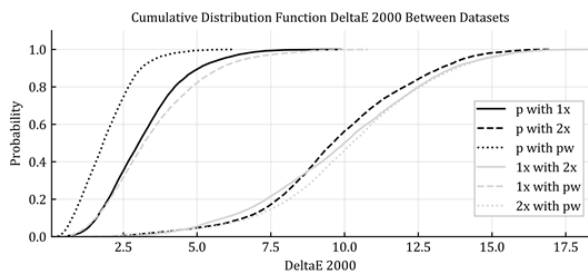
Figure 5: Probability that the color difference between corresponding color patches of two different datasets is less than a certain ΔE_{00} value

The color patches of 'p' and 'pw' are the closest to each other. Accordingly, the gamut of the LEF300 is the closest to the one of the PCOcoated_v3 profile. The difference between 'p' and '1x' is explainable as '1x' is printed on top of one layer of black and three layers of white and therefore on another substrate. The dataset '2x' has the most difference from the other as each color patch is printed with 200% opacity. Therefore, 2x is more saturated, which widens the gamut especially in red, but also limits the gamut in blue.

2.4.3 Organizing the spectral reflectance in arrays

After measuring, the spectral reflectance values of the color patches of a dataset were stored in several csv files. Before this data can be used for training they will be reorganized in np.arrays. Therefore, for each chart the corresponding csv files were opened by calling np.genfromtxt() with the delimeter set to ',' and unpack set to false. As the csv files contains more information than needed, the resulting array was reduced to the spectral reflectance. This information was stored into one array for each chart. Each array has a shape of 400 by 36. Each row represents one color patch while each column represents its spectral reflectance at the corresponding wavelength.

To gather the spectral reflectance of a complete dataset the spectral reflectance arrays of the corresponding charts were combined to a single array. The combined spectral reflectance array has a shape of 10 800 by 36. The patches order in this array is ascending by chart and per chart ascending by row and then ascending by column. So, the first row in the array represents the patch at the first row and first column of the first chart while row 431 in the array represents the patch at the second row and eleventh column of the second chart.

2.4.4 The capturing device

As mentioned in the introduction, the capturing device is a prototype of a 3D scanning system. The housing of the system has the dimensions of 520 x 300 x 300 mm. It is enclosed to lock out extraneous light.
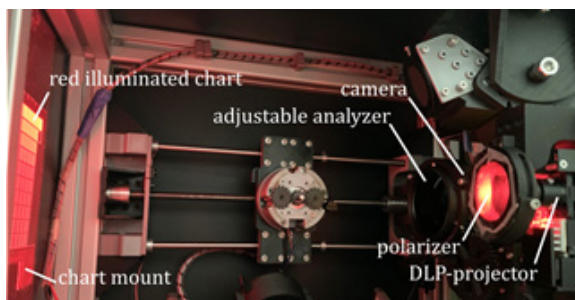
Figure 6: The capturing device with a mounted and red illuminated chart on the left and the DLP projector and M50 camera on the right

On the inside the walls are matte black to reduce internal light scattering. The M50 camera and the DLP projector have a fixed position next to each other on the right side of the box, facing in the direction of the wall on the left site. In the center of this wall is a mount to place a color chart (Figure 6).

Ideally the DLP projector would illuminate the chart at an angle of 45 degree to the camera to avoid reflections. Unfortunately, the angle is limited by the 3D scanning method and the space. To compensate this issue, a polarizing filter in front of the projector serves as polarizer while a polarizing filter in front of the camera serves as analyzer. As polarizer and analyzer were aligned perpendicular to each other, reflections were minimized during capturing (Figure 7).
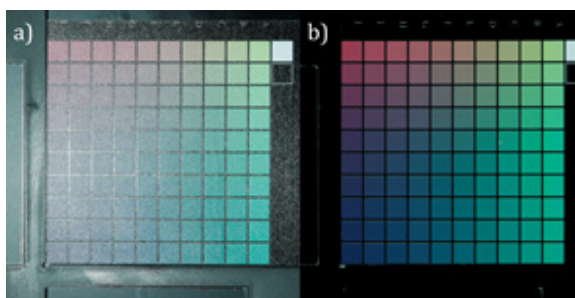
Figure 7: A chart illuminated by white light captured with a) the analyzer aligned parallel to the polarizer and b) the analyzer aligned perpendicular to the polarizer

2.4.5 Capturing the charts

To capture a chart, it has to be placed into the mount. As the substrate printed on is relatively flexible, the chart had to be stiffened. Therefore, each color chart was applied onto white cardboard. Furthermore, each chart had to be divided into four parts (chart parts) to completely fit into the illuminated area (Figure 8).

When the first chart part was placed into the mount, the DLP projector illuminated it subsequently with-
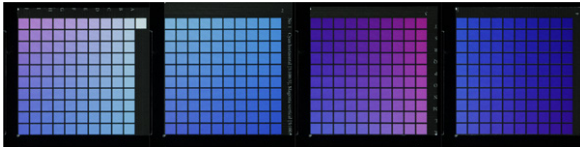
Figure 8: The images of the four chart parts of chart 1 (dataset 'pw') illuminated by white light

white, red, green, blue, cyan, magenta and yellow lights, which can be seen as seven different light sources. With each light source the M50 camera captured an image of the illuminated chart part. When finished, part two to part four of the same chart were captured by following the same procedure. So, each chart part is present in seven images corresponding to the different light sources (Figure 9).
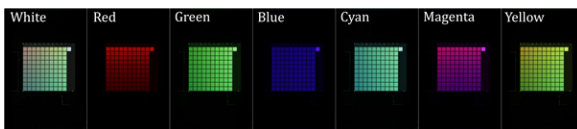
Figure 9: Example of a series of images showing color chart 12 part 1 (dataset 'pw')

This procedure was repeated for each color chart part of each dataset. The resulting images were stored for further processing. Regarding the settings the M50 camera is set to manual control to avoid changing settings due to automated processes. The white balance was set to 5 000 K. The file format for the images was JPEG and the embedded color space was Adobe RGB 1998. Aperture was set to 14, while shutter speed was set to 1 second and ISO was set to 100. Regarding the DLP projector the brightness was set to maximum, while the LEDs were directly controlled using the API provided by Texas Instruments.

2.4.6 Determining the positions and dimensions of the patches in an image of a chart part

To complete the datasets RGB triplets for each color patch had to be extracted from the captured images. Therefore, the positions and dimensions of the colored patches in the images had to be determined. To easily determine position and dimension of each patch despite their changing colors and contrasts to the background, a chart part consisting of only white colored patches was used. The white patches have a high contrast to the black background which eases contour detection. In the following this chart part will be referred as calibration chart. As each colored chart part was captured at the same position as the calibration chart, the determined positions and dimensions of the white patches could be used to extract RGB triplets for each patch on every chart part.
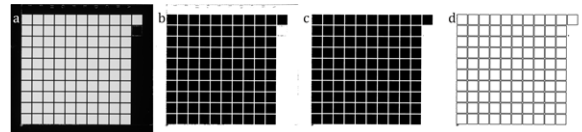
Figure 10: The process of detecting the contour of the color patches: (a) the image of the calibration chart as grayscale image: (b) the image of the calibration chart transformed to binary image: (c) the binary image with less noise: (d) the detected contours

The calibration itself started with capturing the calibration chart resulting in seven images (Section 2.4.5). The calibration chart image illuminated by white light were loaded as grayscale image by calling cv2.imread() with the option cv2.IMREAD_GRAYSCALE (Figure 10a). Calling cv2.threshold() with a threshold of 100, a maximum value of 255 and the type-variable set to cv2.THRESH_BINARY_INV converted the grayscale image into an inverted binary image (Figure 10 b). To remove smaller black parts in the background and smaller white parts in the black patches cv2.morphologyEx() was called with morphological operation set to cv2.MORPH_CLOSE and a 5x5 matrix filled with ones used as kernel (Figure 10c). These preparations optimized the image for calling cv2.findContours() with mode set to cv2.RETR_TREE and method set to cv2.CHAIN_APPROX_SIMPLE. Figure 10d shows the detected contours. To remove false detections, contours with an area (cv2.contourArea()) smaller than 20 000 pixels and greater than 1 000 000 pixels were filtered out. Finally, each contour was simplified to a rectangle (cv2.boundingRect()) defined by its position in the image (*x, y*) and its width and height. This information can be used to find the color patches in each image of a chart part.

2.4.7 Extracting RGB triplets from chart part captures

With the gathered positions and dimensions of each patch in the calibration chart each pixel of each patch in the colored chart parts is addressable. The RGB triplets of all pixels of a patch was reduced to a single RGB triplet. Therefore, each rectangle describing a patch (Section 2.4.6) was shrunk to half its size. Its position was corrected so that the rectangle is centered on the corresponding patch. The average of the RGB triplets of the pixels framed by a rectangle represented the RGB triplet of the corresponding color patch. Figure 11 visualizes the extracted information for the calibration chart.

As each color patch was present in seven images corresponding to the seven light sources, seven RGB triplets had to be extracted for each color patch. As the extraction was done per chart part, the results were gathered and sorted according to the sorting of the
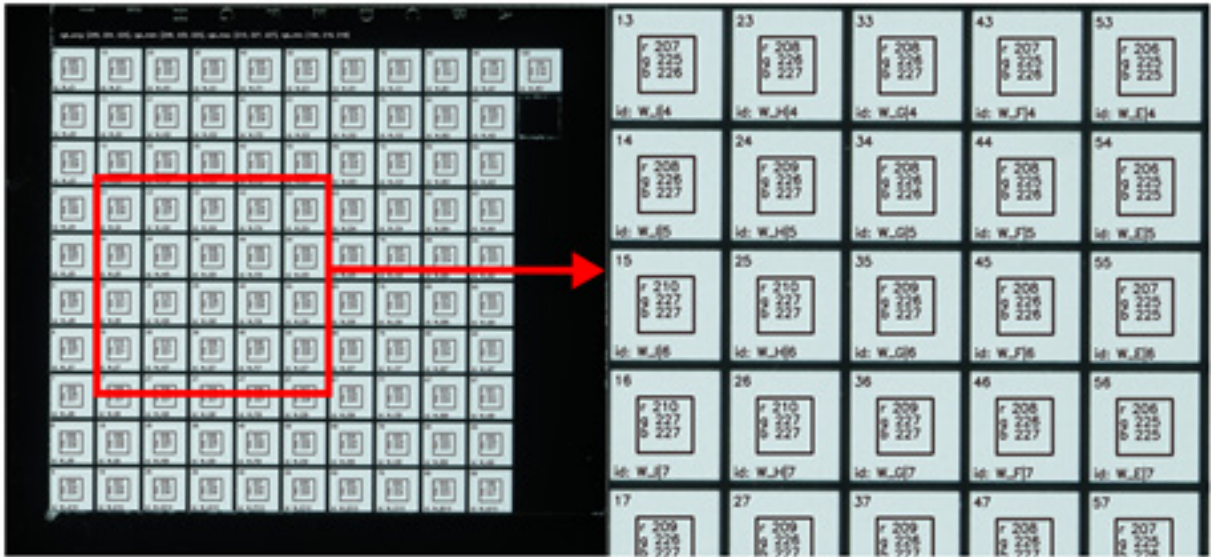
Figure 11: Exemplary RGB triplet extraction for color patches of the calibration chart with white illumination: in the top left of each patch is its number; the rectangle marks the extraction area while r, g, and b are the extracted values and ID describes the patch identity defined by the chart number (here w for white), row and column on the undivided chart

spectral reflectance array (Section 2.4.3). The resulting np.array had a shape of 10 800 by 21, where each row represented a color patch and each column represented a channel of an extracted RGB triplet (R_{white_ls}, G_{white_ls}, B_{white_ls}, ..., R_{yellow_ls}, G_{yellow_ls}, B_{yellow_ls}).

2.4.8 Correcting unevenly distributed illumination

The extracted RGB triplets in Figure 11 also showed that the illumination was uneven. Although, all patches had the same color with the same spectral reflectance the corresponding RGB triplets differ. The minimum values are $\min(R) = 194$, $\min(G) = 216$, $\min(B) = 218$ while the maximum values are $\max(R) = 210$, $\max(G) = 227$, $\max(B) = 227$. To compensate this error for each patch (i) of the calibration chart and each channel of its extracted seven RGB triplets (Kcc_{ij}) corresponding to the seven light sources (j) a correction factor $f_{ij}K$ was computed according to Equation 7. These factors were stored in an np.array. During extraction (Section 2.4.7) these factors were applied to the corresponding extracted values according to Equation 8.

$$f_{ijK} = \frac{\overline{Kcc}}{Kcc_{ij}} \qquad [7]$$

$$Kcrr_{ij} = f_{ijK}\, K_{ij} \qquad [8]$$

where $Kcrr_{ij}$ is the corrected value for K, f_{ijK} is the correction factor, i is the number of patch in a chart part $[0 ; 100]$, j is the illumination (white, red, green, blue, cyan, magenta, yellow), K is the extracted K value

(RGB) of a patch of a color chart, Kcc is the extracted K value of a patch of the calibration chart and $\overline{Kcc}$ is the average of extracted K values of the patches of the calibration chart.

2.5 Splitting the datasets for training, validation and evaluation

Each dataset had to fulfill three purposes. The first purpose is to train the neural network while the second one is to validate the network during training. The third purpose is to test and evaluate the trained network. It is crucial that data used for training is not used for either validation or evaluation, which leads to three subsets. Due to the tests in this article further requirements had to be considered. Firstly, the patches of the subsets had to be equally distributed to represent a wide range of color combinations and to prevent a network to be biased to specific colors (for example reddish colors). Secondly, the subsets had to contain the same patches for each dataset. This enables to compare the performance of networks based on different datasets. It also enabled to test the performance of networks trained with a training subset of one dataset when evaluated with a test subset of another dataset. Thirdly, the training subset had to be reduced systematically. This enabled to test the performance of a network in dependence on the size of the training subset.

To select equally distributed color patches to form the subsets, three cases had to be considered. While the primary colors were distributed linearly, the secondary

S. Ritzmann, P. Urban – J. Print Media Technol. Res. – Vol. 13 No. 2 (2024), 63–79

71

Colors were distributed squarely and the tertiary colors were distributed cubically (Section 2.4.1). For each of these three cases, a step value was calculated according to Equation 9, where the splitting factor was the portion of patches of the dataset. The step value defined the step between color patches in each dimension. In the case of linear distribution, every step-th color patch was used for a subset as the color itself only changed in one dimension. In the case of squared distribution, every step-th color patch (respectively column) from every step-th row of the corresponding chart was part of the subset as one primary color changed per row and the other per column. In the case of cubic distribution, one primary color changed per row, the second per column, and the third per chart. Therefore, from every stepth chart, every step-th color patch from every step-th row was selected.

$$step = 20\left(20^{d}\,f_{split}\right)^{-\frac{1}{d}} = f_{split}^{-\frac{1}{d}} \qquad [9]$$

where step determines the frequency of selected patches (every step-th patch is included in the subset), f_{split} represents the splitting factor $[0.0\,;1.0]$ and d indicates the number of dimensions $[1\,;3]$

In the best-case step is a natural number that directly points to the color patches to select. But it is more likely that step is a rational number. In that case the decimal part of step equaled an error variable and step was rounded off by calling np.floor(). The rounded off step

was used to select the first color patch (or row, column or chart depending on the number of dimensions). For the distance between the last selected and the next color patch the current error was added to step. After that the decimal part again equaled the current error and step was rounded off. This process visualized for the linear, squared and cubic case in Figures 12 to 14. As a result, the error was minimized during selection.

For the test subset, the splitting factor was set to 0.2, and the color patches were selected as described. Depending on the test performed, the splitting factor for the training subset varied. For the main tests, it was set to 1.0. To ensure that each color patch appeared in only one subset, all color patches present in both the test and training subsets were deleted from the training subset. Afterwards, the subsets were shuffled by calling np.random.shuffle() with the seed fixed at 19840924. The splitting factor for the validation subset was set to 0.1. Unlike before, for the validation subset, the first *n* color patches in the shuffled training subset were extracted, where *n* was calculated according to Equation 10. The resulting subsets for the case described above are visualized in Figure 15. Table 1 shows the dataset shares of the subsets corresponding to the previously mentioned splitting factors.

$$n = ceil\left(N_{ts}\,f_{split}\right) \qquad [10]$$

where *n* is the number of patches extracted from training

linear: splitting factor = 0.2, step = 5

step:				5.00				5.00				5.00				5.00		
error:				0.00				0.00				0.00				0.00		
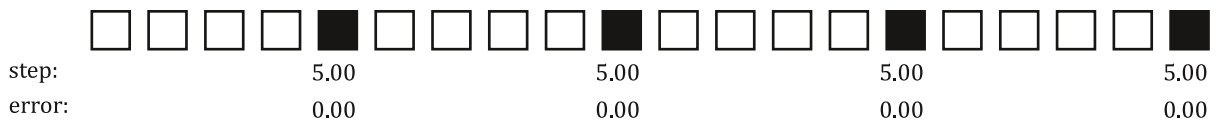
Figure 12: Subset color patch selection in case of linear distribution (primary colors)

squared: splitting factor = 0.2, step = 2,24

step:	2.24	2.48	2.72	2.96		3.20	2.44	2.68	2.92	3.16
error:	0.24	0.48	0.72	0.96		0.20	0.44	0.68	0.92	0.16

Figure 13: One dimension of the subset color patch selection in case of squared distribution (secondary colors)

cubic: splitting factor = 0.2, step = 1,71

step:	1.71		2.42		2.13	1.84		2.55		2.26	1.97		2.68		2.39		2.10	1.81		2.52
error:	0.71		0.42		0.13	0.84		0.55		0.26	0.97		0.68		0.39		0.10	0.81		0.52

Figure 14: One dimension of the subset color patch selection in case of cubic distribution (tertiary colors)

subset, N_{ts} is the number of patches in the training subset and f_{split} is the splitting factor for validation $[0.0 ; 1.0]$
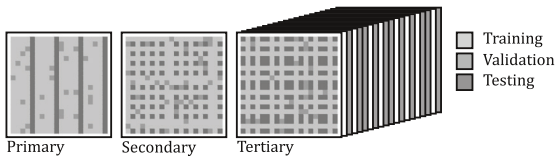
Figure 15: Exemplary RGB-value

Figure 16: Range of the performance of 40 trainings using the same parameters and dataset

Table 1: Splitting factors and resulting dataset shares

	Training	Validation	Testing
Splitting factor	1.00	0.10	0.20
Dataset share [%]	70.88	7.88	21.24
Number of patches	7 655	851	2 294

2.6 Parameters of the neural network

The neural network was a densely connected feed forward network. It had one input layer (keras. Input()), three hidden layers (keras.layers.Dense()) and one output layer (keras.layers.Dense()). Its input layer had 21 Neurons corresponding to the seven RGB triplets of a color patch captured under seven different light sources. Its output layer had 36 neurons representing the spectral reflectance of the same color patch at wavelengths from 380 nm to 730 nm in 10 nm steps. Its first hidden layer had 180 neurons, its second hidden layer had 80 neurons and its third hidden layer had 40 neurons. The rectified linear unit function was the activation function of all neurons in the hidden layers, while the sigmoid function was the one of the neurons in the output layer. During training the loss between the measured and the predicted spectral reflectance was was determined by the mean squared error (MSE) using keras.losses. MeanSquaredError() with reduction set to auto and the other parameters set to default. The ADAM (Adaptive Moment Estimation)-algorithm (Kingma and Ba, 2017) (tf.keras.optimizers. Adam()) minimized the loss during training with its learning rate set to 0.001 and its other parameters set to default. A training ran for a maximum of 2 000 epochs with a batch size of 32. Training was stopped if the validation loss was not decreasing for 50 epochs. In the case of an early stop the best weights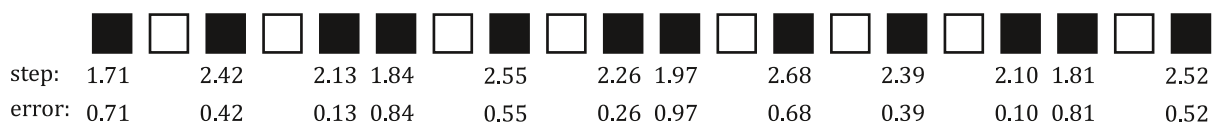 were restored (tf.keras.callbacks.EarlyStopping() with monitor set to 'val_loss', patience set to 50, mode set to 'min' and restore_best_weights set to true).

Before training the RGB triplets of the subsets (Section 2.5) were normalized by dividing by 255. The spectral reflectance values of the subsets were reduced to those obtained with measurement mode M2. The training
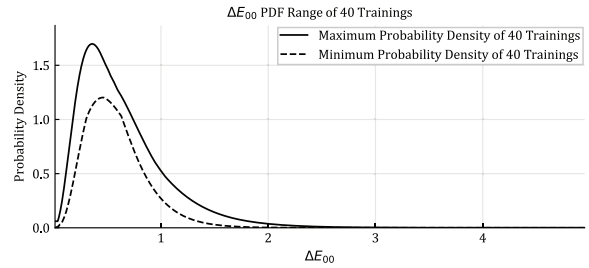
was started by calling keras.model.fit() with the RGB triplets and the spectral reflectance of the training subset set as x and y, the validation subset used as validation data and the other values set as mentioned.

At the start of training, the weights of the neurons were set randomly. These starting weights mainly influenced the training outcome and therefore the performance of a trained network. Figure 16 showed the range of probability density functions (Section 2.7) of 40 trainings using the same parameters and dataset. Due to the randomly chosen starting weights, the performance of the trained networks varied. During pre-testing, 40 trainings were found to be sufficient to cover the entire performance range (which was close to the 41 repetitions used by Lazar, Javoršek, and Hladnik (2020)).

2.7 Evaluation and visualization of the training results

To evaluate a trained network or model, it predicted spectral reflectance from the RGB triplets of the test subset. The predictions were compared to the measured spectral reflectance using two metrics. The first one was the MSE between the predicted and the measured spectral reflectance, which also is the loss function during training. Therefore, the model should be optimized to this metric. The second and mainly used metric is the CIEDE2000 (ΔE_{00}) color difference. To compute the difference, the predicted and corresponding measured spectral reflectance were transformed to the CIELAB color space (Section 2.2).

These metrics were computed for each color patch of the test subset. To analyze the performance of the model as a whole, mean, median, standard deviation, minimum and maximum of these metrics were computed (Tables 2 and 3).

For further visualization the ΔE_{00} metric is used exclusively. To visualize the model performance as a whole a generalized gamma distribution (Stacy, 1962) was fitted to the ΔE_{00} values. Therefore, the ΔE_{00} values of the color patches were sorted ascending by calling

np.sort(). Calling scipy.stats.gengamma.fit() returned the shape parameters *a* and *c* as well as the scale and the location defining the fitted distribution. Calling scipy.stats.gengamma.pdf() with these parameters returns the probability density function (PDF) of the ΔE_{00}-values (e.g. Figure 17). Integrating the PDF on the intervals [0.0; 1.0[, [1.0; 2.0[and [2.0; 3.0[leads to the probability that the color difference lies within these intervals (see Table 2).

The PDF visualizes the model performance regarding the ΔE_{00} values for the whole test subset of a dataset. Furthermore, PDFs are used to visualize the performance of different models in comparison (see Figure 17).

A model with a higher and narrower density peak positioned further left performs better than a network with a lower and wider density peak located further right. The legend in Figure 17 shows the PDFs were sorted descending by their probability to predict a spectral reflectance that leads to a ΔE_{00} less than 1.0.

Regarding the naming each model is assigned to an id. The id consists of the year, month, day, hour, minute and second the training was started. For the PDFs the id is followed by abbreviation of the dataset used for training. In Tables 2–5, 9 and 10 the same dataset can be find in the 'DS' (dataset) column.

3. Results and discussion

3.1 Model performance depending on dataset and measurement mode

Therefore, out of the 40 training runs for each dataset the model with the highest probability to predict a spectral reflectance leading to a ΔE_{00} between 0.0 and 1.0 was chosen as the best performing model. Training with the 'pw' dataset resulted in the best performing model regarding ΔE_{00} (Table 2, Figure 17) and MSE (Table 3) followed by training with the 'p' dataset. Regarding ΔE_{00} the model trained with the '1x' dataset performed better than the one trained with the '2x' dataset (Table 2, Figure 17). Regarding MSE the model trained with '2x' performed better than the one trained with '1x' (Table 3). Due to blocking the optical brighteners during printing (Section 2.3.2) the M2 (UV-cut filter) measurement mode used for training (Section 2.6) should have less influence on the '1x' and '2x' datasets than on the 'p' and 'pw' datasets. To evaluate the influence of the measurement mode on the model performance, the test was repeated with the '1x' and 'pw' dataset. This time the spectral reflectance was obtained using measurement modes M0 and M1. Notation wise the dataset name was complemented by the measurement mode used; e.g. for 'pw-M0' measurement mode M0 was used to obtain the spectral reflectance of the 'pw' dataset. The resulting models were compared to the best performing model so far (20231027075227).

Changing the measurement mode changes the outcome of the training as well. While for 'pw' measurement mode M2 continued to lead to the best performing model, for '1x' M1 leads to the best model (20231122000640) regarding both ΔE_{00} and MSE (Tables 4 and 5, Figure 18). The probability to predict a spectral reflectance leading to a ΔE_{00} less than 1.0 increased from 0.897 (Table 2) with measurement mode M2 to 0.922 (Table 4).

In conclusion, the color management settings, the substrate and the measurement mode of the spectrophotometer used influence the performance of a model. The 'pw' trained model seems to perform slightly

better than the 'p' trained one because of using a wider CMYK simulation target profile (Section 2.4.2). The same color management settings in combination

Table 2: The ΔE_{00} statistics of the best performing models sorted descending by prob.[0;1[

Model id	DS	Mean	Median	StD	Min.	Max.	Prob.[0;1[	Prob.[1;2[	Prob.[2;3[
20231027075227	pw	0.515	0.461	0.280	0.035	2.246	0.938	0.061	0.001
20231006161556	p	0.528	0.479	0.286	0.048	2.177	0.930	0.068	0.001
20231025122410	1x	0.582	0.527	0.318	0.012	2.153	0.897	0.100	0.004
20231026133808	2x	0.737	0.629	0.474	0.030	4.120	0.778	0.201	0.018

Table 3: The MSE statistics of the best performing models sorted ascending by mean

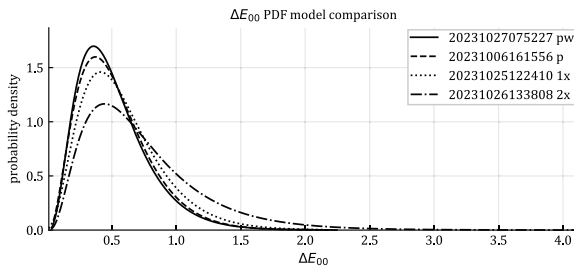| Model id	DS	Mean	Median	StD	Min.	Max.
20231027075227	pw	1.35	6.81×10^{-6}	2.23×10^{-5}	3.50×10^{-7}	3.81×10^{-4}
20231006161556	p	1.38×10^{-5}	7.41×10^{-6}	2.12×10^{-5}	5.79×10^{-7}	2.91×10^{-4}
20231026133808	2x	1.41×10^{-5}	8.12×10^{-6}	1.81×10^{-5}	4.43×10^{-7}	2.45×10^{-4}
20231025122410	1x	1.53×10^{-5}	9.95×10^{-6}	1.95×10^{-5}	4.99×10^{-7}	3.84×10^{-4}

Figure 17: The ΔE_{00} PDFs of the best performing model from each dataset in comparison (ascending sorted by Prob.[0;1[in legend)
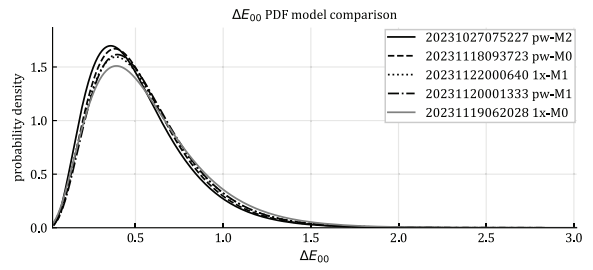
Figure 18: The ΔE_{00} PDFs of the model performance depending on the measurement mode
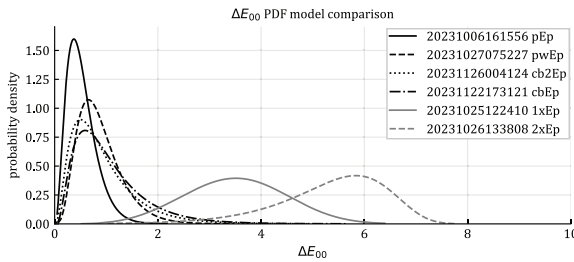
Figure 19: The ΔE_{00} PDFs of all models evaluated with the 'p' test subset
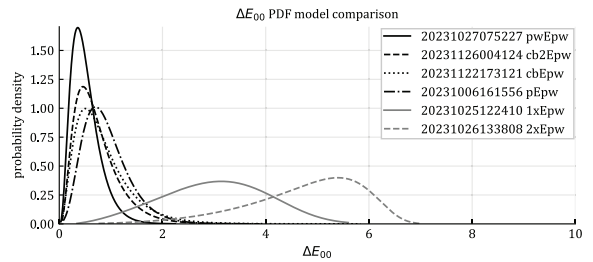
Figure 20: The ΔE_{00} PDFs of all models evaluated with the 'pw' test subset
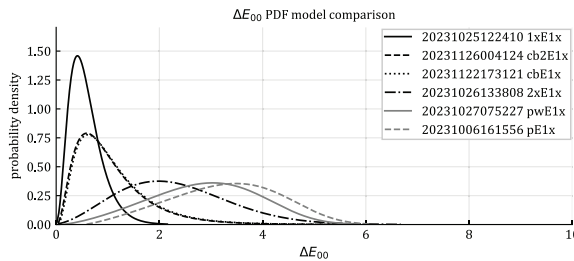
Figure 21: The ΔE_{00} PDFs of all models evaluated with the '1x' test subset
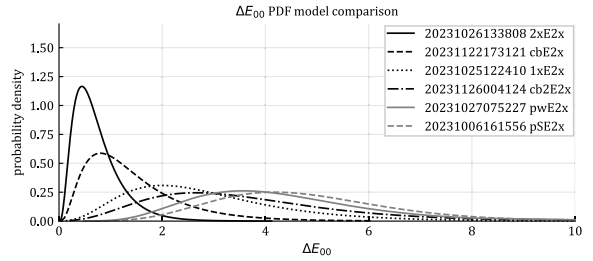
Figure 22: The ΔE_{00} PDFs of all models evaluated with the '2x' test subset

Table 4: The ΔE_{00} statistics for testing the influence of the measurement modes

Model id	DS	Mean	Median	StD	Min.	Max.	Prob.[0;1[	Prob.[1;2[	Prob.[2;3[
20231027075227	pw-M2	0.515	0.461	0.280	0.035	2.246	0.938	0.061	0.001
20231118093723	pw-M0	0.535	0.486	0.285	0.054	2.833	0.931	0.067	0.001
20231122000640	1x-M1	0.546	0.489	0.297	0.027	1.918	0.922	0.076	0.006
20231200013 33	pw-M1	0.551	0.502	0.296	0.034	2.845	0.922	0.076	0.001
20231190620 28	1x-M0	0.566	0.508	0.318	0.030	3.016	0.905	0.092	0.002

Table 5: The MSE statistics for testing the influence of the measurement modes

Model id	DS	Mean	Median	StD	Min.	Max.
20231027075227	pw-M2	1.35×10^{-5}	6.81×10^{-6}	2.23×10^{-5}	3.50×10^{-7}	3.81×10^{-4}
20231122000640	1x-M1	1.45×10^{-5}	9.84×10^{-6}	1.46×10^{-5}	4.50×10^{-7}	1.75×10^{-4}
20231119062028	1x-M0	1.56×10^{-5}	1.05×10^{-5}	1.67×10^{-5}	6.04×10^{-7}	2.10×10^{-4}
20231118093723	pw-M0	1.60×10^{-5}	8.67×10^{-6}	2.80×10^{-5}	6.26×10^{-7}	5.75×10^{-4}
20231120001333	pw-M1	1.99×10^{-5}	9.51×10^{-6}	5.73×10^{-5}	8.32×10^{-7}	1.66×10^{-3}

with the different substrates 'p' and '1x' are printed on cause the performance of the '1x' trained model to decrease in comparison. The performance of a '2x' trained model seems to decrease because of the 200% opacity (Section 2.4.2) compared to a '1x' trained one. The performance of a '1x' trained model increases when using measurement mode M1 instead of M2, seemingly, because these measurement modes deal differently with the fluorescence of ink and substrate. In theory, each of these assumptions should not influence the training of a neural network as long as the RGB triplets correlates well with the corresponding spectral reflectance. So, the final assumption is that the different datasets influence this correlation. Within the scope of this work the exact reasons are not clear and should be topic of further investigation.

3.2 Model generalization

This test examineed if a model is specialized on the dataset used for training or if it is generalized. Therefore, each model determined in 3.1 was evaluated with the test subsets of the datasets that are not related with its training. Furthermore, the datasets weree combined to train more generalized models. So, the training subsets of all datasets were combined to one training subset ('cb' for combined). The second combined training subset ('cb2') did not include the '2x' training subset. Regarding the notation for the PDF, the first subset is the subset the model was trained with followed by 'E' (for evaluate) as divider and then by the subset used for evaluation. So, 'pwE1x' shows the performance of a model trained with 'pw' and evaluated with the test subset of '1x'. Due to the number of models (26) the statistics were reduced to two values for each test and training subset combination. The two values are the mean ΔE_{00} with its added standard deviation (Table 6) and the probability that that the ΔE_{00} of a sample is less than 3.0 (Table 7).

In general, the performance of a model went down if the test subset was from another dataset than the training subset. Figures 19 to 22 each show the PDFs of the models evaluated with one test subset. For both test subsets 'p' (Figure 19) and 'pw' (Figure 20) the

models trained with '1x' and '2x' performed the worst with a mean ΔE_{00} with its added standard deviation between 4.042 and 6.450 (Table 6) and a probability between 0.032 and 0.482 that a prediction results in a ΔE_{00} less than 3.0 (Table 7). The corresponding PDFs have a noticeably lower peak located far right from the other PDFs (Figures 19 and 20). The test subsets '1x' (Figure 21) and '2x' (Figure 22) each have two PDFs with similar characteristic corresponding to the models trained with 'pw' and 'p'. While the mean ΔE_{00} with its added standard deviation range between 3.926 and 6.741 (Table 6) is close to before, the probability that a prediction leads to a ΔE_{00} less than 3.0 between 0.137 and 0.528 (Table 7) is slightly better. The common property between '1x' and '2x' which differs from the common property of 'p' and 'pw' is the substrate. In contrast, the datasets 'p' and '1x' as well as 'pw' and '1x' are closer to each other than '1x' and '2x' (Figure 5). This observation lead to the assumption that accuracy of the prediction of a model increases if the sample is printed on the same substrate.

Overall, the non-combined datasets ('p', 'pw', '1x', '2x') have an average mean ΔE_{00} with its added standard deviation between 3.103 and 4.228 (Table 6). The two models trained with a combination of all datasets on the other hand perform noticeable better with an average mean ΔE_{00} with its added standard deviation of 1.868 for 'cb' and 2.629 for 'cb2'. The probability to predict a spectral reflectance resulting in ΔE_{00} less than 3.0 is between 0.928 and 0.994 for 'cb'. As 'cb2' does not include the '2x' training subset the probability decreases from 0.928 to 0.425 for the '2x' test subset compared to 'cb' (Table 7). The probability for the other test subsets increases slightly from 0.974 to 0.977 for '1x', 0.978 to 0.987 for 'p' and 0.994 to 0.997 for 'pw'.

In conclusion, training with a combination of multiple training subsets leads to a generalized model. If a single subset is neglected during training, the performance of the corresponding test subset decreases significantly more than the performance increases for the other test subsets. Furthermore, the performance of the generalized models decreases compared to the

Table 6: The mean ΔE_{00} added by the standard deviation of training and test subset combinations

Test	1x	2x	p	pw	cb	cb2
1x	0.900	3.365	4.337	3.926	1.840	1.795
2x	5.062	1.211	6.741	6.365	2.450	5.984
p	4.491	6.450	0.814	1.325	1.764	1.563
pw	4.042	5.885	1.362	0.795	1.419	1.175
avg.	3.624	4.228	3.314	3.103	1.868	2.629

Table 7: Probability that the ΔE_{00} of a sample is less than 3.0

Test	1x	2x	p	pw	cb	cb2
1x	1.000	0.755	0.385	0.528	0.974	0.977
2x	0.608	0.997	0.137	0.228	0.928	0.425
p	0.307	0.032	1.000	0.997	0.978	0.987
pw	0.482	0,078	0.997	1.000	0.994	0.997
avg.	3.624	4.228	3.314	3.103	1.868	2.629

Table 8: Splitting factors of training subsets and resulting dataset share

	0.15	0.25	0.39	0.52	0.71	0.80	0.89
Dataset share [%]	9.91	19.86	29.76	39.38	50.62	60.21	69.51
n-patches train	1 070	2 145	3214	4 253	5 467	6 503	7 507
n-patches validation	119	239	358	473	608	723	835

Table 9: The ΔE_{00} statistics of the models with reduced size of the training subset

Model id	DS	Mean	Median	StD	Min.	Max.	Prob.[0;1[	Prob.[1;2[	Prob.[2;3[
2023111145455	pwR89	0.524	0.469	0.293	0.018	2.931	0.933	0.066	0.001
2023111011123	pwR80	0.551	0.504	0.298	0.011	2.693	0.921	0.077	0.001
20231109211733	pwR71	0.579	0.524	0.302	0.050	2.857	0.907	0.091	0.001
20231109024923	pwR52	0.601	0.534	0.343	0.021	3.433	0.882	0.114	0.003
20231108163826	pwR39	0.621	0.562	0.339	0.024	3.322	0.872	0.124	0.003
20231106043622	pwR25	0.729	0.639	0.440	0.015	4.815	0.789	0.196	0.013
20231107221515	pwR15	0.776	0.679	0.475	0.052	5.504	0.754	0.225	0.018
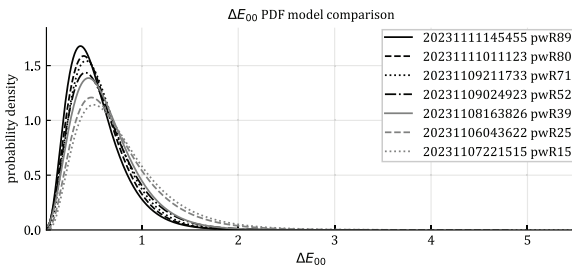
Figure 23: The ΔE_{00} PDFs of the models trained with reduced training subsets
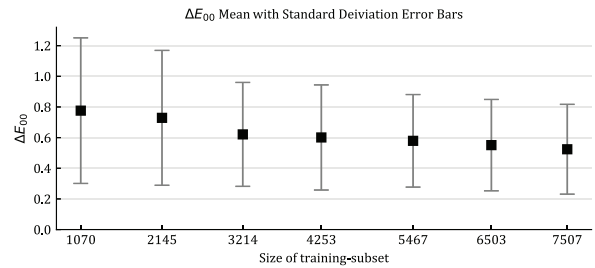
Figure 24: The ΔE_{00} means depending on the size of the training subset

performance of a model trained and evaluated with the subsets of the same dataset.

3.3 Decreasing size of the training subset

This test examines the performance of a model depending on the size of the training subset. Therefore, the 'pw' dataset that results in the best performing model (Section 3.1) is used for training. The size of the training subset is decreased from 70 % of the size of the dataset down to 10 % in 10 %-steps by reducing the splitting factor of the training subset (Section 2.5). Due to the reduction logic a splitting factor of 0.7 does not equal a share of 70% of the dataset. The used splitting factors and the resulting shares of the dataset are shown in Table 8. The dataset name is complemented by 'R' (for reduction test) followed by the corresponding splitting factor in percentage.

With the decreasing size of the training subset the peaks of the corresponding PDFs flatten out and shift to the right indicating a decreasing performance (Figure 23). If the number of color patches is reduced from 7507 (pwR89) to 1070 (pwR15) the probability to predict a spectral reflectance that leads to an error less

than 3.0 ΔE_{00} decreases slightly from 1.0 to 0.997. If a ΔE_{00} less than 1.0 is needed the probability drops from 0.933 to 0.754 (Table 9). The expected error range lies between 0.231 and 0.817 ΔE_{00} for a training subset size of 7507 color patches. This range extends to a range from 0.301 to 1.251 ΔE_{00} if the training subset size is reduced to 1 070 color patches (Figure 24). In conclusion, the performance of a model decreases with the size of the training subset.

3.4 Number and combination of light sources

This test examined the performance of a model depending on the number and different combinations of light sources. Therefore, the RGB triplets (Section 2.4.7) were reduced and recombined. The tested light sources are white (W), a combination of red, green and blue (RGB) and a combination of cyan, magenta and yellow (CMY). Using two complementary colors should, in theory, cover the whole spectrum with no overlaps. That leads to the combination of red and cyan (RC), green and magenta (GM) and blue and yellow (BY). To test if more overlapping colors influence the performance a combination of cyan and yellow (CY) was added. For comparison the best performing

Table 10: The ΔE_{00} statistics of the models trained with different light sources

| Model id	DS	Mean	Median	StD	Min.	Max.	Prob.[0;1[	Prob.[1;2[	Prob.[2;3[
20231027075227	WRGBCMY	0.515	0.461	0.280	0.035	2.246	0.938	0.061	0.001
20231207114655	CMY	0.569	0.502	0.321	0.028	2.213	0.902	0.096	0.004
20231213171513	CY	0.640	0.565	0.367	0.030	3.312	0.853	0.140	0.001
20231212090246	BY	0.660	0.584	0.375	0.044	2.744	0.839	0.154	0.003
20231205190528	RGB	0.669	0.598	0.387	0.025	3.104	0.832	0.159	0.007
20231210141326	GM	0.681	0.612	0.388	0.037	3.887	0.827	0.164	0.007
20231208225150	RC	0.697	0.611	0.401	0.038	3.668	0.814	0.176	0.009
20231203213010	W	0.878	0.749	0.580	0.048	5.265	0.680	0.278	0.035
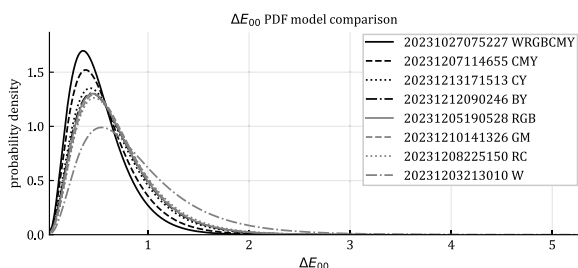
Figure 25: The ΔE_{00} PDFs of the models trained with different light sources

model from Section 3.1 (20231027075227) was used as it combines all seven light sources (WRGBCMY). Therefore, the other models were trained and evaluated using the 'pw' dataset. In Figure 25, the PDF with the highest peak located the furthest left corresponds to the combination of all light sources followed by the PDF of the CMY trained model. It is noticeable, that the PDFs of the models trained with the light source combinations CY, BY, RGB, GM and RC are close to each other whereby the PDF of CY has a slightly higher peak located more left (Figure 25). The PDF with the lowest peak located the furthest right corresponds to the W trained model. The results indicate that the model performance increases with the spectral overlap of the light sources used.

As long as two light sources were used for training the probability that the prediction leads to an error less than 3.0 ΔE_{00} was at least 0.999 (Table 10). If a ΔE_{00} less than 1.0 is needed the probability was at least 0.814 (Table 10). In the case of a single white light source the 3.0 ΔE_{00} probability was 0.993 while the 1.0 ΔE_{00} probability was 0.68 (Table 10). Finally, Figure 26 shows a multispectral image of a print processed by a model of this paper. It has to be mentioned, that the accuracy of this prediction was not tested. This is something to be done in the future.

4. Conclusion

In summary, the results show that a neural network can be used to predict the spectral reflectance of prints with at least acceptable tolerance. In practice it will be useful to have a more generalized network. Therefore, one should gather similar substrates with similar color management settings in groups and train a network for each group. Capturing thousands of color patches takes time (in this paper approximately 3 hours per dataset). If necessary this time can be reduced by reducing the number of light sources and the number of color patches. Reducing the number of color patches and light sources will not
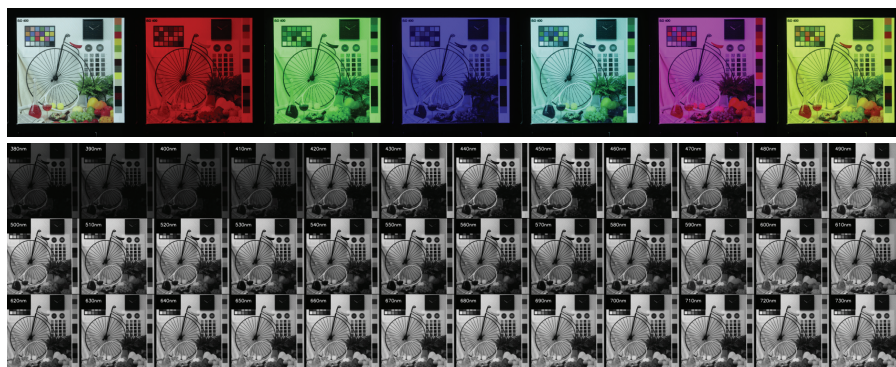

Figure 26: The print illuminated by the seven light sources (top) and the spectral reflectance predicted by the network of this paper (bottom). The printed image is part of the Image Quality Testform Package (Fogra, 2024).

only reduce the time needed for capturing but also the time needed for training. Although the reduction influences the performance negatively, the prediction results still are decent even in the worst scenarios. In fact, one has to find the perfect compromise regarding time and prediction accuracy for each use case. Finally, it should be mentioned that especially the light source has an influence on the research results. In this paper the light source was optimized for 3D scanning. Therefore, optimizing the light source for the purpose to reconstruct spectral reflectance should further improve the performance. Zhang, et al. (2021) identify such optimal projector spectra in a simulated environment.

References

Adobe Inc., 2023. Adobe InDesign (18.1). [computer program] Adobe Inc.. Available at: <https://www.adobe.com/de/products/indesign.html> [Accessed 07 August 2023].

Arad, B., Ben-Shahar, O., Timofte, R., Van Gool, L., Zhang, L., Yang, M. -H., Xiong, Z., Chen, C., Shi, Z., Liu, D., Wu, F., Lanaras, C., Galliani, S., Schindler, K., Stiebel, T., Koppers, S., Seltsam, P., Zhou, R., El Helou, M., Lahoud, F., Shahpaski, M., Zheng, K., Gao, L., Zhang, B., Cui, X., Yu, H., Can, Y. B., Alvarez-Gila, A., van de Weijer, J., Garrote, E., Galdran, A., Sharma, M., Koundinya, S., Upadhyay, A., Manekar, R., Mukhopadhyay, R., Sharma, H., Chaudhury, S., Nagasubramanian, K., Ghosal, S., Singh, A. K., Singh, A., Ganapathysubramanian, B. and Sarkar, S., 2018. NTIRE 2018 Challenge on spectral reconstruction from RGB images. In: *IEEE/CVF Conference on Computer Vision and Pattern Recognition Workshops* (CVPRW). Salt Lake City USA, 18–22 June 2018. https://doi.org/10.1109/CVPRW.2018.00138.

Arad, B., Timofte, R., Ben-Shahar, O., Lin, Y. -T., Finlayson, G., Givati, S., Li, J., Wu, C., Song, R., Li, Y., Liu, F., Lang, Z., Wei, W., Zhang, L., Nie, J., Zhao, Y., Po, L. -M., Yan, Q., Liu, W., Lin, T., Kim, Y., Shin, C., Rho, K., Kim, S., Zhu, Z., Hou, J., Sun, H., Ren, J., Fang, Z., Yan, Y., Peng, H., Chen, X., Zhao, J., Stiebel, T., Koppers, S., Merhof D., Gupta, H., Mitra, K., Fubaram, B.J., Sedky, M., Dyke, D., Banerjee, A., Palrecha, A., Sabarinathan, S., Uma, K., Vinothini, D.S., Sathya Bama, B. and Roomi, S.M.M., 2020. NTIRE 2020 Challenge on Spectral Reconstruction from an RGB Image. In: IEEE, IEEE/CVF Conference on Computer Vision and Pattern Recognition Workshops (CVPRW). Virtual, 14–19 June 2020. https://doi.org/10.1109/CVPRW50498.2020.0023.

Arad, B., Timofte, R., Yahel, R., Morag, N., Bernat, A., Cai, Y., Lin, J., Lin, Z., Wang H., Zhang, Y., Pfister, H., Van Gool, L., Liu, S., Li, Y., Feng, C., Lei, L., Li, J., Du, S., Wu, C., Leng, Y., Song, R., Zhang, M., Song, C., Zhao, S., Lang, Z., Wei, W., Zhang, L., Dian, R., Shan, T., Guo, A., Liu, J., Agarla, M., Bianco, S., Buzzelli, M., Celona, L., Schettini, R., He, J., Xiao, Y., Xiao, J., Yuan, Q., Kwon, T., Ryu, D., Bae, H., Yang, H.-H., Chang, H.-E., Huang, Z.-K., Chen, W.-T., Kuo, S. -Y., Chen, J., Li, H., Sabarinathan, S., Uma, K., Bama, B. S. and Roomi, S.M.M., 2022. NTIRE 2022 Spectral Recovery Challenge and Data Set. In: *IEEE/CVF Conference on Computer Vision and Pattern Recognition Workshops (CVPRW)*. New Orleans USA, 19–24 June 2022. https://doi.org/10.1109/CVPRW56347.2022.00102.

Bradski, G., 2000. The OpenCV Library. Dr. Dobb's Journal of Software Tools. vol. 25, no. 11, pp. 120–125.

Drouin, M. and Beraldin, J., 2020. Active Triangulation 3D Imaging Systems for Industrial Inspection. In: Liu, Y., Pears, N., Rosin, P.L., Huber, P.ed. *3D Imaging, Analysis and Applications*. Cham: Springer International Publishing. https://doi.org/10.1007/978-3-030-44070-1.

International Organization for Standardization. 2020a. *ISO/CIE 11664-1:2019, Colorimetry – Part 1: CIE standard colorimetric observers*. Berlin: Beuth Verlag GmbH.

International Organization for Standardization. 2022a. *ISO/CIE 11664-2:2022, Colorimetry – Part 2: CIE standard illuminants.* Berlin: Beuth Verlag GmbH.

International Organization for Standardization. *2020b. ISO/CIE 11664-3:2019, Colorimetry – Part 3: CIE tristimulus values*. Berlin: Beuth Verlag GmbH.

International Organization for Standardization. 2020c. *ISO/CIE 11664-4:2019, Colorimetry – Part 4: CIE 1976 L*a*b* colour space*. Berlin: Beuth Verlag GmbH.

International Organization for Standardization. 2023. *ISO/CIE DIS 11664-5:2023, Colorimetry – Part 5: CIE 1976 L*u*v* colour space and u', v' uniform chromaticity scale diagram*. Berlin: Beuth Verlag GmbH.

International Organization for Standardization. 2022b. *ISO/CIE 11664-6:2022, Colorimetry – Part 6: CIEDE2000 colour-difference formula.* Berlin: Beuth Verlag GmbH.

Fogra Forschungsinstitut für Medientechnologien e.V., 2024. Image Quality Testform Package [pdf] Fogra Forschungsinstitut für Medientechnologien e.V.. Available at: < https://fogra.org/fileadmin/files/7_downloads/Testformen/ImageQuality_Testforms_2024_Jan.pdf > [Accessed 11 March 2024]

gPhoto - opensource digital camera access and remote control, 2022. gphoto2 (2.5.28). [computer program] Available at: < http://www.gphoto.org/ > [Accessed 08 December 2023].

Harris, C.R., Millman, K.J., van der Walt, S.J., Gommers, R., Virtanen, P., Cournapeau, D., Wieser, E., Taylor, J., Berg, S., Smith, N.J., Kern, R., Picus, M., Hoyer, S., van Kerkwijk, M.H., Brett, M., Haldane, A., Del Río, J.F., Wiebe, M., Peterson,

P., Gérard-Marchant, P., Sheppard, K., Reddy, T., Weckesser, W., Abbasi, H., Gohlke, C. and Oliphant, T.E. 2020, Array programming with NumPy, Nature. [e-journal] vol. 585, no. 7825, pp. 357–362. https://www.doi.org/10.1038/s41586-020-2649-2.

Hunter, J.D. 2007, Matplotlib: A 2D Graphics Environment, Computing in Science & Engineering. [e-journal] vol. 9, no. 3, pp. 90–95. https://www.doi.org/10.1109/MCSE.2007.55.

Kingma, D. P. and Ba, J. 2017, Adam: A Method for Stochastic Optimization [PDF]. https://doi.org/10.48550/arXiv.1412.6980.

Lazar, M., Javoršek, D., i Hladnik, A. 2020, Study of Camera Spectral Reflectance Reconstruction Performance using CPU and GPU Artificial Neural Network Modelling. Tehnički vjesnik. [e-journal] vol.27, no. 4, pp. 1204-1212. https://doi.org/10.17559/TV-20190526202030.

Lazar, M. and Hladnik, A., 2023. Comparison of Artificial Neural Network and Polynomial Approximation Models for Reflectance Spectra Reconstruction. Sensors. [e-joural] vol. 23, no. 2. https://doi.org/10.3390/s23021000.

Mansencal, T., Mauderer, M., Parsons, M., Shaw, N., Wheatley, K., Cooper, S., Vandenberg, J.D., Canavan, L., Crowson, K., Lev, O., Leinweber, K., Sharma, S., Sobotka, T. J., Moritz, Do., Pppp, M., Rane, C., Eswaramoorthy, P., Mertic, J., Pearlstine, B., Leonhardt, M., Niemitalo, O., Szymanski, M., Schambach, M., Huang, S., Wei, M., Joywardhan, N., Wagih, O., Redman, P., Goldstone, J., Hill, S., Smith, J., Savoir, F., Saxena, G., Chopra, S., Sibiryakov, I., Gates, T., Pal, G., Tessore, N., Pierre, A., Thomas, F.-X., Srinivasan, S. and Downs, T., 2022. Colour 0.4.2. https://doi.org/10.5281/zenodo.7367239.

Park, J. -I., Lee, M. -H., Grossberg, M. D. and Nayar, S. K., 2007. Multispectral Imaging Using Multiplexed Illumination. In: IEEE, IEEE 11th International Conference on Computer Vision. Rio de Janeiro, Brazil, 2007, pp. 1-8. https://www.doi.org/10.1109/ICCV.2007.4409090.

Roland Digital Group Corporation 2023, VersaWorks 6 RIP Software (6.17.0). [computer program] Roland Digital Group Corporation Available at: < https://www.rolanddg.eu/de/produkte/software/versaworks-6-rip-software> [Accessed 11 March 2024].

Stacy, E. W. 1962. A Generalization of the Gamma Distribution. The Annals of Mathematical Statistics, vol. 33, no. 3, pp. 1187–1192 [Online]. Available at: <http://www.jstor.org/stable/2237889> [Accessed 11 March 2024]

Virtanen, P., Gommers, R., Oliphant, T.E., Haberland, M., Reddy, T., Cournapeau, D., Burovski, E., Peterson, P., Weckesser, W., Bright, J., van der Walt, S.J., Brett, M., Wilson, J., Millman, K.J., Mayorov, N., Nelson, A.R.J., Jones, E., Kern, R., Larson, E., Carey, C.J., Polat, İ., Feng, Y., Moore, E.W., VanderPlas, J., Laxalde, D., Perktold, J., Cimrman, R., Henriksen, I., Quintero, E.A., Harris, C.R., Archibald, A.M., Ribeiro, A.H., Pedregosa, F. and van Mulbregt, P. 2020, SciPy 1.0: fundamental algorithms for scientific computing in Python, Nature methods. [e-journal] vol. 17, no. 3, pp. 261–272. https://www.doi.org/10.1038/s41592-019-0686-2.

TensorFlow Developers, 2023. TensorFlow. https://doi.org/10.5281/zenodo.8118033

Zhang, J., Meuret, Y., Wang, X. and Smet, K. A. G. 2021, Improved and Robust Spectral Reflectance Estimation. LEUKOS. [e-joural] vol. 17, no. 4, pp. 359–379. https://doi.org/10.1080/15502724.2020.1798246

Zhang, J., Su, R., Fu, Q., Ren, W., Heide, F. and Nie, Y. 2022, A survey on computational spectral reconstruction methods from RGB to hyperspectral imaging. Scientific Reports. vol. 12, no. 1, p. 11905. https://doi.org/10.1038/s41598-022-16223-1

N. Nuwan, M. Shukri and A. Khatibi – J. Print Media Technol. Res. – Vol. 13 No. 2 (2024), 83–95

81

Fostering organisational resilience in print and media industry in Sri Lanka: The role of dynamic capability and strategic orientation

Nalinda Nuwan[1], Mohd Shukri[2] and Ali Khatibi[2]

[1]Office on Missing Persons,   nalinda.n@bms.ac.lk
  No. 40, Buthgamuwa Road, Rajagiriya, Sri Lanka
[2]Graduate School of Management, Management & Science University,
  University Drive, Off Persiaran Olahraga, Section 13, 40100 Shah Alam, Malaysia

Abstract

Organisational resilience has gained significant prominence as a result of unprecedented shocks in the corporate marketplace, where print and media enterprises are particularly vulnerable. Therefore, print and media enterprises are required to develop organisational resilience strategically, focusing on fostering business resilience. In this context, the theory of dynamic capability offers a framework for print and media enterprise leaders to navigate capabilities toward potential opportunities. This research provides an extensive framework to examine the relationship between organisational resilience and dynamic capability. Primary data were gathered from 300 print and media enterprise leaders in Sri Lanka using a structured questionnaire. The data was analysed using SPSS and AMOS. The findings indicate that a well-combined set of dynamic capabilities, centered around seizing new opportunities, has a significant effect on improving company resilience in the PME sector. Moreover, strategic orientation plays a significant role as a mediator between dynamic capability and organisational resilience. A key finding of this study further reveals that company characteristics and market conditions also have a considerable effect on fostering organisational resilience. The study suggests that older print and media enterprises must adopt a more strategic orientation and reforms must be implemented to enhance company resilience in the print and media industry in Sri Lanka.

Keywords: organisational resilience, dynamic capability, strategic orientation, print and media enterprises, business leaders

1. Introduction

Print media is an incredible instrument that works best when combined with other advertising and marketing channels. The success of the advertising sector is strongly dependent on the formulation of strategies and the way they are navigated. Although there has been steady expansion in recent decades, the industry as a whole is facing unprecedented challenges due to alarming technological advancements and market uncertainty. However, organisational resilience (OR) is required to establish a strategic road map in order to effectively manage the obstacles it faces, grasp opportunities for growth and maintain a competitive advantage in the ever-changing advertising landscape. Therefore, the print and media industry needs OR to overcome the challenges it faces and thrive in a continually changing market. Organisational resilience is a multidisciplinary concept with different meanings and aspects depending on context (Duchek and Raetze, 2020; Saad, et al., 2021). Based on prior studies, OR is a capacity that allows businesses to foresee and survive changes by modifying their business processes, making it essential to their long-term viability and success (Granig and Hilgarter, 2020; Kantur and Iseri-Say, 2012). According to Annarelli and Nonino (2016), resilience is an organisational characteristic that is connected to strategic awareness and enables businesses to deal with shocks proactively. Furthermore, OR can assist companies in dealing with disruptive occurrences and expediting recovery (Annarelli and Nonino, 2016). According to Duchek, Raetze and Scheuch (2020), previous research generally examined OR in terms of an organisation's ability to restore itself to its original

condition. However, it is increasingly acknowledged as a dynamic process that requires enterprises to actively engage in controlling disruptions (Duchek, Raetze and Scheuch (2020); Burnard and Bhamra, 2019). Consequently, Linnenlucke, et al. (2011) opines that resilience has two dimensions: the first relates to an organisation's ability to cope with disruptions, while the second refers to its ability to recover and return to its normal condition. Conversely, the idea of resilience is seldom restricted to replication and recuperation, as scholars stress the role of preparation and planning to foster OR (Zighan and Ruel, 2021; Lisdiono, et al., 2022; Iborra, Safón and Dolz, 2020; Sahebjamnia, Torabi and Mansouri, 2015). Considering the preceding perspectives, OR, on the other hand, is distinct from adaptation, agility, flexibility, improvisation, recovery, redundancy and robustness. Resilience is the organisation's reaction to damage, emphasizing the ability to recover and develop in a context of uncertainty, discontinuity and emergency (Xiao and Cao, 2017). According to Xiao and Cao (2017), OR has three specific capabilities:

1) Resilience focuses on survival, adaptation, bounce-back and development in the face of adversity.

2) Resilience is a capability that develops in the face of a discontinuous, evolving internal and external environment.

3) OR is a multi-level concept that includes organisational resources, routines and processes.

In this article, OR is described as an organisation's ability to return to its previous state or to learn a new skill in the face of adversity.

In the light of these concerns, OR is a companies ability to anticipate potentially unfavorable events and resist by adapting possible counter measures and recovering by restoring the organisation or a situation where it bounces back to normalcy (Burnard and Bhamra, 2019; Umoh, Amah and Wokocha, 2013). The ability of companies to absorb shock by developing a resistance mechanism in the face of various disruptions that arise in the corporate context may be a measure of how prepared the organisation is for unanticipated occurrences (Umoh, Amah and Wokocha, 2013; Yuan, et al., 2022). Scholars have long suggested OR should be explored according to the context on which resources and capacity depend (Lengnick-Hall and Beck, 2011;). Nonetheless, OR skills in print and media enterprises (PMEs) have been largely ignored and even fewer studies have been conducted to better understand how strategic decisions contribute to OR in an uncertain economic environment. The environment in which PMEs presently operate is undergoing rapid change and upheaval, which will have an influence on how

these businesses expand and compete. Consequently, PMEs confront significant problems in maintaining competitiveness in volatile market condition due to limited human capital, minimal strategies, organisational and financial resources and skills. On the other hand, PMEs are more adaptable to shifting circumstances than large enterprises (Detarsio, North, and Ormaetxea, 2013; Corvello, et al., 2022). Leaders are overburdened by day-to-day operations and are under pressure to delegate and integrate new avenues (Van Bruysteg, et al., 2008; Fadahunsi, 2022). Limited access to information and markets, insufficient access to skills and technology, insufficient access to finance and poor strategic management direction are key obstacles. In order to meet this issue, some scholars advise that businesses acquire dynamic capability (DC) to renew, reconfigure and adjust existing firm-specific resources in response to the rapidly changing environment (Teece, Pisano and Shuen, 1997). Organisational resilience is a critical component of crisis management and DC also goes hand in hand. The study on the concept and assessment of OR, on the other hand, is still in its early stages. To present, research on OR has given contradicting results, making it impossible to provide clear guidance for business leaders to apply proper strategies. The role of leadership is critical in actively facilitating resilience to manage crises and concentrate on recovery (James, Wooten and Dushek, 2011). However, very limited studies have been conducted on how leaders create strategic resilience (SR) in the print and media industry. Moreover, organisational framework for navigating strategies towards company resilience is also somewhat unclear (Andersson, et al., 2019). In light of the above concern, PME leaders have a bigger role in navigating strategies towards OR. Therefore, it is necessarily worthwhile to study the relationship between DC, strategic orientation (SO) and OR.

2. Theory

According to Annarelli and Nonino (2016), OR may primarily be divided into dynamic resilience and static resilience. Static resilience is about strategic efforts for resilience based on managing internal and external resources, whereas dynamic resilience focuses on DC that enables businesses to manage unanticipated challenges and hazards (Annarelli and Nonino, 2016). The concepts of proactive resilience and reactive resilience coexist with static resilience, dynamic resilience, according to Hall, et al. (2018). According to Somers (2009), proactive resilience refers to purposeful actions that increase the ability to deal with future risks, whereas reactive resilience refers to the organisation's ability to bounce back to its regular condition without suffering significant harm or loss. Pre-disaster environments call for proactive resilience,

whereas post-disaster environments call for reactive resilience (Wildavsky, 1988). According to Somers (2009), proactive and reactive views are frequently used to define and describe OR. These perspectives are more relevant from a practical standpoint and are frequently employed in various research (e.g. Bode and Macdonald, 2016; Lengnick-Hall and Beck, 2011; Linnenluecke, et al., 2012; McManus, et al., 2008; Sawalha, 2015; Fadahunsi, 2022; Seville el at., 2008). In addition, Linnenluecke, Griffiths and Winn (2012) argued that it is critical to include both viewpoints on OR in a single research on OR since it can provide light on how the two forms of OR interact to one another in various fields or circumstances. In this study, proactive OR and reactive OR are the two ways that OR is characterized.

Dynamic capability and OR are interconnected concepts that have their roots in several theories and have gained significance throughout the last decades. The two most well-known theories in strategic and operational management are the subject of this study. An explanation of how businesses adjust to quickly changing setting is given by the DC and OR viewpoints (Siguaw, Simpson and Enz, 2006). According to Pavlou and El Sawy (2011), the boundary conditions of the constructs have come under greater examination from strategy and management researchers. This is especially true when it comes to print and media context as the leaders of PMEs have to navigate the right balance of strategies in accordance with company characteristic and market condition in particular when the market is highly uncertain. Similarly, to how the alignment of DC and OR is critical for survival in turbulent environments (as the level of turbulence increases, more of these capabilities are required), the planning and strategy associated with such implementation must be considered.

When opportunities are recognized, PME leaders need to gain advantage by reconfiguring the resources in the company when the market and/or technology inevitably undergo another transformation (Teece, Pisano and Shuen, 1997). This is the foundation of the DC, which goes hand in hand with PME sector resilience. Numerous researches conducted in western and European Nations have revealed significant correlations between DC and adaptability as a metric for OR. Itkien, et al. (2015), focused their research on Slovenian service companies in order to study the impact of DCs on service innovation. They used a comparative analysis study design to acquire data from existing literature (secondary data). They found that DCs are critical for service-oriented organisations because they allow companies to detect market opportunities and customer requirements to foster OR, act on those possibilities by arranging existing resources and gain a competitive market advantage in the long run. Furthermore, Morales, et al. (2019) stated that OR is heavily reliant on leaders' ability and capability to develop effective responses and achieve satisfactory recovery to crises caused by disruptive events and DC co-exists with the perspectives of proactive resilience and reactive resilience. Manfield and Newey (2018) define resilience as a portfolio of skills that includes diverse capability responses to various threats, disorder and direction (bounce-back or bounce-forward). Various capacities created by leaders to promote OR have been studied in various studies. Organisational resilience is derived from organisational skills (Douglas, 2021) and is linked to managerial procedures of efficiently managing and distributing primary resources through DC (Weaven, et al., 2021; Barghersad and Zobel, 2021). Furthermore, recognizing valued resources and competencies is critical for an organisation to work towards and respond to disruptions proactively (Sullivan-Taylor and Branicki, 2011; Jia, et al., 2020). Additionally, when the leaders of organisations navigate DC, well-established activities across departments and management competence can aid in mitigating disruptive occurrences (Paul, Parthasarathy and Gupta, 2017). It is important to highlight that large enterprises frequently have more capacity to respond to and recover from disruptive events since they have access to more resources (Barghersad and Zobel, 2021). However, PMEs are often less efficient in terms of OR than large enterprises due to possible resource and capacity limits (Sullivan-Taylor and Branicki, 2011). Therefore, developing a DC is especially vital for PME sector companies in emerging nations, given their tumultuous and unusual settings. Despite increased interest in the dynamic capacity viewpoint, most studies remain theoretical and conceptual and additional empirical research is needed to explore and validate this approach (Levin, 2006). As a result, conversations about how organisations generate DC remain under-developed. Therefore, SO as a mediator may give a source that helps organisations establish DC in rapidly changing contexts to foster long-term resilience.

Strategic orientation refers to the processes, practices, principles and decision-making styles that guide enterprises' activities, particularly in the context of the external environment and corporate development, to significantly influence competitive advantage and OR (Jantunen, et al., 2008; Crovini, Santoro and Ossola, 2021). Companies must actively monitor their rivals in a highly competitive market to grasp their relative position in the market in comparison to that of rivals (Han, Kim and Srivas, 1998; Al-Kwifi, Farha and Zaraket, 2020). In this light, the SO is a key factor that plays a significant role between DC and OR in exceptional performance in developing econo-

mies. Strategic orientation is concerned with how businesses should connect with their external surroundings, such as clients, rivals and technology (Day, 1994; Gatignon and Xuereb, 1997; Lin and Kunnathur, 2019). Once opportunities are identified, it is crucial to assess how well the external environment and strategic choices align from an external perspective. Dynamic capability, on the other hand, provides a deeper understanding on how to combine and reenergize corporate resources and capabilities in a new manner. Organisational resilience is defined by Annarelli and Nonino (2016) and Annarelli, Battistella and Nonino,(2020) as the company's ability to survive disruptions and unanticipated changes based on its strategic awareness and cooperation between internal and external capabilities. Despite the variety of resilience measures, adaptability and agility are recognized as determinants of SO and used in this study as the indicators of OR. In order to develop DCs, companies should acquire, allocate and use resources according to their strategic direction. Therefore, combining these two techniques offer fresh perspectives on how SO influences internal processes like resource reconfiguration and modification. However, existing literature does not address the significance of SO and DC in establishing OR amid economic uncertainty when PMEs are considered, indicating a large study vacuum. In order to address these research gaps, this article examines the effects of DC on SOs in the context of PMEs of Sri Lanka by focusing particularly on company characters and market situation to foster OR.

3. Methods

A framework for this study was set up and offered as the overall research plan in order to achieve the primary goal of our investigation. Accordingly, the overall research design process consisted of four steps, including the identification of primary data sources, data collection and data analysis. Sri Lanka lacks an established and up-to-date PME list in terms of the identification of the right PMs for this research. The

Ministry of Industries and the Chamber of Commerce, however, have different lists of PMEs. Consequently, companies that fall under PME were carefully selected and entered into one database by removing some multiple entries and this final list ended up with 1 438 PMEs for the study as the target audience. In the literature, the response rate was 35 % and 857 questionnaires were distributed among PME leaders to select 300 responses. Literature further highlighted that common method variance (CMV) is one of the key issues that need to be managed in terms of achieving high accuracy of raw data. In terms of avoiding CMV problems, however, one tactic is to gather data from several sources within the same organisation (Wall and Wood, 2005). More precisely, this involves choosing multiple key informants who respond to questions that better suit their areas of expertise or about which they are more knowledgeable (Huselid and Becker, 2000). To increase our understanding of the causes of OR, this study therefore proposes a multiple-key informant method for data collection. Accordingly, the owner of each PME unit was contacted by phone and explained the primary objective of the survey. In this process, in addition to the owner manager of PME unit, one of the leaders from this category was asked to be nominated, such as the CEO, Managing Director, Director, Finance Manager and Accountant. Based on the sample size calculation, a simple random sampling process was used to select 150 PMEs and 300 PME leaders from a newly created list. Accordingly, the illustration in Figure 1 describes the whole identifying procedure.

The primary data was gathered through an online survey approach with a 43 items structured questionnaire that was circulated to PME leaders via Google Forms. Items for every construct were also adapted from previous research. The conceptual framework in Figure 2, which includes three exogenous factors, two mediating variables and one dependent variable, was developed in accordance with theory and literature to achieve the study's ultimate purpose. These mediating variables are favored by OR, which focuses
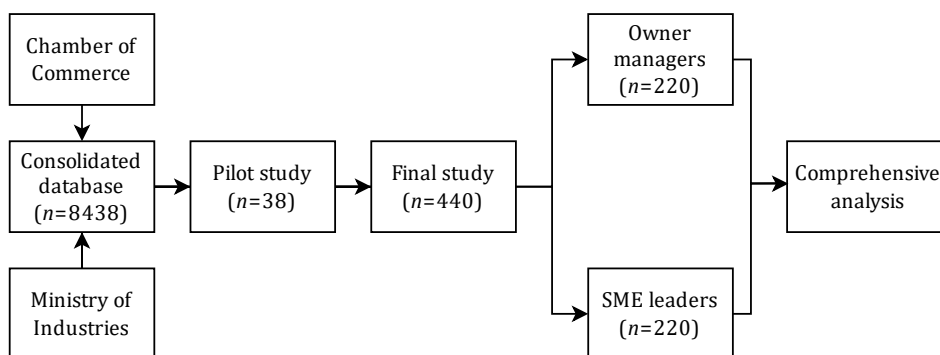

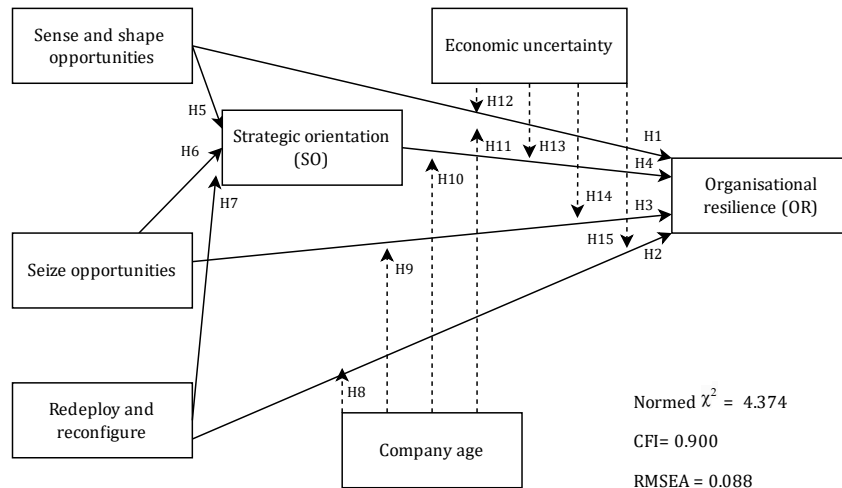*Figure 1: Summary of identification procedure*

Figure 2: Conceptual framework

on enhancing firms' capacity to identify and reconfigure the need for responding to changing environmental situations. Organisational resilience is a significant factor in helping firms deal with SO of the firm and that goes hand in hand with characteristics of the firm and market situation (Lengnick-Hall and Beck, 2011; Teece, 2020). The following conceptual framework was constructed in line with the theory and the literature including three independent variables, one mediating variable and two moderating variables to achieve the overall objective of the study.

3.1 Hypotheses

In line with the objectives and above conceptual frame (Figure 2), the following hypotheses were formulated.

H1: Sensing and shaping opportunities has significant positive effect on OR.

H2: Seizing opportunities has significant positive effect on OR.

H3: Redeploying and reconfigure has significant positive effect on OR.

H4: Strategic orientation has significant positive effect on OR.

H5: Strategic orientation mediates the relationship between sensing and shaping opportunities and OR.

H6: Strategic orientation mediates the relationship between seize opportunities and OR.

H7: Strategic orientation mediates the relationship between reconfiguring opportunities and OR.

H8: Company age moderates the relationship between sensing and shaping opportunities and OR.

H9: Company age moderates the relationship between seizing opportunities and OR.

H10: Company age moderates the relationship between SO and OR.

H11: Company age moderates the relationship between redeploying and reconfiguring opportunities and OR.

H12: Economic uncertainty moderates the relationship between sensing and shaping opportunities and OR.

H13: Economic uncertainty moderates the relationship between SO and OR.

H14: Economic uncertainty moderates the relationship between seizing opportunities and OR.

H15: Economic uncertainty moderates the relationship between redeploying and reconfiguring opportunities and OR.

3.2 Data analysis

Data analysis process in this study was performed in three steps: In step (1), a preliminary analysis of the scale was performed by exploratory factor analysis (EFA) using maximum likelihood and varimax rotation through SPSS. In step (2), further validating the factor structure, which was the output of EFA sent to CFA conducted through AMOS. Step (3) was performed in order to test the hypotheses by assessing the structural model related to OR using AMOS. Accordingly, the results of EFA analysis are provided in Table 1.

Table 1: Exploratory factor analysis results

Kaiser-Meyer-Olkin measure of sampling adequacy.		0.843
Bartlett's test of sphericity	Approx. chi-square	3607.237
	Degrees of freedom	120
	P	0.000

4. Results

Based on the results of EFA analysis presented in Table 1, the Kaiser-Meyer-Olkin value exceeded 0.50, indicating that the sampling adequacy criteria were met. The Bartlett's test of sphericity was statistically significant ($P < 0.05$), suggesting that the correlation matrix significantly differs from an identity matrix, as expected. Consequently, the components were classified into eight categories, as outlined in Appendix 1. The results of the EFA confirmed an eight-factor solution, with all items loading above 0.5 on their respective factors. This solution accounted for 75.4 % of the total variance. The EFA findings demonstrated a high level of factor validity. To further validate these findings, a CFA was conducted.

The initial CFA model, shown in Figure 3, provided a graphical representation of the factors. The CFA results confirmed that the factors exhibit a high degree of validity. Additionally, further tests were carried out to assess reliability, convergent validity and discriminant validity. Based on the results in Table 2, the fit indices demonstrate that the model shows a good fit, with strong validity and reliability. The fit statistics include X^2 (chi-squared test), df (degrees of freedom), RMSEA (root mean square error of approximation), SRMR (standardized root mean square residual), GFI (goodness of fit) and CFI (comparative fit index). The accepted and recommended values based on the suggestions of Hu and Bentler (1999); Browne and Cudeck (1992); Cline, Huckaby and Zullo, (2023) are as follows: $X^2 / df < 5$, RMSEA < 0.08, SRMR < 0.05, CFI > 0.90,). All items standardized factor loadings were above 0.60 and AVE (average variance extracted) was is also above 0.50.

Therefore, it is a valid indication of good convergent validity. Another evidence of convergent validity is that the maximum shared variance was less than the respective average variance extracted for all dimensions. The Cronbach alpha and composite reliability for all constructs were above 0.70. Hence the results of the study can be established that the considered constructs have good reliability. However, testing
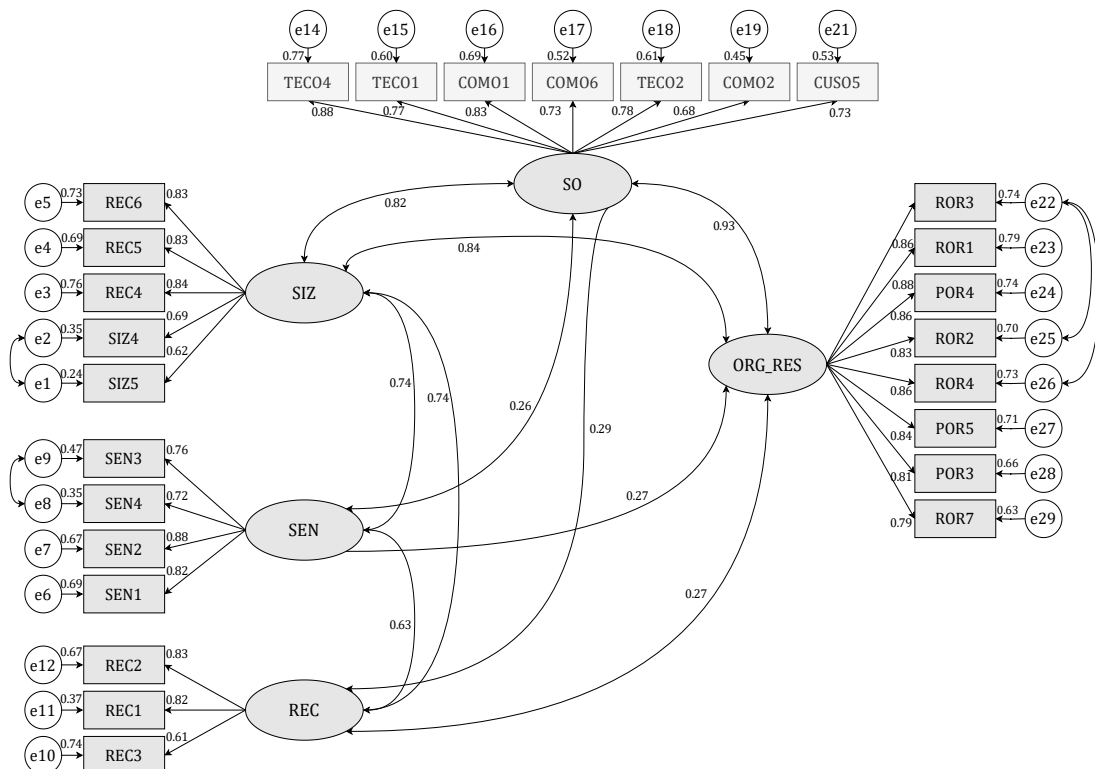

Figure 3: Confirmatory factor analysis model

Table 2: Reliability and convergent validity

Variables	Items	Standardized factor loadings	Cronbach alpha	Composite reliability	Average variance extracted	Maximum shared variance
Sense and shape opportunities	SEN5	0.534				
	SEN4	0.715				
	SEN1	0.815	0.88	0.719	0.632	0.168
	SEN3	0.757				
	SEN2	0.875				
Redeploy and reconfigure	REC3	0.609				
	REC2	0.829	0.792	0.708	0.524	0.128
	REC1	0.82				
Seize opportunities	SIZ4	0.688				
	REC5	0.834				
	REC6	0.832	0.879	0.729	0.693	0.356
	REC4	0.839				
	SIZ5	0.622				
	SEN6	0.687				
Strategic orientation	TECO4	0.877				
	TECO1	0.773				
	COMO1	0.834				
	COMO6	0.725	0.918	0.796	0.615	0.356
	TECO2	0.776				
	COMO2	0.682				
	CUSO5	0.725				
Organisational resilience	ROR3	0.863				
	ROR1	0.888				
	POR4	0.861				
	ROR2	0.827	0.953	0.893	0.683	0.168
	ROR4	0.858				
	POR5	0.843				
	POR3	0.814				
	ROR7	0.787				

Model fitness: $\chi^2 = 1342.822$; df = 307; χ^2 / df = 4.374; RMSEA = 0.088; SRMR = 0.0447; GFI = 0.826; CFI = 0.904

Table 3: Discriminant validity

	Sense and shape opportunities	Redeploy and reconfigure	Seize opportunities	Strategic orientation	Organisational resilience
Sense and shape opportunities	0.795				
Redeploy and reconfigure	0.358	0.731			
Seize opportunities	0.340	0.296	0.832		
Strategic orientation	0.410	0.305	0.400	0.827	
Organisational resilience	0.284	0.146	0.597	0.319	0.785

discriminant validity was also required in this process. Based on the analysis of Table 3, the Fornell and Larcker (1981) criteria were used in terms of testing discriminant validity. The values in the diagonal were square root of AVE and other values were inter-variable correlation. The basic requirement was that the diagonal bold values should be higher than other values in its respective row and column, which was met as can be seen in the Table 3. Thus, it can be confirmed that the considered variables have good discriminant validity as well. In addition to the Fornell and Larcker test, the HTMT ratio (heterotrait-monotrait ratio of correlations) was also tested and all values were lower than 0.85. Accordingly, the model has met all criteria required for the reliability and validity of the model.
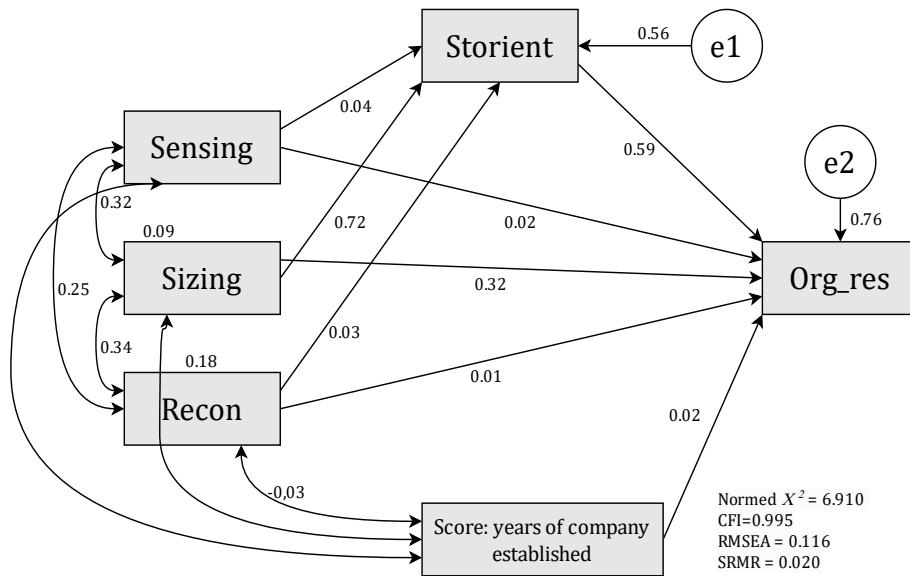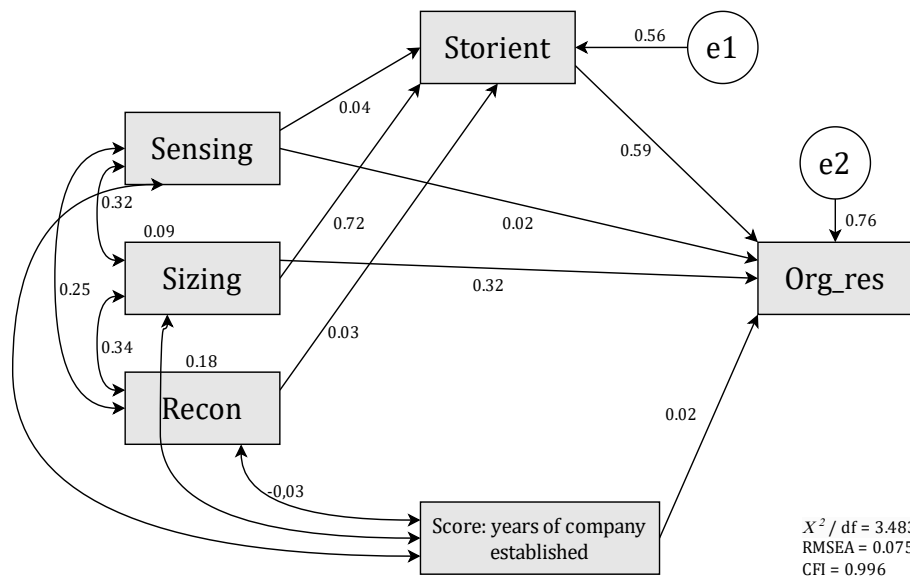
Figure 4: Proposed structural model

Figure 5: Tested structural model

Table 4: Hypothesis testing

H. No.	Paths	Estimate	S.E.	C.R.	P	Remarks
H1	Sensing and shaping → Organisational resilience	0.015	0.023	0.653	0.514	Not supported
H2	Seizing and shaping → Organisational resilience	0.362	0.041	8.925	0.000	Supported
H3	Redeploying and reconfiguring → Organisational resilience	0.027	0.031	0.868	0.386	Not supported
H4	Strategic orientation → Organisational resilience	0.578	0.034	16.794	0.001	Supported

Model fitness: X^2 = 6.9, df = 2, X^2 / df = 3.48, RMSEA = 0.075, SRMR = 0.026, GFI = 0.995, CFI = 0.996

S.E. = standardized estimate, C.R. = critical rate, *P* as used above

Table 5: Mediation analysis

H.No	Relationship	Direct effect	Indirect effect	Confidence interval		P	Conclusion
				Lower bond	Upper bond		
H5	Sense and shape opportunities → Strategic orientation → Organisational resilience	0.028	0.0456	−0.014	0.133	0.325	No mediation effect – not supported
H6	Seize opportunities → Strategic orientation → Organisational resilience	0.252	0.8207	0.581	0.985	0.000	Partial mediation – supported
H7	Redeploy and reconfigure → Strategic rientation → Organisational resilience	-0,030	0.0152	−0.047	0.086	0.258	No mediation effect – not supported

5. Analysis of the structural model

In order to study the relationship between DC, SO and OR the structural equation modeling was used by means of AMOS path analysis by imputing the factor score from CFA. The graphical representation of the structural model is represented in Figure 4. Results indicated a good fit for the model presented including RMR (root mean square residual) of 0.026, GFI of 0.970 and CFI of 0.995. However, the RMSEA failed to achieve the desired values as RMSEA should be less than 0.08 to achieve model fitness. Moreover, the χ^2 / df value was also above 5. Therefore, the proposed model was retested after removing the diagonal relationship between redeploying and reconfiguring and OR. Accordingly, the results indicate that by the new model, OR in print and media sector is 76 % explained by the factors of DC and SO, which means that the new model is successful and applicable for hypothesis testing. However, the model was further modified as per the scheme in Figure 5. Results related to the newly tested model (Figure 5)

indicated a good fit for the model presented including SRMR of 0.026, GFI of 0.995 and CFI of 0.996. Further, the generalizability of the model indicates a RMSEA of 0.075 and a χ^2 / df value of 3.48, which achieved the high level of model fitness. Accordingly, hypotheses were tested as shown in Table 4.

Hypotheses resulting based on path analysis (Table 4) showed that seizing opportunity is positively and significantly associated with OR ($\beta = 0.362$, P < 0.05) which means that seizing new opportunities in print and media industry leads to foster OR. Moreover, SO is also positively and significantly associated with OR ($\beta = 0.578$, P < 0.05). In other words, a good combination of customer orientation, competitor orientation and technology orientation enhances the resiliency of PMEs. However, other two constructs (sensing and shaping and redeploying and reconfiguring) are insignificantly associated with OR. Based on these results, alternative hypothesis was accepted for H2 and H4 and null hypothesis was accepted for H1 and H3.

Table 6: Moderation testing

H. No.	Moderating effect	Estimate	S.E.	C.R.	P	Remarks
H8	Interaction sensing and shaping * company age → OR	.025	.026	.967	.334	Not Supported
H9	Interaction seizing opportunities * company age → OR	.001	.022	1.97	.002	Supported
H10	Interaction SO * company age → OR	.059	.024	2.477	.013	Supported
H11	Interaction reconfiguring oppotunities * company age → OR	.003	.026	.117	.907	Not Supported
H12	Interaction sensing and shaping * economic uncertainity → OR	-.002	.025	-.087	.930	Not Supported
H13	Interaction SO * economic uncertainty → OR	.848	.038	22.202	.000	Supported
H14	Interaction seizing opportunities * economic uncertainty → OR	-.031	.025	-1.979	.000	Supported
H15	Interaction redeploying and reconfiguring * economic uncertainty → OR	0.030	0.026	1.150	0.250	Not supported

5.1 The role of strategic orientation between dynamic capabilities and organizational resilience

The mediation analysis was performed by treating three meta capabilities of dynamic capability as independent variables, OR as dependent variable and SO as mediator. The mediation analysis was based on the analysis of indirect effects based on the guideline by Baron and Kenny (1986) classical approach. Accordingly, mediation analysis was tested by using the direct and indirect effects based on bootstrap procedures (500 samples) and bias-corrected bootstrap confidence interval (95 %). The results are provided in the Table 5.

In accordance with the results shown in Table 5, it becomes visible that SO is partially mediating the relationship between seizing opportunity and OR as indirect effects are statistically significant ($\beta = 0.82$, $P < 0.05$), which means that PME resilience is possible to achieve by seizing opportunities at the right time through SO. Based on these results, alternative hypothesis was accepted only for H6 and null hypothesis was accepted for other hypotheses H5 and H7.

5.2 Analysis of company age and economic uncertainty as moderators

The moderation analysis was performed by treating sensing and shaping, seizing and redeploying and reconfiguring as independent variables, OR as dependent variable and company age and economic uncertainty as moderator variables. The results were calculated by creating interaction terms from standardized score of variables using SPSS.

In this study, two moderating effects (company age and economic uncertainty) were tested with DC and OR. According to Table 6, the analysis suggests that the company's growth strengthens the positive relationship between size and opportunities (OR), indicating that as the company matures, it must seize new opportunities. Moreover, findings reveal that economic uncertainty strengthens the positive relationship between seizing
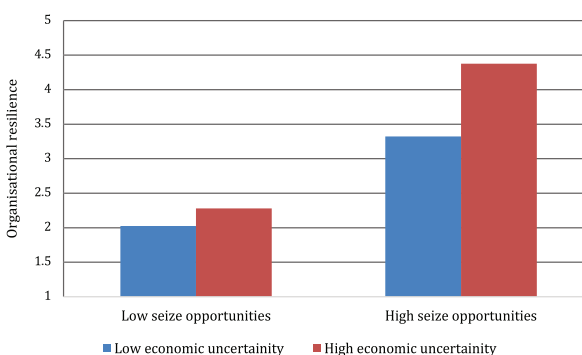
opportunities and OR. The graphical representation of both impacts is provided in Figures 6 and 7.

Analysis of Figures 6 and 7 highlights that the age of the company and economic uncertainty both strengthen the relationship between SO and OR. In other words, SO is mostly required for older PMEs. Accordingly, alternative hypotheses were accepted for H9, H10, H13 and H14, which indicate that there was statistical support for the moderating role of company age and economic uncertainty on seizing opportunity, SO and OR.

6. Discussion and implications

The results demonstrated show that a good combination of DCs (sensing and shaping, seizing and redeploying and reconfiguring capabilities) centered around seizing new opportunities have a significant effect on improving the degree of company resilience among PME sector organisations. Moreover, SO plays a significant role as a mediator in between DC and OR. The key finding of this study further revealed that company characteristics and market condition also have a considerable effect in terms of fostering OR. Similarly when it comes to literature, Kanten, et al. (2017), used a structural equation model to analyze data from 176 employees in order to investigate the impact of dynamic capability on organisational agility in the Turkish retail sector. The analysis's conclusion showed that the merchants' agility is favorably and strongly influenced by the dynamic capacity characteristics. Additionally, Kanten, et al. (2017) pointed out that in order to foster a companies agility in a quickly evolving business environment with a high degree of uncertainty, DC of detecting, seizing and transforming must be strategically wedded with the companies strategy. The impact of DC on service innovation was also examined by Žitkienė, Kazlauskienė and Deksnys (2015), who concentrated their study on Slovenian service companies. They concluded that DCs are crucial for service-oriented businesses because they
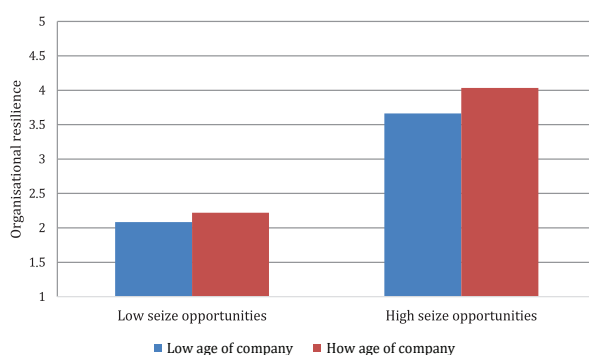

Figure 6: Company age moderates OR and seizing.

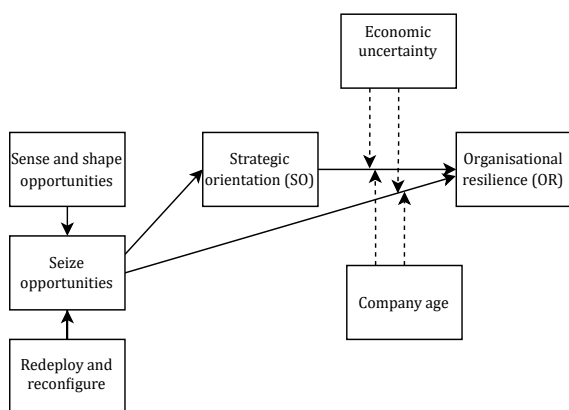*Figure 7: EU moderates OR and seizing.*

Figure 8: The identified model

enable them to recognize market opportunities and customer needs, seize those opportunities by allocating available resources and gain a competitive edge in the process of company resilience. However, these findings lack clarity on the overall integration of DCs with SO considering the market situation and company characteristics.

The findings of this study articulate several remarkable additions to OR, thus contributing to theory and practice. From the theoretical point of view, this study makes the following contributions. To begin with, this is among the pioneer studies that contribute to the scant research on exploring OR in the field of PMEs in Sri Lanka. In contrast to prior research exploring OR in large and longer-established companies such as multinational enterprises (e.g. Pereira, et al., 2018), the contribution of this research focuses on PME sector, which aims to exploit new ventures in order to survive in the market. This is particularly crucial for service and manufacturing PMEs since they have a high degree of restrictions, such as limited resources as well as capabilities and knowledge that make them fragile in competitive and uncertain markets (Ratten, Ferreira and Fernandes, 2016; Sadeghi and Biancone, 2018; Sukumar, et al., 2020), whereas SO needs to mediate them in order to foster OR in the long run.

Furthermore, findings elaborate that OR is not a stand-alone characteristic but seizes opportunity with the other set of two capabilities that help PMEs remain in the competitive market. Through the lens of DC, the study's findings contribute to existing research by exploring and evaluating three meta-capabilities, along with SO, which address company characteristics and market conditions.Accordingly, the framework shown in Figure 8 was identified and proposed for PME sector particularly in times of economic uncertainty.

Moreover, in relation to the practical implications, the findings of this study highlighted that PMEs need to leverage DC and SO at a more strategic level considering internal and external resources. When the companies are small-scale, inherent resources are also limited, the new market is highly volatile and unknown, SO can enable them to survive in the market (Hagen, Zucchella and Ghauri, 2019). The findings further highlighted that identifying and seizing long-term new business opportunities and seeking survival and growth in uncertain markets paves the way to foster resiliency. Given the ever-changing and dynamic business environment, organizations are continually presented with unanticipated disruptions and problems. As a result of limited resources and a limited capacity to plan for crisis occurrences, PMEs are more exposed to external shocks than larger organizations. As a result, PME leaders have to establish a high degree of OR skills to deal with any future shocks. In this case, being strategically oriented allows PMEs to start with a new concept, test it and monitor competitors activities to make quick decisions to seize untapped opportunities. In this regard, the findings of this study imply that such PME leaders have to extend their present activities while also implementing essential creative efforts in their business processes. As a result, leaders of PMEs can use the most recent techniques as a short-term solution or expand on their R&D operations, which contribute to long-term benefits. Moreover, the findings, on the other hand, emphasize that PME leaders may utilize new knowledge and opportunities to foster resilience.

7. Conclusion

This study empirically demonstrates that dynamic capability, including sensing and shaping, seizing and redeploying and reconfiguring capabilities, significantly enhance the resilience of print media enterprises. Strategic orientation particularly in times of economic uncertain plays a significant role in terms of fostering long term resilience however age of the company also needs to be well considered. The findings concluded that a well-balanced dynamic capability is essential and PME leaders, in particular, have to seize new opportunities in terms of specialized competencies and expertise related to the business process in order to achieve organisational resilience. The findings also revealed that strategic orientation has a crucial role in the relationship between dynamic capability and organisational resilience during highly uncertain economic situations, that older companies (PMEs) have to be more strategically oriented and that reforms must be made in order to build resilience in print media enterprises sector in

Sri Lanka. However, the reconfiguration process or sensing process cannot be done to achieve organisational resilience without the support of strategic orientation. Accordingly, the following three conclusions can be derived:

1) Seizing opportunity is the most important pillar of dynamic capability mobilization of resources to fulfill demands and opportunities, while the other two capacities are interconnected, creating absorptive capacity in the PME sector in times of economic uncertainty.

2) The involvement of strategic orientation is highly essential in PME sector in fostering organisational resilience.

3) Young companies are more prone to adapting strategic orientation quickly than older firms. Therefore, adaptation of strategic orientation is required for matured PMEs.

Findings elaborated that organisational resilience is not a stand-alone characteristic but seizing opportunity with the other set of two capabilities of dynamic capability that help PMEs remain in the competitive market. Hence, through the lens of dynamic capability, the findings of the study enrich the extant research by exploring and evaluating three meta capabilities along with strategic orientation that deal with firm characteristics and market conditions. Accordingly, a newly tested framework (Figure 8) identified and proposed for PME sector particularly in times of economic uncertainty.

8. Recommendations

The findings of the study yield to the following recommendations:

1) Leaders of print media enterprises need to take efforts to strengthen their ability to anticipate probable changes in the highly unpredictable environment. Therefore, leaders have to plan and alter their internal processes to adapt to new changes in terms of building long term resilience.

2) Leaders of print media enterprises in Sri Lanka need to strategically seize new opportunities and capabilities to be more competitive in order to find and gain external information about their market, technology and industry. This will allow print media enterprises to adjust to economic uncertainty swiftly, in keeping with their age and to survive in the market in the long run.

3) Strategic orientation should be well adopted by PME leaders to successfully combine new externally sourced capabilities with current internal capabilities into creative combinations. This will result in mature company seizing untapped opportunities and improved business processes, as well as the company's resilience.

4) Leaders of print media enterprises should monitor potential changes in consumer demands and preferences in order to respond quickly and foster resilience by adjusting procedures to meet the needs of customers, competitors and technology. Therefore, leaders of print media enterprises have a very crucial role to play in seizing the right opportunities at the right time.

References

Al-Kwifi, O.S., Farha, A.K.A. and Zaraket, W.S., 2020. Competitive dynamics between multinational companies and local rivals in emerging markets. *FIIB Business Review*, 9(3), pp. 189–204. https://doi.org/10.1177/2319714520939673.

Andersson, T., Cäker, M., Tengblad, S. and Wickelgren, M., 2019. Building traits for organizational resilience through balancing organizational structures. *Scandinavian Journal of Management*, 35(1), pp. 36–45. https://doi.org/10.1016/j.scaman.2019.01.001.

Annarelli, A. and Nonino, F., 2016. Strategic and operational management of organizational resilience: Current state of research and future directions. *Omega*, 62, pp. 1–18. https://doi.org/10.1016/j.omega.2015.08.004.

Annarelli, A., Battistella, C. and Nonino, F., 2020. Competitive advantage implication of different product service system business models: Consequences of 'not-replicable' capabilities. *Journal of Cleaner Production*, 247: 119121. https://doi.org/10.1016/j.jclepro.2019.119121.

Baghersad, M. and Zobel, C.W., 2021. Organizational resilience to disruption risks: Developing metrics and testing effectiveness of operational strategies. *Risk Analysis,* 42(3), pp. 561–579. https://doi.org/10.1111/risa.13769.

Baron, R.M. and Kenny, D.A., 1986. The moderator–mediator variable distinction in social psychological research: Conceptual, strategic and statistical considerations. *Journal of Personality and Social Psychology,* 51(6), pp.1173–1182. https://doi.org/10.1037/0022-3514.51.6.1173.

Burnard, K.J. and Bhamra, R., 2019. Challenges for organisational resilience. *Continuity & Resilience Review*, 1(1), pp. 17–25. https://doi.org/10.1108/CRR-01-2019-0008.

Corvello, V., Verteramo, S., Nocella, I. and Ammirato, S., 2022. Thrive during a crisis: The role of digital technologies in fostering antifragility in small and medium–sized enterprises. *Journal of Ambient Intelligence and Humanized Computing*, pp. 1–13. https://doi.org/10.1007/s12652-022-03816-x.

Day, G.S., 1994. The capabilities of market–driven organizations. *Journal of Marketing*, 58(4), pp. 37–52. https://doi.org/10.1177/002224299405800404.

Detarsio, R., North, K. and Ormaetxea, M., 2013. Sobrevivir y competir en tiempos de crisis: Casos de estrategias de PYMES argentinas. *Economía Industrial*, 388, pp. 145–154.

Douglas, S., 2021. Building organizational resilience through human capital management strategy. *Development and Learning in Organizations*, 35(5), pp. 19–21. https://doi.org/10.1108/dlo-08-2020-0180.

Duchek, S., Raetze, S. and Scheuch, I., 2020. The role of diversity in organizational resilience: A theoretical framework. *Business Research*, 13(2), pp. 387–423. https://doi.org/10.1007/s40685-019-0084-8.

Fadahunsi, O.A., 2022. Strategies for reducing employee turnover in small and medium enterprises. Doctoral dissertation, Walden University. https://scholarworks.waldenu.edu/dissertations/13344.

Gatignon, H. and Xuereb, J.M., 1997. Strategic orientation of the firm and new product performance. *Journal of Marketing Research*, 34(1), pp. 77–90. https://doi.org/10.1177/002224379703400107.

Granig, P. and Hilgarter, K., 2020. Organisational resilience: A qualitative study about how organisations handle trends and their effects on business models from experts' views. *International Journal of Innovation Science*, 12(5), pp. 525–544. https://doi.org/10.1108/ijis-06-2020-0086.

Hagen, B., Zucchella, A. and Ghauri, P.N., 2019. From fragile to agile: Marketing as a key driver of entrepreneurial internationalization. *International Marketing Review*, 36(2), pp. 260–288. https://doi.org/10.1108/IMR-01-2018-0023.

Han, J.K., Kim, N. and Srivastava, R.K., 1998. Market orientation and organizational performance: Is innovation a missing link? *Journal of Marketing*, 62(4), pp. 30–45.

Iborra, M., Safón, V. and Dolz, C., 2020. What explains the resilience of SMEs? Ambidexterity capability and strategic consistency. *Long Range Planning*, 53(6), p: 101947. https://doi.org/10.1016/j.lrp.2019.101947.

James, E.H., Wooten, L.P. and Dushek, K., 2011. Crisis management: Informing a new leadership research agenda. *Academy of Management Annals*, 5(1), pp. 455–493. https://doi.org/10.1080/19416520.2011.589594.

Jia, X., Chowdhury, M., Prayag, G. and Chowdhury, M.M.H., 2020. The role of social capital on proactive and reactive resilience of organizations post–disaster. *International Journal of Disaster Risk Reduction*, 48, p: 101614. https://doi.org/10.1016/j.ijdrr.2020.101614.

Kanten, P., Kanten, S., Keceli, M. and Zaimoglu, Z., 2017. The antecedents of organizational agility: Organizational structure, dynamic capabilities and customer orientation. *PressAcademia Procedia*, 3(1), pp. 697–706.

Kantur, D. and Iseri-Say, A., 2012. Organizational resilience: A conceptual integrative framework. *Journal of Management and Organization*, 18(6), pp. 762–773. https://doi.org/10.1017/S1833367200000420.

Lavie, D., 2006. Capability reconfiguration: An analysis of incumbent responses to technological change. *Academy of Management Review*, 31(1), pp. 153–174.

Lengnick-Hall, C.A., Beck, T.E. and Lengnick-Hall, M.L., 2011. Developing a capacity for organizational resilience through strategic human resource management. *Human Resource Management Review*, 21(3), pp. 243–255. https://doi.org/10.1016/j.hrmr.2010.07.001.

Levin, K.A., 2006. Study design III: Cross–sectional studies. *Evidence–Based Dentistry*, 7(1), pp. 24–25. https://doi.org/10.1038/sj.ebd.6400375.

Lin, C. and Kunnathur, A., 2019. Strategic orientations, developmental culture and big data capability. *Journal of Business Research*, 105, pp. 49–60. https://doi.org/10.1016/j.jbusres.2019.08.036.

Linnenluecke, M.K., Griffiths, A. and Winn, M., 2011. Extreme weather events and the critical importance of anticipatory adaptation and organizational resilience in responding to impacts. *Business Strategy and the Environment*, 21(1), pp. 17–32. https://doi.org/10.1002/bse.708.

Lisdiono, P., Said, J., Yusoff, H. and Hermawan, A.A., 2022. Examining leadership capabilities, risk management practices and organizational resilience: The case of state-owned enterprises in Indonesia. *Sustainability*, 14(10): 6268. https://doi.org/10.3390/su14106268.

McManus, S., Seville, E., Vargo, J. and Brunsdon, D., 2008. Facilitated process for improving organizational resilience. *Natural Hazards Review*, 9(2), pp. 81–90. https://doi.org/10.1061/(ASCE)1527–6988(2008)9:2(81).

Morales, S.N., Martínez, L.R., Gómez, J.A.H., López, R.R. and Torres-Argüelles, V., 2019. Predictors of organizational resilience by factorial analysis. *International Journal of Engineering Business Management*, 11, pp. 1–13. https://doi.org/10.1177/1847979019837046.

Paul, J., Parthasarathy, S. and Gupta, P., 2017. Exporting challenges of SMEs: A review and future research agenda. *Journal of World Business*, 52(3), pp. 327–342. https://doi.org/10.1016/j.jwb.2017.01.003.

Pavlou, P.A. and El Sawy, O.A., 2011. Understanding the elusive black box of dynamic capabilities. *Decision Sciences*, 42(1), pp. 239–273. https://doi.org/10.1111/j.1540-5915.2010.00287.x.

Pereira, V., Mellahi, K., Temouri, Y., Patnaik, S. and Roohanifar, M., 2018. Investigating dynamic capabilities, agility and knowledge management within EMNEs: Longitudinal evidence from Europe. *Journal of Knowledge Management*, 23(9), pp.1708–1728. https://doi.org/10.1108/JKM-06-2018-0391.

Ratten, V., Ferreira, J. and Fernandes, C., 2016. Entrepreneurial and network knowledge in emerging economies: A study of the Global Entrepreneurship Monitor. *Review of International Business and Strategy*, 26(3), pp.392–409.

Sadeghi, V.J. and Biancone, P.P., 2018. How micro, small and medium–sized enterprises are driven outward: The superior international trade performance? A multidimensional study on the Italian food sector. *Research in International Business and Finance*, 45, pp.597–606. https://doi.org/10.1016/j.ribaf.2017.07.136.

Siguaw, J.A., Simpson, P.M. and Enz, C.A., 2006. Conceptualizing innovation orientation: A framework for study and integration of innovation research. *Journal of Product Innovation Management*, 23(6), pp. 556–574. https://doi.org/10.1111/j.1540-5885.2006.00224.x.

Saad, M.H., Hagelaar, G., Van Der Velde, G. and Omta, S.W.F., 2021. Conceptualization of SMEs' business resilience: A systematic literature review. *Cogent Business and Management*, 8(1): 1938347, https://doi.org/10.1080/23311975.2021.1938347.

Sahebjamnia, N., Torabi, S.A. and Mansouri, S.A., 2015. Integrated business continuity and disaster recovery planning: Towards organizational resilience. *European Journal of Operational Research*, 242(1), pp. 261–273. https://doi.org/10.1016/j.ejor.2014.09.055.

Siguaw, J.A., Simpson, P.M., & Enz, C.A. 2006. Conceptualizing innovation orientation: A framework for study and integration of innovation research. *Journal of Product Innovation Management*, 23(6), pp. 556–574. https://doi.org/10.1111/j.1540-5885.2006.00224.x.

Somers, S., 2009. Measuring resilience potential: An adaptive strategy for organizational crisis planning. *Journal of Contingencies and Crisis Management*, 17(1), pp. 12–23. https://doi.org/10.1111/j.1468-5973.2009.00558.x.

Sullivan-Taylor, B. and Branicki, L., 2011. Creating resilient SMEs: Why one size might not fit all. *International Journal of Production Research*, 49(18), pp. 5565–5579. https://doi.org/10.1080/00207543.2011.563837.

Sukumar, A., Jafari-Sadeghi, V., Garcia-Perez, A. and Dutta, D.K., 2020. The potential link between corporate innovations and corporate competitiveness: Evidence from IT firms in the UK. *Journal of Knowledge Management*, 24(5), pp.965–983. https://doi.org/10.1108/JKM-10-2019-0590.

Teece, D. J., 2007. Explicating dynamic capabilities: The nature and microfoundations of (sustainable) enterprise performance. *Strategic Management Journal,* 28(13), 1319–1350.

Teece, D.J., Pisano, G. and Shuen, A., 1997. Dynamic capabilities and strategic management. *Strategic Management Journal*, 18(7), pp. 509–533. https://doi.org/10.1002/(SICI)1097-0266(199708)18:7<509::AID-SMJ882>3.0.CO;2-Z

Umoh, G.I., Amah, E. and Wokocha, I.H., 2013. Production improvement function and corporate growth in the Nigerian manufacturing industry. *Industrial Engineering Letters*, 3(9), pp. 3–7 https://www.iiste.org/Journals/index.php/IEL/article/view/7506.

Van Bruystegem, K., Van De Woestyne, M. and Dewettinck, K., 2008. Human resource challenges for growing SMEs: How Flemish entrepreneurs attract, develop and retain employees. *Vlerick Leuven Gent Management School Working Paper Series 2008-24.*

Weaven, S., Quach, S., Thaichon, P., Frazer, L., Billot, K. and Grace, D., 2021. Surviving an economic downturn: Dynamic capabilities of SMEs. *Journal of Business Research*, 128, pp. 109–123. https://doi.org/10.1016/j.jbusres.2021.02.009.

Wildavsky, A., 1988. Searching for safety. New Brunswick, NJ: Transaction Books.

Xiao, L. and Cao, H., 2017. Organizational resilience: The theoretical model and research implication. *The 4th Annual International Conference on Information Technology and Applications (ITA 2017)*. ITM Web of Conferences, 12: 04021. https://doi.org/10.1051/itmconf/20171204021.

Yuan, R., Luo, J., Liu, M.J. and Yu, J., 2022. Understanding organizational resilience in a platform-based sharing business: The role of absorptive capacity. *Journal of Business Research*, 141, pp. 85–99. https://doi.org/10.1016/j.jbusres.2021.11.012.

Zighan, S. and Ruel, S., 2021. SMEs' resilience from continuous improvement lenses. J*ournal of Entrepreneurship in Emerging Economies*, 15(2), pp. 233–253. https://doi.org/10.1108/JEEE-06-2021-0235.

Žitkienė, R., Kazlauskienė, E. and Deksnys, M., 2015. Dynamic capabilities for service innovation. *Managing sustainable growth: Proceedings of the Joint International Conference / Management International Conference* – MIC 2015, 28–30 May 2015, Portorož, Slovenia. Portorož: University of Primorska, Faculty of Management. ISBN 9789612661816.

Appendix

Table A1: Rotated factor matrix

	Factor							
	1	**2**	**3**	**4**	**5**	**6**	**7**	**8**
SEN2	0.829							
SEN3	0.820							
SEN1	0.805							
SEN4	0.797							
SEN5	0.695							
SIZ1	0.640							
SIZ3	0.545							
REC4		0.820						
REC6		0.807						
REC5		0.800						
SIZ4		0.766						
SIZ5		0.756						
SEN6		0.694						
REC1			0.860					
REC2			0.859					
REC3			0.718					
LU1				0.813				
LU3				0.768				
STS4				0.747				
STS5				0.739				
LU2				0.733				
STS2					0.838			
STS1					0.824			
LU5					0.790			
LU4					0.779			
RF2						0.912		
RF1						0.901		
RF3						0.771		
TECO4							0.859	
TECO1							0.849	
COMO1							0.840	
COMO6							0.822	
TECO2							0.822	
COMO2							0.786	
COMO5							0.770	
CUSO5							0.724	
ROR3								0.896
ROR1								0.894
POR4								0.887
ROR2								0.879
ROR4								0.871
POR5								0.844
POR3								0.838
ROR7								0.837

Extraction Method: Maximum Likelihood. Rotation Method: Varimax with Kaiser Normalization. a. Rotation converged in 5 iterations.

Modeling the process of ink transfer from the gravure printing plate to the printing substrate

Svitlana Havenko[1], Jerzy Czubak[2], Yosyf Piskozub[3], Yaroslav Uhryn[2] and Marta Labetska[2]

[1]Center of Papermaking and Printing,
 Lodz University of Technology,
 Str. Wólczańska, 223, Lodz, Poland, 90-924
[2]Printing Art and Media Technologies Institute,
 Lviv Polytechnic National University,
 Bandera St., 12, Lviv, Ukraine, 79000,
[3]Department of Applied Mathematics,
 Faculty of Computer Science and Telecommunications,
 Cracow University of Technology,
 Warszawska Str. 24, Cracow, Poland, 31-155

svitlana.havenko@p.lodz.pl
jerzyczubak2022@gmail.com
yosyf.piskozub@pk.edu.pl
yaroslav.m.uhryn@lpnu.ua
marta.t.labetska@lpnu.ua

Abstract

The article presents a mathematical model of imprint formation in gravure printing on cardboard substrates. The focus is on ensuring imprint quality by balancing interactions between the structural subsystems of the printing press, specifically the plate cylinder, ink, printing system, and substrate. Using mathematical models, the behavior of the printing substrate and printing plate elements system is investigated by determining the stress–strain state of the contacting elements during imprint formation. The study describes the ink transfer process from the gravure printing plate to the substrate, considering factors such as substrate weight and structure, technical characteristics of the printing press, and its structural subsystems. The method for calculating printing pressure is also examined. At higher printing speeds and pressures, cylinder coatings can be damaged, leading to overheating and cracking, which necessitates cylinder cooling. Increased press width requires greater pressure to achieve the desired contact area, causing cylinder deflection and uneven pressure distribution, affecting image quality and color matching. Morphological analysis confirmed the significant influence of the printing and inking systems of web-fed gravure presses on pressure distribution in the printing zone. The stress–strain state of objects in direct contact is a key factor in imprint quality. Therefore, studying the micromechanics of contacting surfaces during printing is crucial for high-quality images. Mathematical modeling allows calculation and control of the load in the contact zone between the substrate and ink-filled printing elements, ensuring the quality of gravure imprints on various materials.

Keywords: gravure printing, mathematical models, control, print quality

1. Introduction

Despite its high image quality, gravure printing was considered conservative, not very innovative and less profitable compared to flexographic printing a few years ago. This opinion about gravure printing has recently changed thanks to many technological innovations (Anon., 2006). Innovative processes of automation of prepress preparation, as well as the faster process of engraving the printing plates and the shorter preparation time of the gravure printing press, have greatly increased productivity and cost-effectiveness. In Stefanyshena and Zorenko (2020), modern trends in the development of gravure printing are considered based on the analysis of patent sources and scientific and technical literature regarding the technologies of manufacturing printing plates, printing equipment, consumables and areas of application in different geographical regions. Due to its unique reproduction properties, gravure printing is primarily used for high-quality illustrative products, such as labels, packaging, and advertising catalogues. This specialization

makes gravure printing a focal point for researchers, especially in understanding the factors that influence the quality of printed images.

A detailed analysis of the basic principles of gravure printing is given in Szentgyörgyvölgyi (2016). In particular, special attention is paid to the transfer of ink at high speeds (in 1 – 3 ms), because, with the help of gravure printing, a much larger amount of ink can be transferred to the imprint than in most other printing technologies, thereby ensuring the reproduction of a wide range of tones.

Gladwell (1980) emphasizes that the ideal substrates for gravure printing are paper, cardboard, and film materials with a smooth surface (i.e., coated, super-calendered) since effective ink transfer depends on the full contact of the printing plate with the printing substrates. In Nandakumar and Paramasivam (2006), the authors note that gravure printing can reproduce images with a high screen ruling: 100, 120, 150, 175, 225, and 300 lines/cm. Printing using 175 lines/cm is popular.

As is known, the printing section of the gravure printing press consists of an ink supply system, a gravure and impression cylinder and a blade (Kipphan, 2001, p. 48). For high-speed printing presses, the best option is to use a closed ink system, thanks to which the evaporation of the solvent is reduced, in contrast to an open system, where there is no control of the evaporation of the solvent and the ink does not mix well. The closed system also uses ink viscosity control. In this system, every time the ink is returned from the ink fountain, it is filtered, and a solvent is added to maintain the desired viscosity of the ink. In addition to this closed ink application system, a spray system is also used for very high-speed printing presses, where an ink pump feeds ink to nozzles directed towards the cylinder. The surface of the nozzle always remains wet and never dries out. This system is also completely closed.

Gravure printing presses use several different designs of doctor blade, which is set at a certain angle (55 – 65 degrees) and removes the remaining ink from the non-image areas of the printing plate.

A steel printing cylinder is usually made with a hard rubber coating that can withstand high pressure. The rubber coating has a thickness of 12 to 20 mm. Its hardness ranges from 60 to 100 according to Shore A, depending on the type of the printing substrate. The amount of pressure in the printing zone (up to $\sim$ 500 N/m^2) depends on the characteristics of the elasticity of the cylinder coating, the properties of the substrate, and the type of image being printed.

One of the challenges in ensuring the quality of imprints is the well-established balance of the interaction of the structural subsystems of the printing press, in particular plate cylinder and the inking and printing units with the substrate. It is known that the design of the impression cylinder significantly affects the deformation of its coating during printing. It was investigated that with constant deformation of the coating of the impression cylinder, the internal tension decreases and a relaxation phenomenon is observed, which leads to a gradual decrease in pressure in the printing area (Davies, et al., 2006). The larger the width of the printing press, the more pressure must be applied to obtain the desired width of the printing area. Significant pressure on the edges of a large-diameter cylinder causes deflection of the cylinder and resulting uneven distribution of pressure in the printing area. In such cases, there is a difference in image quality across the printing width and problems related to the passage of the reel substrate, which affects the quality of the printed image. Due to the high speed of gravure printing presses, ink transfer takes 1–3 ms. In this short time, the ink must be uniformly transferred from the small cells of the printing plate to the surface of the substrate (Davies, et al., 2006).

Therefore, it is relevant to study the behaviour of the the behavior of the printing substrate and printing plate elements system, to determine the factors affecting the stress–strain state of the contacting elements during the formation of an imprint in gravure printing presses.

The work reported here is aimed at studying the process of ink transfer from the gravure printing plate to the printing substrate using mathematical modelling to assist in ensuring the quality of the obtained imprints.

2. Objectives and methods of research

The objective of the research was to improve the process of obtaining imprints on a BOBST Lemanic 820 Riviera gravure printing press on cardboards with a grammage of 200 to 500 g/m^2 at a printing speed of v = 250 m/min. It was assumed that the plate cylinder should have the same diameter along the entire length, allowable micro-uniformity of 0.01 to 0.02 mm, a certain stiffness and maximum deflection within 0.05 to 0.1 mm.

The plate cylinder is made of steel, with a top coating of nickel, copper, and chrome. Thus, the tonal coverage of the image on the imprint from the lightest to the darkest areas is determined by different depths, as well as the distances between the screen cells. The

impression cylinder is covered with elastomer with a thickness of 30 to 40 mm. The thicker and more elastic the coating of the impression cylinder, the lower the pressure over the total contact surface during printing. When the cylinder coating thickness decreases, the required printing pressure increases.

The ratio of screen cells and the distances between them (cell walls) is an important parameter that affects the volume of the cell, the quality of imprints and the mechanical stability of the plate. The width of the cell wall affects the ability of the engraved surface to transfer ink. If the width of the cell wall between cells is large, then, when printing, a drop of ink must move across the width between cells when contacted with the substrate, which has no ink, to form a continuous image. The consequence of this failing to occur is results in unevenness of the image, on which it is then possible to see the screen structure.

The area occupied by screen lines is the absorption area of some part of the image itself. Accordingly, the wider the screen cell wall separation, the larger the area of the reproduced image is lost, and it is printed with certain defects. These defects, however, are almost invisible without special devices. This happens because the screen lines are so small in width (with a ratio of cells to cell separation greater than 1:2) that they cannot be noticed with the naked eye. The screen line carries a mechanical load. To provide it with the necessary mechanical stability, the minimum possible width of the inter-cell wall should be provided. Therefore, screens with a different width ratios of transparent and opaque elements in the range from 1:1 to 1:9 are used.

For the BOBST Lemanic 820 Riviera press considered in this study, the ratio of the width of print element and non-print element on the printing plate was 1:3. It should be noted that the researchers recommend creating wider lines on the printing plate (1:5; 1:6; 1:7; 1:8; 1:9) with increased printing speed to increase the durability of the plate.

It is known that for a square screen with a different ruling, but the same ratio of cell walls and cells, the area occupied by the cells in percentage terms, is the same, and the volume of the cells depends only on the depth of the cell and the angle of inclination of the edges of the cell. At higher printing press speeds and high pressure, the cylinder coating is severely damaged, heated and often cracked. Therefore, in many solutions to the problem in the printing press, the cylinder is cooled.

Mathematical modelling methods were used for theoretical research into the abovementioned phenomena.
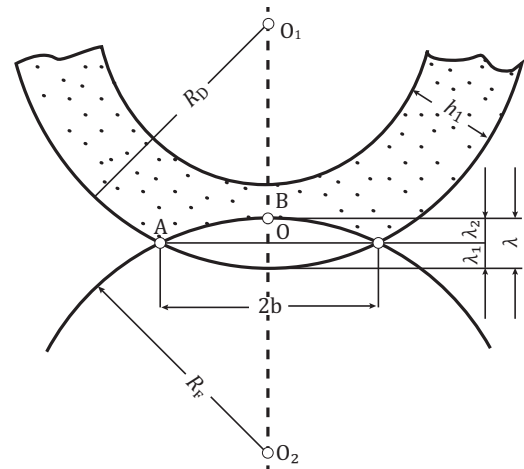

Figure 1: Scheme for calculating the pressure when printing by the gravure printing method where R_D is the radius of the impression cylinder, R_F is the radius of the plate cylinder and λ is the deformation

3. The proposed model and its discussion

Let us consider an example of calculating pressure when printing on a gravure printing press (Figure 1).

$$2b = \sqrt{\frac{2R_D R_F \lambda}{R_D + R_F}} \tag{1}$$

According to Equation [1], for the radius of the plate cylinder R_F = 318 mm and the radius of the impression cylinder R_D = 180 mm, the width of the printing contact area 2b will be 15.2 mm at deformation (compression) of the coating λ = 0.5 mm and 21.4 mm at λ = 1.0 mm. The relative deformation, i.e. applied strain ε, of the cylinder coating during printing is determined by the Equation [2], where $h1$ is the coating thickness (see Figure 1):

$$\varepsilon = \frac{\lambda}{H} \tag{2}$$

Hooke's purely elastic law does not work in practice between the stress of the load and its deformation (where the stress is directly proportional to the relative deformation of the material).

According to the equation of Tir (1965):

$$\sigma = \left(E\varepsilon\right)^{\frac{1}{m}} \tag{3}$$

where σ is the stress, m is the power factor, which depends on the material properties, and E is the elastic modulus of the material. ε is the relative strain.

In the article (Raske, Hewson, Kapur and Boer, 2017), the authors provide a heterogeneous model for the formation of gravure imprints with discrete cells and partially consider the conditions of contact of the printed roll material with the printing plate. However, they focus their research on the relationship between the properties of inks and the shape of the coating layer. However, they do not detail the stress-strain state of the elements of the printing system. Studies (Tir, 1965) have shown that with constant deformation of the coating of a printing cylinder, the internal stress decreases and the relaxation phenomenon is observed, which leads to a gradual decrease in the pressure of the coating in the printing zone and stresses in it. The pressure concerning load relaxation is calculated using Maxwell's equation:

$$P = P_0 e^{\frac{-t}{T}} \qquad\qquad [4]$$

where P is the printing pressure when the cylinder coating operates with a constant deformation, P_0 is the printing pressure when the coating operates with a variable deformation, e is the natural logarithm base, t is the duration of the printing pressure, T is the relaxation time corresponding to the time of change in the cylinder coating stress.

Depending on the pressure force in the printing area, the width of the contact strip between the printing plate and the coating of the impression cylinder ranges from 10 to 25 mm (Chubak and Uhryn, 2023). The larger the width of the printing press, the more external force must be applied to provide the necessary contact pressure to obtain the required width of the printing area. In practice, this force is often referred to as "pressure" because it is adjusted via a hydraulic pressure mechanism, but the resultant is nonetheless a force. However, due to the force being applied to the ends of the cylinder, significant pressure on the end edges of a large-diameter cylinder causes deflection of the cylinder and hence uneven distribution of pressure in the printing area. In such cases, there is a difference in image quality across the print width and problems related to the passage of the web (printing substrate), which affects the accuracy of both colour matching and image alignment.

Modern presses use pressure-compensated impression cylinders, which consist of a core with bearings and a rotating shell with a skin, where two independent sources of force significantly affect the deflection curve of the cylinder: one of them acts on both edges, the other on the trunnions. Axial pressure is transmitted to the rotating shell through bearings located in the middle of the impression cylinder. By changing the hydraulically generated forces, the necessary linear profiles of optimal pressure can be obtained to ensure

consistent quality printing and correct, precise transport of the reel substrate through the printing and inking units of the printing press. There are well-known NIPCO cylinders that allow precise pressure to the plate cylinder to be set within the printing area over its entire width. Such cylinders consist of a fixed axis, on which a special steel cape covered with elastomer with a hardness of 80÷850 shore A is placed. The elastomeric coating makes it possible to ensure the same uniform pressure along the entire length of the printing area and ensure the proper quality of imprints.

The conducted morphological analysis of the structure of the printing and inking units of web-fed gravure printing presses confirmed the significant influence of their design on the distribution of pressure in the printing area and ensuring the appropriate quality of imprints (Chubak and Uhryn, 2023).

As previously mentioned, one of the main quality parameters is the full correspondence of the imprint to the original, including the geometric accuracy of image reproduction. One of the determining factors in this regard is the stress–strain state of the objects in direct contact during the printing process. The macro mechanics of the contact of cylindrical bodies, including those with an elastomeric or other nonlinearly elastic coating, have been studied quite fully, starting with the classic works of Hertz (1881; 1882), Boussinesq (1885) and Reynolds (1876) and mentioning several reviews of individual aspects of contact problems (Sulym, 2007; Kozachok, Martyniak and Slobodian, 2018; Sulym and Piskozub, 2004; Goryacheva, 1998; Martynyak and Serednytska, 2017; Ballarini, 1990; Gladwell, 1999; Johnson, 1985; Nemat-Nasser, 1999; Batra, Levinson and Betz, 1976; Bentall and Johnson, 1967).

However, macro mechanics of contact do not provide an opportunity to control the micro properties of contacting elements in the printing process, in particular raster elements, the size of which are orders of magnitude smaller than the size of the area of direct contact between the impression cylinder and the printing substrate. If there is a need for precision micro printing, it is necessary to consider the micromechanics of contact.

The area of direct contact S is surrounded by a dashed frame in Figure 2. To consider the features of mechanical contact in the direct printing area, it is enough to consider the contact problem of two half-spaces with different mechanical properties, at the contact boundary of which there are inhomogeneities, the presence of which significantly disturbs the stress-deformed state in their vicinity (Figure 3) (Muskhelishvili, 1953; Sulym, 2007; Sulym and Piskozub, 2004; 2017; Gladwell, 1980;

1999; Johnson, 1985; Nemat-Nasser, 1999; Sulim and Piskozub, 2008; Boussinesq, 1885; Hertz, 1881; 1882).

We will consider the quasi-static contact of the half-space S_2 with the rigid S_1 base (Figure 3). We assume that the stress–strain state in the centre of the contact area for reasons of symmetry corresponds to the conditions of plane deformation. Shallow hole cells with a length of $2a$ and a height of $h(x)$ are located at the contact boundary of the base with the substrate with a regular spacing period $d\,(2a \gg h, 2a < d)$.
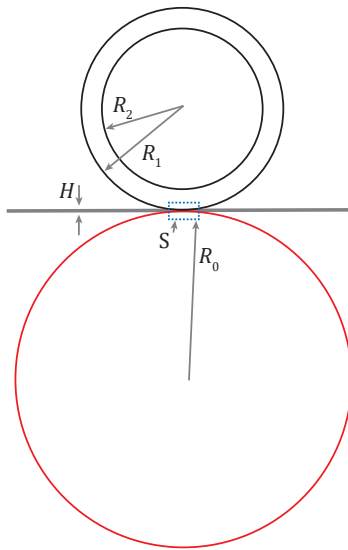
Figure 2: Model of contact of impression cylinders with the printing substrate in the gravure printing process (R_0- radius of the plate cylinder , R_1 and R_2 - radius of the impression cylinder with and without coating, H - thikness of printing substrate, S - zone of direct microcontact)
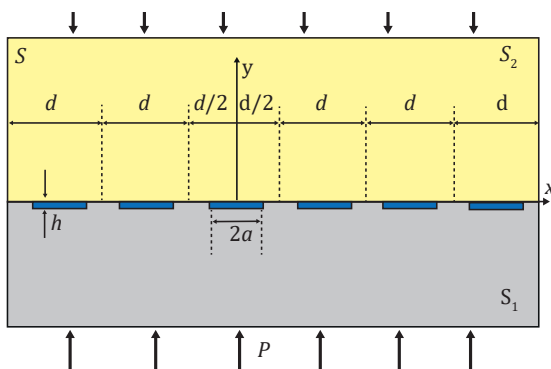

Figure 3: Micromechanical contact of raster cells with the substrate in the direct printing area (P – external pressure, 2a – cell width, h – cell depth, S – area of direct contact)

Boundary conditions in the areas of direct contact S_1 and S_2 expressed in spatial tensor components:

$$a \le |x - nd| \le \frac{d}{2}, \quad n = 0, \pm 1, \pm 2, \ldots \qquad [5]$$

$$\sigma_{xy}(x \pm 0) = 0, \quad u_y(x \pm 0) = 0$$

and in the areas of contact of the cell material with S_2:

$$|x - nd| < a, \quad n = 0, \pm 1, \pm 2, \ldots \qquad [6]$$

$$\sigma_{xy}(x \pm 0) = 0, \quad \sigma_{yy}(x \pm 0) = -P(x)$$

where $P(x)$ is the contact pressure caused by the presence of a liquid filler in the cells.

According to the methodology (Muskhelishvili, 1953; Sulym, 2007; Kozachok, Martyniak and Slobodian, 2018; Sulym and Piskozub, 2004; 2008; 2017; 2021; Piskozub, 2020; Pasternak and Sulym, 2011), the presence of thin inhomogeneities (cells) is modelled by an unknown jump of stresses and strains on their middle surface

$$\left(\sigma_{yy1}(\varsigma) - i\sigma_{xy1}(\varsigma)\right) - \left(\sigma_{yy2}(\varsigma) - i\sigma_{xy2}(\varsigma)\right) = \qquad [7]$$
$$f_1(\varsigma) - if_2(\varsigma),$$

$$\left(u'_{y1}(\varsigma) + iu'_{x1}(\varsigma)\right) - \left(u'_{y2}(\varsigma) + iu'_{y2}(\varsigma)\right) =$$
$$f_3(\varsigma) + if_4(\varsigma),$$

$$\varsigma = x + nd \quad (n = 0, \pm 1, \pm 2, \ldots)$$

Here σ_{yy1}, σ_{xy1} and σ_{yy2}, σ_{xy2} denote the normal and tangential stresses in the contact zone of the half-spaces S_1 and S_2, respectively. u'_{y1}, u'_{x1}, u'_{y2}, u'_{y2} denotes the respectively strains.

And due to boundary conditions (5), (6)

$$f_j(\varsigma) = f_j(x) \quad (j = 1, 2, 3, 4) \qquad [8]$$

$$f_j(\varsigma) = 0 \quad (j = 1, 2, 3, 4) \text{ at}$$

$$x \in [-d; d] \setminus [-a; a]$$

In addition, we have

$$f_j(\varsigma) = 0 \quad (j = 1, 2, 3) \text{ on the entire axis} \qquad [9]$$

$$Ox : x \in (-\infty; \infty)$$

Taking into account the periodicity of the problem, the field of stresses and displacements can be represented in the form of a superposition (Muskhelishvili, 1953; Kozachok, Martyniak and Slobodian, 2018;

Martynyak and Kryshtafovych, 2000; Martynyak and Serednytska, 2017):

$$\sigma_{yy}(z) - i\sigma_{xy}(z) = \sigma_{yy}^0(z) - i\sigma_{xy}^0(z) + \tag{10}$$

$$\sum_{n=-\infty}^{\infty}\left(\hat{\sigma}_{yy}^{(n)}(z) - i\hat{\sigma}_{xy}^{(n)}(z)\right), \qquad z \in S$$

$$u_y(z) + iu_x(z) = u_y^0(z) + iu_x^0(z) +$$

$$\sum_{n=\infty}^{\infty}\left(\hat{u}_y^{(n)}(z) + i\hat{u}_x^{(n)}(z)\right)$$

where $\sigma_{yy}^0(z), \sigma_{xy}^0(z), u_y^0(z), u_x^0(z)$ are components of the stress-strain state known from the homogeneous problem of contact of two half-spaces S_1 and S_2 without inhomogeneities in the contact area, and $\hat{\sigma}_{yy}^{(n)}(z), \hat{\sigma}_{xy}^{(n)}(z), \hat{u}_y^{(n)}(z), \hat{u}_x^{(n)}(z)$ are the unknown perturbations from jumps, $f_j(\varsigma)(j=1,2,3,4)$ caused by the presence of hole-cells.

The components of the stress tensor under plane deformation conditions can be expressed through a Airy function $U(x,y)$ (Muskhelishvili, 1953; Sulym, 2007; Kozachok, Martyniak and Slobodian, 2018)

$$\sigma_{xx} = \frac{\partial^2 U}{\partial x^2}, \; \sigma_{yy} = \frac{\partial^2 U}{\partial y^2}, \; \sigma_{xy} = -\frac{\partial^2 U}{\partial x \partial y} \tag{11}$$

which makes it possible to write the equilibrium equation in the form of a biharmonic equation

$$\Delta\Delta U = 0 \tag{12}$$

Using the well-known presentation of the biharmonic function through the Kolosov-Mushkelishvili complex potentials $\Phi(z), \Psi(z)$ (Muskhelishvili, 1953) and the methodology of works (Muskhelishvili, 1953; Sulym, 2007; Sulym and Piskozub, 2004; 2008; 2017; 2021; Piskozub, 2020; Martynyak and Kryshtafovych, 2000; Martynyak and Serednytska, 2017; Pasternak and Sulym, 2011) the components of the stress tensor and the displacement vector in each of considered S_k for a plane problem can be written using two complex potentials

$$\sigma_{yyk} - i\sigma_{xyk} = \Phi_k(z) + \overline{\Phi_k(z)} + \tag{13}$$

$$z\overline{\Phi_k'(z)} + \overline{\Psi_k(z)},$$

$$2G_k\left(u_{xk}' + iu_{yk}'\right) = \kappa_k\Phi_k(z) -$$

$$\overline{\Phi_k(z)} - z\overline{\Phi_k'(z)} - \overline{\Psi_k(z)}$$

$$\left(z = x + iy \in S_k; \leftrightarrows \leftrightarrows k = 1,2\right),$$

which are holomorphic in these half-planes and going to zero at infinity.

We define the functions $\Phi_1(z)$ in the upper half-plane and $\Phi_2(z)$ in the lower half-plane as follows (analytical continuation through unloaded sections) (Muskhelishvili, 1953; Sulym, 2007; Sulym and Piskozub, 2008):

$$\Phi_k(z) = -\overline{\Phi_k}(z) - z\overline{\Phi_k}(z) - \overline{\Psi_k}(z) \tag{14}$$

$$\left(z \in S_l; k, l = 1,2; l = 3 - k\right)$$

From here, replacing $z = x + iy$ with $\bar{z} = x - iy$, its complex conjugate, we get

$$\overline{\Psi_k(z)} = -\overline{\Phi_k(z)} - \Phi_k(\bar{z}) - \bar{z}\Phi_k'(z) \tag{15}$$

$$\left(z \in S_k; \; k = 1,2\right)$$

Substituting this Equation [15] into Equation [13], and assuming that it is loaded by a field of uniform stresses at infinity $\sigma_{yy}^\infty = -P$, we get

$$\sigma_{yyk}(z) - i\sigma_{xyk}(z) = \tag{16}$$

$$\Phi_k(z) - \Phi_k(\bar{z}) + (z - \bar{z})\overline{\Phi_k'(z)} + \sigma_{yy}^\infty, \quad (z \in S_k)$$

$$2G_k\left[u_{xk}'(z) + u_{yk}'(z)\right] =$$

$$\kappa_k\Phi_k(z) + \Phi_k(\bar{z}) - (z - \bar{z})\overline{\Phi_k'(z)} - \frac{3 - \kappa_k}{4}\sigma_{yy}^\infty;$$

Here G_k – shear modules, v_k – Poisson's coefficients, such that $\kappa_k = 3 - 4v_k$ – Mushelishvili's constants for plane deformation of half-space materials S_k. Passing in [16] to the limit at $z \to x$, taking into account the fact that $\lim_{z \to x}\left[(\bar{z} - \bar{z})\Phi'(z)\right] = 0$, and also that if z goes to the $0x$ axis from the lower (respectively, upper) half-plane S_k, then $\bar{z}$ goes to the same point on the $0x$ axis, only moving from the upper (lower) half-plane, we get

$$\sigma_{yyk}(x) - i\sigma_{xyk}(x) = \Phi_k^\pm(x) - \Phi_k^\mp(x), \quad k = \begin{Bmatrix} 2 \\ 1 \end{Bmatrix} \tag{17}$$

$$2G_k\left(u_{xk}'(x) + iu_{yk}'(x)\right) = \tag{18}$$

$$\kappa_k\Phi_k^\pm(x) + \Phi_k^\mp(x), \qquad k = \begin{Bmatrix} 2 \\ 1 \end{Bmatrix}$$

Values in curly brackets mean that in equations [17], [18] and similar ones, the upper sign corresponds to the value $k = 2$; the lower one is $k = 1$. Applying the methodology of works [9-11, 21] can be obtained

$$\hat{\sigma}_{yy}^{(n)}(z) - i\hat{\sigma}_{xy}^{(n)}(z) = \tag{19}$$

$$\Phi_k(z) - \Phi_k(\bar{z} + 2nd) +$$

$$(z - \bar{z} - 2nd)\overline{\Phi_k'(z)},$$

$$2G_k\left(\hat{u}_y^{(n)}(z) - i\hat{u}_x^{(n)}(z)\right) =$$

$$\kappa_k\Phi_k(z) + \Phi_k(\bar{z} + 2nd) -$$

$$(z - \bar{z} - 2nd)\overline{\Phi_k'(z)} \qquad z \in S$$

where

$$\Phi_k(z) = -\frac{(-1)^{3-k}}{\pi\Upsilon} \sum_{n=-\infty}^{\infty} \int_{-a+nd}^{a+nd} \frac{f_4(t)}{t-z} \mathrm{d}t \qquad [20]$$

$$z \in S_k \, (k=1,2),$$

$$\Upsilon = \frac{1+\kappa_1}{2G_1} + \frac{1+\kappa_2}{2G_2}$$

Using the summation equation

$$\sum_{n=-\infty}^{\infty} \frac{1}{z-nd} = \frac{\pi}{d} \mathrm{ctg}\left(\frac{\pi z}{d}\right) \qquad [21]$$

we will rewrite the potentials [19] in the form

$$\Phi_k(z) = \frac{(-1)^{3-k}}{d\Upsilon} \int_{-a}^{a} f_4(t)\,\mathrm{ctg}\frac{(t-z)}{d}\mathrm{d}t, \qquad [22]$$

$$z \in S_k \, (k=1,2)$$

Then the contact pressure defined by Equation [6] can be calculated using the Equation [23]

$$P(x) = -\sigma_{yy}(x,\pm0) \qquad [23]$$

$$= -\frac{2}{d\Upsilon} \int_{-a}^{a} f_4(t)\,\mathrm{ctg}\frac{\pi(t-z)}{d}\mathrm{d}t - \sigma_{yy}^{\infty}$$

from which it is easy to obtain the singular integral equation with the Hilbert kernel to determine the unknown jump $f_4(x)$

$$\frac{2}{d} \int_{-a}^{a} f_4(t)\,\mathrm{ctg}\frac{\pi(t-z)}{d}dt = \Upsilon(P - P(x)) \qquad [24]$$

To solve Equation [24], it is convenient to use the substitution of variables

$$\xi = \mathrm{tg}\left(\frac{\pi x}{d}\right), \quad \eta = \mathrm{tg}\left(\frac{\pi t}{d}\right), \qquad [25]$$

$$\alpha = \mathrm{tg}\left(\frac{\pi a}{d}\right), \quad \beta = \mathrm{tg}\left(\frac{\pi b}{d}\right)$$

Then Equation [24] transforms into a Equation [25] with a Cauchy-type kernel

$$\int_{-\alpha}^{\alpha} \frac{f_4(\eta)}{\eta-\xi} d\eta = F(\eta) = \qquad [26]$$

$$\frac{\Upsilon d}{2(1+\xi^2)}(P - P(\xi)),$$

$$|\xi| \le \alpha$$

which has a solution

$$f_4(\xi) = \frac{1}{\pi^2 \sqrt{\alpha^2 - \xi^2}} \qquad [27]$$

$$\left\{ -\int_{-\alpha}^{\alpha} \frac{\sqrt{\alpha^2-\eta^2}\,F(\eta)}{\eta-\xi} \mathrm{d}\eta + \int_{-\alpha}^{\alpha} f_4(\xi)\mathrm{d}\xi \right\}$$

Taking into account that at the ends of the cells $\hat{u}_y^{(n)}(x \pm na) = -h \, (n=0,\pm1,\pm2,\ldots)$, we have an additional condition

$$\int_{-\alpha}^{\alpha} f_4(\xi)\mathrm{d}\xi = 0 \qquad [28]$$

The pressure $P(\xi)$ can be found using the equation of state of a compressible barotropic fluid (Muskhelishvili, 1953; Sulym, 2007; Kozachok, Martyniak and Slobodian, 2018)

$$V_h e^{\frac{P_h}{B}} = V_0 \qquad [29]$$

where $V_0 = 2ah$ is the initial volume of a rectangular cell in profile, V_h is the volume of liquid per unit cell length in the transverse direction, and B is modulus of volume elasticity of liquid.

From Equation [27] taking into account Equation [26], we get the solution

$$f_4(\xi) = \frac{\Upsilon d(P-P_h)\xi\sqrt{\alpha^2+1}}{2\pi(1+\xi^2)\sqrt{\alpha^2-\xi^2}}, \quad |\xi| \le \alpha \qquad [30]$$

Integrating Equation [30], we get increase in cell volume

$$\Delta u_y(\xi) = \int_{-\alpha}^{\xi} f_4(\xi)d\xi = \qquad [31]$$

$$-\frac{\Upsilon d(P-P_h)}{2\pi}\mathrm{arcth}\left(\frac{\sqrt{\alpha^2-\xi^2}}{\sqrt{\alpha^2+1}}\right)+$$

$$h, \quad |\xi| \le \alpha$$

Then the contact pressure of the surfaces can be calculated from the equation

$$P(x) = \qquad [32]$$

$$\frac{\left|\mathrm{tg}\left(\frac{\pi x}{d}\right)\right|\sqrt{\mathrm{tg}^2\left(\frac{\pi a}{d}\right)+1}}{\sqrt{\mathrm{tg}^2\left(\frac{\pi x}{d}\right)-\mathrm{tg}^2\left(\frac{\pi a}{d}\right)}}(P-P_h)+P_h,$$

$$a \le |x-kd| \le \frac{d}{2}$$

Equation [29] for determining the fluid pressure P_h after applying the substitution of variables [27] and taking into account

$$V_0 = \frac{dh}{\pi} \int_{-\alpha}^{\alpha} \frac{d\xi}{1+\xi^2} = \frac{2hd \cdot \mathrm{arctg}(\alpha)}{\pi} \qquad [33]$$

takes the form

$$e^{\frac{P_h}{B}}\left(-\frac{\Upsilon d\left(P-P_h\right)}{4}\right) \qquad [34]$$

$$\left(\ln\left(\alpha^2+1\right)+2h\cdot\text{arctg}\left(\alpha\right)\right)-2h\cdot\text{arctg}\left(\alpha\right)=0$$

This equation does not have an analytical solution, so it should be solved by numerical methods. It is worth noting that the less compressible the liquid is, the less the contact pressure changes over the entire contact surface, including the intervals of direct contact of the half-spaces. The direction in [34] of the modulus of volume elasticity of the liquid to infinity (incompressible fluid, $B \to \infty$) leads to the result that the pressure of an incompressible fluid is equal to the applied load $P(x) = P$ and therefore, the pressure over the entire surface of the body is also constant and equal to the applied load. That is, there is no effect of the presence of hole cells as perturbations of the stress-strain state in the contact area.

With the help of the method, it is possible to carry out several numerical calculations for various parameters of changing the size and location of the cells on the printing plate, as well as changes in the mechanical proper-

ties of materials of half-spaces and fluids under external load in the range $0 < P < P^\infty$, where

$$P^\infty = \Upsilon B \ln\left(\begin{array}{c}\text{arctg}\left(\alpha\right)\\\left(\frac{\pi \ln\left(\alpha^2+1\right)}{\ln\left(\sqrt{\alpha^2+1}+\alpha\right)}+4\,\text{arctg}\left(\alpha\right)\right)^{-1}\end{array}\right)+ \qquad [35]$$

$$\frac{2\pi h}{d\ln\left(\sqrt{\alpha^2+1}+\alpha\right)}$$

i.e. the load at which the contact of the border of the half-space S_2 with the base of the cells at depth y = −h.

4. Conclusions

Thus, taking into account the theoretical principles of macro- and micromechanics of the contact of system elements in the gravure printing process, it is possible to control their properties. Using the method of mathematical modelling, it is possible to calculate and control the load in the contact area of the printing substrate and printing plate with ink-filled printing elements, ensuring the quality of imprints on various materials, taking into account their structure and thickness.

References

Anon., 2006. Trends in digital engraving. *Flexo & Gravure International*, 2, pp. 20–24.

Ballarini, R., 1990. A rigid line inclusion at a bimaterial interface. *Engineering Fracture Mechanics*, 37(1), pp. 1–5. https://doi.org/10.1016/0013-7944(90)90326-c.

Batra, R.C., Levinson, M. and Betz, E., 1976. Rubber covered rolls – the thermoviscoelastic problem. A finite element solution. *International Journal for Numerical Methods in Engineering*, 10 (4), pp. 767–785. https://doi.org/10.1002/nme.1620100405.

Bentall, R. H. and Johnson, K. L., 1967. Slip in the rolling contact of two dissimilar elastic rollers. *International Journal of Mechanical Sciences*, 9(6), pp. 389–404. https://doi.org/10.1016/0020-7403(67)90043-4.

Boussinesq, J., 1885. *Application des potentiels à l'étude de l'équilibre et du mouvement des solides élastiques*. Paris: Gauthier-Villars.

Chubak, Y. and Uhryn, Y., 2023. Morphological analysis of problems of the imprints quality related to the structure of printing and inking systems of gravure printing presses. *Printing and Publishing*, 2(86), pp. 91–101.

Davies, G.R. and Claypole, T. C., 2006. Effect of viscosity on ink transfer in gravure printing. In: *Proceedings of the 33rd International Research conference of Iarigai*, Leipzig, Germany, pp. 235–244.

Drago, A. and Pindera, M., 2007. Micro-macromechanical analysis of heterogeneous materials: Macroscopically homogeneous vs periodic microstructures. *Composites Science and Technology*, 67(6), pp. 1243–1263. https://doi.org/10.1016/j.compscitech.2006.02.031.

Gladwell, G.M., 1999. On inclusions at a bi-material elastic interface. *Journal of Elasticity*, 54(1), pp. 27–41.

Gladwell, G.M.L., 1980. *Contact problems in the classical theory of elasticity.* Dordrecht: Springer Netherlands.

Goryacheva, I.G., 1998. *Contact mechanics in tribology*. Dordrecht: Springer Netherlands. https://doi.org/10.1007/978-94-015-9048-8.

Hertz, H., 1881. Über die Berührung fester elastischer Körper. *Journal für die reine und angewandte Mathematik*, 92, pp. 156–171.

Hertz, H., 1882. Über die Berührung fester elastischer Körper und über die Harte. *Verhandlungen des Vereins zur Beförderung des Gewerbfleißes*, 1882, pp. 449–463.

Johnson, K.L., 1985. *Contact Mechanics*. Cambridge: Cambridge University Press.

Kipphan, H., 2001. *Handbook of Print Media: Technologies and Production Methods.* Berlin: Springer. ISBN 978-3540673262.

Kozachok, O., Martynyak, R., and Slobodian, B., 2018. *Vzaemodiia til z rehuliarnoho reliiefu za naiavnosti mizhkontaktnoho seredovyshcha*. Lviv, Ukraine: Rastr-7 (in English: *Interaction Between Bodies with Regular Relief in the Presence of an Interstitial Medium*).

Martynyak, R. and Kryshtafovych, A., 2000. Friction contact of two elastic half-planes with local recesses in boundary. *Journal of Friction and Wear*, 21(4), pp. 6–15.

Serednytska, K. and Martynyak, R., 2017. *Контактні задачі термопружності для міжфазних тріщин в біматеріальних тілах.* (in English: *Contact problems of thermoelasticity for interface cracks in bimaterials*).

Muskhelishvili, N. I., 1953. *Some basic problems of the mathematical theory of elasticity: Fundamental equations, plane theory of elasticity, torsion and bending. Groningen*: Noordhoff.

Nandakumar, M. and Paramasivam, A., 2006. *Gravure, flexo and screen printing*. Sivakasi: Arasan Ganesan Polytechnic College.

Nemat-Nasser, S. and Hori, M., 1999. *Micromechanics: Overall Properties of Heterogeneous Materials*. 2nd rev. ed. Cambridge: Cambridge University Press.

Pasternak, Y.M. and Sulym, G.T., 2011. Models of Fine Inhomogeneities Considering the Possibility of Their Non-Ideal Contact with the Environment. *Dnipro University Bulletin: Mechanics Series*, 15(5), pp. 200–210.

Piskozub, Y. Z. and Sulym, H. T., 2021. Modeling of deformation of the bimaterial with thin Non-linear interface inclusion. *Researches in Mathematics and Mechanics*, 2(36), pp. 40–57. https://doi.org/10.18524/2519-206x.2020.2(36).233748.

Piskozub, Y.Z., 2020. Effect of surface tension on the antiplane deformation of bimaterial with a thin interface microinclusion. Mathematical Modeling and Computing, 8(1), pp. 69–77. https://doi.org/10.23939/mmc2021.01.069.

Raske, N., Hewson, R., Kapur, N. and Boer, G., 2017. A predictive model for discrete cell gravure roll coating. *Physics of Fluids*, 29(6), 062101. https://doi.org/10.1063/1.4984127.

Reynolds, O., 1876. On rolling friction. *Philosophical Transactions of the Royal Society of London*, 166, pp. 155–175.

Stefanyshena, O. B. and Zorenko, O.V., 2020. Modern trends in the development of gravure printing. Technology and Technique of Typography, 3(69), pp. 34–42. https://doi.org/10.20535/2077-7264.3(69).2020.224199.

Sulim, G. T. and Piskozub, J. Z., 2008. Thermoelastic equilibrium of piecewise homogeneous solids with thin inclusions. *Journal of Engineering Mathematics*, 61, pp. 315–337. https://doi.org/10.1007/s10665-008-9225-3.

Sulym, G. and Piskozub, Y., 2004. Conditions of contact interaction of bodies: an overview. *Mathematical Methods and Physical and Mechanical fields*, 47(3), pp. 110–125.

Sulym, G. and Piskozub, Y., 2017. Nonlinear deformation of a thin interfacial inclusion. *Physical and Chemical Mechanics of Materials*, 53(5), pp. 24–30.

Sulym, G.T., 2007. *Fundamentals of the mathematical theory of thermoelastic equilibrium of deformable solids with thin inclusions*. Lviv: Research and Publishing Center of the National Academy of Sciences.

Szentgyörgyvölgyi, R., 2016. Gravure printing. In: J. Izdebska, S. Thomas, eds., eds. 1st ed. *Printing on Polymers*. Waltham: William Andrew. pp. 199–215. https://doi.org/10.1016/B978-0-323-37468-2.00012-9.

Tir, K.V., 1965. *Mechanics of printing machines*. Moscow.

TOPICALITIES

Edited by Markéta Držková

CONTENTS

News & more – J. Print Media Technol. Res. – Vol. 13 No. 2 (2024), 109–110

109

News & more

Recently ending EU-funded projects

This time, the regular overview includes the printing-related projects funded by Horizon 2020 and, in part, already by Horizon Europe, the EU's 7-year programmes for research and innovation. Besides the selection presented below, 3DBIOLUNG, which received the ERC Starting Grant, applied bioengineering approaches to generate constructs mimicking lung tissue using 3D bioprinting of hybrid bioink reinforced with extracellular matrix, and the innovation action Caladan used micro-transfer printing to incorporate lasers and electronics into photonic integrated circuits for efficient manufacturing of optical transceivers to increase communication throughput in data centres. Other examples include the Horizon Europe projects with the ERC Proof of Concept funding, dealing with in-situ monitoring for fused deposition modelling, novel support material for 3D bioprinting and post-printing tissue growth, 3D-printed electromagnetic interference shielding solutions based on 2D nanomaterials inks, and many more.

GrapheneCore3 – Graphene Flagship Core Project 3

Successfully building on the previous stages, see JPMTR Vol. 10, No. 2 (2021), also this third one, with a budget of 150 million EUR and about two hundred participants, contributed to the state of the art in graphene technologies.

RealNano – In-line and real-time digital nano-characterization technologies for the high yield manufacturing of flexible organic electronics

The outcomes of this research and innovation action include the tools and methods based on spectroscopic ellipsometry, Raman spectroscopy, imaging photoluminescence and laser beam induced current mapping for real-time and non-destructive in-line characterising, and analysing optical, structural, electrical and electronic properties of organic electronics materials and devices to significantly improve their performance and the manufacturing process control and reduce the development time and resources consumption.

RoLA-FLEX – Roll-2-roll and photolithography post-processed with laser digital technology for flexible photovoltaics and wearable displays

The progress made within this research and innovation action towards commercial flexible organic and large-area electronics, presented in over 20 papers, helped to develop organic photovoltaics with a significantly longer lifetime and an organic LCD prototype enabled by organic thin-film transistors.

PRIME – Advanced and versatile printing platform for the next generation of active microfluidic devices

This research and innovation action, aiming to integrate all the fluidic and sensing functions into a single device, involved the 4D printing of novel liquid crystal elastomers as smart materials responsive to temperature and light. The underlying research is described in about 20 papers.

Impressions from drupa 2024 sharing a positive spirit

Having the possibility to simply visit the fair, wander through the halls, let the exhibitors catch the attention by showcasing their solutions, learn interesting details and gain insights into areas of particular interest, meet colleagues and share the news – that all may seem ordinary, but after the long eight years it just feels good.

The overall picture provided by this year's drupa fair is optimistic, with many new developments, partnerships and cooperations. In numbers, over 1 500 exhibitors filled almost every spot. Among nearly 50 countries, clear leaders were China and Germany, each with about 400 companies, followed by Italy with nearly 140, then India, the UK, the USA, the Netherlands and other, mainly European and Asian countries. Looking across the halls, the large exhibitors included Heidelberg, Müller Martini, Masterwork, Kolbus, Kurz, Kodak, Epson, Barberán, Horizon, Duplo, Canon, Ricoh, Screen, Kyocera, Fujifilm, Konica Minolta, Hanglory, Esko, Landa, EFI, Uflex, Bobst, Comexi, Uteco, UP Group, Line O Matic, Xeikon, Fangbang, Zenbo, Emmeci, Komori, Windmöller & Hölscher, Koenig & Bauer, Durst, RMGT, Manroland Goss, and HP. Regarding trends, the universal concept was automation, encountered in various contexts: as an integral aspect of digital machines, software and system solutions, an essential driver behind the increasing performance of all kinds of conventional equipment, and eye-catching robotic extensions and autonomous trolleys. Other clear trends include product portfolios adapting to the strength of the packaging sector and the emphasis on environmental considerations. The time for disruptive solutions exploiting the progress in artificial intelligence is yet to come.

The Intergraf activities during the last year

In the context of the ongoing digital transformation, several

INTERGRAF

Intergraf activities highlighted the role of print. The joint statement with Cepi, UNI Europa Graphical & Packaging, FEPE, and IndustriAll Europe draws attention to essential paper and print products, aspects of their sustainability and circularity, benefits of reading in print for quality education and preventing the exclusion due to the excessive digitalisation, and the often omitted fact that the use of digital technologies is not environmentally neutral. With respect to environmental concerns, Intergraf, with other members of the World Print & Communication Forum, recognised the need for a common approach in the assessment of carbon footprint for the printing industry, and with UNI Europa Graphical & Packaging supported the European Parliament definitions of composite packaging, plastic packaging and high-quality recycling, and the coexistence of both reuse and recycling schemes, i.e. the concepts underlying the packaging and packaging waste regulation. Also, the first version of the Intergraf method for the assessment of environmental schemes for printed products was published in April. It defines the significant environmental parameters, following a life-cycle approach and adding the use of chemical substances in printed products, consumption of organic solvents and emissions of volatile organic solvents, along with classification criteria and the corresponding classification of environmental parameters.

In June, Intergraf released its regular annual reports. The Intergraf Activity Report provides an overview of the organisation and its operations in the past months. The relevant statistics collected in the 2024 Intergraf Economic Report mostly keep the values from the previous one. Considerable changes and differences among individual countries again show EU electricity prices, which are included in the market report section.

ApPEARS – Appearance Printing – European Advanced Research School

In this project, eight participating universities and research institutes with expertise in appearance characterisation have joined to facilitate innovative training of young scientists. The advances in the field are presented in dozens of scholarly publications, including a thesis assessing 2.5D print quality. Other topics include structural colourants, methods for reproducing the colour of translucent objects, 3D adaptive digital halftoning, and others.

T-Sense Cold – Printed temperature sensitive labels for products in cold chain

This project was funded through the SME Instrument and focused on developing a series of irreversible temperature-sensitive colour-changing labels for packages to increase the level of control across the whole cold supply chain. It comprised synthesising active materials, formulating inks, and thoroughly testing their functionality, safety, and sustainability.

ASTRABAT – All solid-state reliable battery for 2025

The objective of this research and innovation action was to contribute to developing a safe, high-energy, sustainable and marketable battery for green mobility. It addressed the challenges in terms of new materials for electrodes and electrolytes, including fluorine-free lithium salts and ionic liquid plasticizers, as well as cell architecture, eco-design, and manufacturing. Inkjet printing was proposed as a promising fabrication method for advanced 3D electrodes.

NewMEAT – New micro-extrusion advanced technology for plant-based whole-cut meat substitutes

This two-year project, funded within Horizon Europe under the European Innovation Council, utilised tissue engineering, food science and 3D printing to develop a micro-extrusion technology capable of mimicking the texture, appearance, flavour and nutritional properties of meat whole-cuts using a wide range of sustainable plant-based proteins and produce meat alternatives meeting consumer expectations at industrial scale.

PEP2D – Printable electronics on paper through 2D materials based inks

The published results of this long-term project that received the ERC Consolidator Grant present a wide range of low-dimensional materials and their use in different paper-based components and devices, including a novel anti-counterfeiting tag, naturally degradable photonic devices and many more.

PeroCUBE – High-performance large area organic perovskite devices for lighting, energy and pervasive communications

This innovation action explored new materials, device architectures and characterisation methods for perovskite photovoltaics and light-emitting diodes with a focus on their scalable manufacturing, e.g. by roll-to-roll printing.

SYMPHONY – Smart hybrid multimodal printed harvesting of energy

Among other outcomes of this research and innovation action, the energy-autonomous sensor system for smart tyres, which was integrated inside the bicycle tube, recently received the OE-A (Organic and Printed Electronics Association) award for the best publicly funded project demonstrator.

Bookshelf – J. Print Media Technol. Res. – Vol. 13 No. 2 (2024), 111–116

111

Bookshelf

Transfer Printing Technologies and Applications

This new book presents transfer printing as a highly versatile class of technologies for micro- and nanofabrication and deterministic large-scale assembly of various advanced materials or integrated devices. With almost 50 contributors, the book reflects the recent progress and aims to facilitate the choice of proper transfer-printing technique for a given application.

Eight chapters of the first part introduce the essential fundamentals of transfer printing, i.e. the analytical mechanical models, novel structures and functional materials, and then detail the individual methods, their working principles, specific characteristics and applications. The text describes the transfer printing by kinetic control of adhesion, with rate-dependent mechanical transfer of graphene as an example, the thermal release tape-enabled transfer printing techniques, where it discusses the mechanism of thermal release tape stamp with thermally expandable microspheres for large adhesion switchability, laser thermal treatment, shape-conformal thermal release tape stamp for curve electronics and roll-to-roll processing enabling large-scale transfer printing, and the laser-driven noncontact transfer printing technique making use of interfacial delamination. Further, it covers magnetic-assisted transfer printing techniques, transfer printing techniques enabled by advanced carbon nanomaterials, and water-assisted transfer printing techniques with self-assembled monolayer-based release layer or with sacrificial layer. Additionally it introduces novel nontraditional transfer printing technologies, which include the methods using shape memory polymer as a manipulator or a stamp coated with thin photoresist film, transfer printing of elastic membrane for pattern generation and epoxy-based subtractive transfer printing.

In the second part, nine chapters present the state-of-the-art applications in different areas enabled by transfer printing. These include optical systems, different types of flexible sensors, namely strain, pressure, thermal, electrophysiological and chemical sensors, flexible transistors based on Si, compound semiconductors, carbon materials, ion gel, oxides and other materials, functional devices for biomedical applications, micro-light-emitting diode display produced with contact or noncontact laser-driven transfer printing techniques, and energy systems, i.e. rechargeable batteries, supercapacitors, fuel cells and water splitting and solar cells. Among materials, the text deals with the transfer printing of metal films; it discusses environmentally-assisted bonding and debonding of the metal–substrate interfaces and the eletromechanical behaviour of ultrathin metal films bonded on a substrate. It also describes the stacking of 2D materials and its implementation in electronics, namely 2D layer-based logic devices, optoelectronics and memories. The last chapter identifies the major challenges in transfer printing, e.g. high costs and limited scalability, and future research directions, such as hybrid materials, roll-to-roll printing, system integration and the Internet of Things.
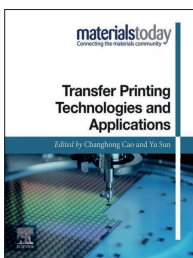
Editors: Changhong Cao, Yu Sun

Publisher: Elsevier
1st ed., January 2024
ISBN: 978-0-443-18845-9
538 pages
Softcover
Available also as an eBook

Industrial Strategies and Solutions for 3D Printing Applications and Optimization

Editors: Hamid Reza Vanaei, Sofiane Khelladi, Abbas Tcharkhtchi

Publisher: Wiley
1st ed., March 2024
ISBN: 978-1394150304
320 pages
Hardcover
Also as an eBook
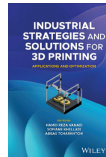
This book takes the interdisciplinary approach to encompass all aspects of the 3D printing process and properties of 3D-printed parts, with an emphasis on the importance of multi-objective evaluation. Written by 30 experts active in the field worldwide, the text highlights the essential features of 3D printing, discusses the possibility of upscaling in the context of state-of-the-art materials and techniques used in 3D printing, as well as the range of its applications, and identifies the current challenges. Further, it details the evaluation methods, controlling factors, physical and chemical properties of 3D-printed parts, rheology, mechanical performance, thermal modelling and temperature monitoring, along with the benefits of optimising and machine learning.

3D Printing and Sustainable Product Development

Editors: Mir I. U. Haq, Ankush Raina, Nida Naveed

Publisher: CRC Press
1st ed., September 2023
ISBN: 978-1032306803
240 pages, 60 images
Hardcover
Also as an eBook
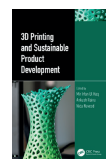
Also dealing with the fast progress in the field of additive manufacturing, this book identifies the opportunities and challenges of 3D printing in developing new products and reviews best practices to facilitate its industrialisation. It discusses the role of 3D printing towards sustainability and product safety, including the environmental impact

Robotics, Vision and Control
Fundamental Algorithms in Python

This appreciated and informative book presents the title topics not only separately but also together as robotic vision. The author, with about 40 years of experience in the field, highlights the factors behind the fast evolution of robotics and machine vision of all kinds. Besides significant advances in computational power, sensors, cameras and other components and technologies, as well as their affordability, it is the open-source Robot Operating System platform and improvements in sensory data processing. Over ten years after the first edition, the current one uses Python with the relevant toolboxes ported from MATLAB. The algorithms in MATLAB are provided in the alternative third edition, coauthored by W. Jachimczyk and R. Pillat.

After the introduction, the content is divided into five parts. Foundations include the extensively rewritten chapter on representing position and orientation in 2D and 3D and another one dealing with aspects related to time and motion. Two parts present mobile robotics and robot manipulators, with an improved coverage of robot arm kinematics. The part dedicated to computer vision explains the concepts of light and colour, such as spectral representation, colour temperature, colour constancy, white balancing, dichromatic reflection and gamma. It also details methods for obtaining and processing images, feature extraction, image formation and use of multiple images. The last part deals with vision-based control, discussing both common and advanced visual servoing. The book also provides rich supplementary information.
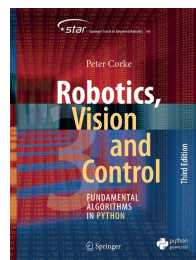
Author: Peter Corke

Publisher: Springer
3rd ed., August 2023
ISBN: 978-3-031-06468-5
850 pages, 635 images
Softcover
Available also as an eBook

Computational Imaging for Scene Understanding
Transient, Spectral, and Polarimetric Analysis

About 20 authors of this new book review the recent progress in computer vision techniques beyond the usual RGB images captured at standard frame rates. The first part presents the approaches to transient imaging, including the methods for non-line-of-sight imaging, transient convolutional imaging using correlation image sensors, and time-of-flight rendering. The second part deals with hyperspectral imaging, obtaining the reflectance and fluorescence spectra from scenes, shape reconstruction of transparent objects,

Editors: Takuya Funatomi, Takahiro Okabe

Publisher: Wiley-ISTE
1st ed., May 2024
ISBN: 978-1-789-45150-4
338 pages
Hardcover
Available also as an eBook
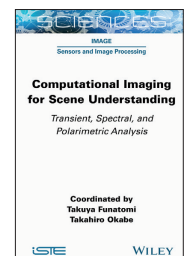
thermal photometric stereo, and synthetic wavelength imaging based on interferometry. The third part discusses polarimetric imaging, shape estimation using the shading and polarisation fusion approach, shape recovery in outdoor environments by considering polarised illumination, and multispectral polarisation filter array using a photonic crystal.

Multimedia Foundations
Core Concepts for Digital Design

This revised edition incorporates the changes in multimedia technologies and their use in digital media production since the second edition published in 2016, building on the recent data. The text introduces the components of multimedia design and explains the related concepts, including design thinking, inclusive design, colour theory, interview, secondary footage acquisition techniques, and photography composition, exemplified by new illustrations. Also, it covers the main stages of the editing process and postproduction workflows. The content is organised into five sections, which deal with multimedia basics, asset management and project planning, elements and principles of visual design, text, graphics and photography, digital recording, audio and video production and non-linear editing, and interactive media. For this last section, Q. Xu revised the chapter on user interface design, and K. Furnas contributed the chapter on coding for web and mobile media.
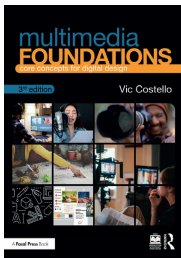
Author: Vic Costello

Publisher: Focal Press
3rd ed., July 2023
ISBN: 978-1-138-39153-6
512 pages, 376 images
Hardcover
Available also as an eBook

Foundations of Visual Communication
How Visuals Appear in Daily Life

The authors of this book, illustrated by a variety of examples ranging from commonly encountered symbols, images and media to art history, focus on interaction with and among visuals. They discuss a changing visual landscape and intercultural influences, visual culture studies, factors shaping visual communication and its outcomes dependent on general or immediate context, individual perception and reception. The text also presents fundamental concepts and approaches to creating and interpreting visuals, visual cues, storytelling and interaction. The final chapter deals with visuals transforming in time and space and finding new roles.

Authors: Yvonne Eriksson, Anette Göthlund

Publisher: Routledge
1st ed., June 2023
ISBN: 978-0-367-77155-3
142 pages, 59 images
Hardcover
Available also as an eBook
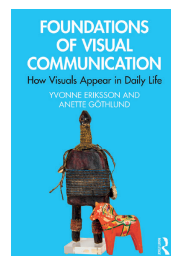
of metal additive manufacturing and the use of polymeric materials based on spent coffee grounds and recycled polyethylene terephthalate. In addition, four chapters deal with dental and orthodontic applications, nanomaterials and 4D printing of magnetic-based robotic materials.

Designing Brand Identity
A Comprehensive Guide to the World of Brands and Branding

Authors: Alina Wheeler, Rob Meyerson

Publisher: Wiley
6th ed., March 2024
ISBN: 978-1119984818
352 pages
Hardcover
Also as an eBook

The first part of this neatly arranged book explains the basic concepts of branding, brand ideals, elements, dynamics and redesign. The second one focuses on the design process, its important aspects and essential phases, i.e. conducting research, clarifying strategy, designing identity, creating touchpoints, and managing assets. The last part presents over 50 new case studies to highlight best practices. The current revised edition reflects the recent advances and changes, covering artificial intelligence, virtual reality, social justice and evidence-based marketing.

The Book of Printed Fabrics
From the 16th Century Until Today

Author: Aziza Gril-Mariotte

Publisher: Taschen
1st ed., April 2024
ISBN: 978-3836562768
888 pages
Hardcover
Also as an eBook

Page spreads of these two volumes present the hundreds of printed textiles from four continents, with a vast range of motifs carefully selected from a unique collection of the Musée de l'Impression sur Étoffes in Mulhouse and introduced in English, French and German.

Carbon-Based Conductive Polymer Composites
Processing, Properties, and Applications in Flexible Strain Sensors

Author: Dong Xiang

Publisher: CRC Press
1st ed., February 2023
ISBN: 978-1032111582
175 pages, 87 images
Hardcover
Also as an eBook
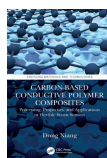
This book deals with advances in conductive polymer composites based on carbon nanomaterials. It introduces their preparation, processing, and properties, as well as specially designed structures and applications in flexible strain sensors. It presents characteristics of compression moulded and biaxially stretched composites and blown film extrusion of different types of composites. Further, it discusses the stimuli-resistivity behaviour of carbon-based conductive polymer composites and details three types of flexible strain sensors, including those prepared by 3D printing.

Graphene Based Biomolecular Electronic Devices

Authors: Bansi D. Malhotra, Sharda Nara

Publisher: Elsevier
1st ed., January 2023
ISBN: 978-0128215418
262 pages
Softcover
Also as an eBook

The authors of this book focus on the devices that make use of the charge transfer between graphene and biomolecules. After an overview of graphene fundamentals, they present graphene-based transduction systems in biosensors and graphene in biosensors based on field-effect transistors, protein and nucleic acid biosensors, wearable biosensors, microbial fuel cells and drug delivery systems. They also deal with 3D-printed graphene in bioelectronics and the prospects and challenges.

Functionalized Nanomaterials Based Supercapacitor
Design, Performance and Industrial Applications

This comprehensive reference summarises the development of supercapacitors based on functionalised nanomaterials and in related areas. The first three parts provide the fundamental background. One chapter introduces nanotechnology, supercapacitors, functionalised nanomaterials and trends in their use as supercapacitor devices. The next details fabrication methods, including additive manufacturing of relevant functionalised nanomaterials, photolithography for supercapacitor electrodes, 3D printing and inkjet printing of supercapacitors together with recent advances in printable composite materials, and also the methods used for pre- and post-treatment of functionalised nanomaterials for supercapacitor electrodes. The third chapter is dedicated to functionalisation techniques for carbon-based nanomaterials, their forms and electrochemical properties, and the development of supercapacitors based on metal-oxide/hydroxides and conducting polymers. Then, four parts present the application possibilities in energy storage, the food and beverage industry, water treatment, health care and other emerging areas. The last two parts focus on the aspects of economics and commercialisation and discuss future development.

Editors: Chaudhery M. Hussain, M. Basheer Ahamed

Publisher: Springer
1st ed., September 2023
ISBN: 978-981-99-3020-3
713 pages, 243 images
Hardcover
Available also as an eBook
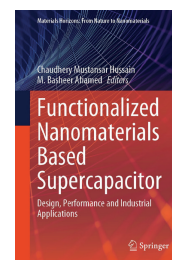
3D Graphene
Fundamentals, Synthesis, and Emerging Applications

This volume reviews the progress in fabricating 3D graphene structures and their use. Three chapters introduce the unique properties of 3D graphene and describe its synthesis and printing. The next one deals with different architectures of 3D graphene and analyses relevant chemical aspects. The main part presents a wide range of applications. These include biosensors, electrochemical, optical and flexible sensors, remediating hydrogen sulfide gas, removing inorganic pollutants and pharmaceutical residues, metal-ion, metal–air, flexible and wearable batteries, flexible electronics, supercapacitors, photovoltaics, fuel cells, electrocatalysts and photocatalysts for water splitting, capacitive de-ionization of water and theranostic uses. Toxicity, stability, recycling and risk assessments are discussed in the last chapter.

Editor: Ram K. Gupta

Publisher: Springer
1st ed., July 2023
ISBN: 978-3-031-36248-4
449 pages, 130 images
Hardcover
Available also as an eBook

Bookshelf – J. Print Media Technol. Res. – Vol. 13 No. 2 (2024), 111–116

115
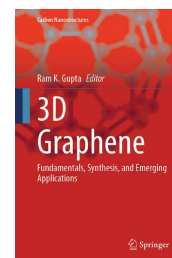
Bookshelf

Academic dissertations

Development of 3D Printable, Hydrophilic, and Rapidly Curing Silicone-Based Ink Formulations for Various Biomedical Applications

This thesis facilitated the progress in the 3D printing of elastic biomimetic structures towards higher precision needed to fabricate functional human-mimetic substitutes. The approach was based on developing silicone elastomer materials suitable for 3D micro-extrusion, namely UV-curable and hydrophilic ink formulations with tunable mechanical and rheological features to address the issues due to slow curing, low viscosity and hydrophobicity.

The dissertation provides the relevant background on 3D printing methods commonly used for bioprinting, 3D-printable biomaterials based on ceramics, different types of polymers, hydrogels and composites, collagen, carbon nanotubes and nanocelluse as additive components, and considerations regarding 3D printing in biomedical applications, especially for fabricating cartilage and microfluidic devices. The experimental work is described in two chapters. One details the development of inks with the desired characteristics achieved using the formulations consisting of aminosilicone to increase substrate affinity, cellulose nanocrystals as a hydrophilic nanosized rheology modifier, and methacrylate anhydride with a photoinitiator for rapid curing, which enables creating the overhanging structures without supports. The developed hybrid inks and optimised printing parameters allowed the 3D printing of biocompatible human articular cartilage substitutes with a complex biomimetic multizonal 3D structure with a controlled change in stiffness and enhanced mechanical fastness. The work proposes a possible use of these novel inks also for in-situ surgical applications. The next step comprised the micro-extrusion of one developed ink to demonstrate the one-step and time-efficient fabrication of highly flexible microfluidic devices, including the T-junction and Y-channel types. Besides optimising basic printing parameters, attention was paid to the proper setting of bridging angle, bridge flow ratio and bridging speed to minimise sagging and blockage or leakage of microfluidic channels.

Doctoral thesis – Summary

Author:
Hossein Golzar

Speciality field:
Chemistry – Nanotechnology

Supervisor:
Xiao-Wu Tang

Defended:
*20 December 2022,
University of Waterloo,
Department of Chemistry
Waterloo, Canada*

Contact:
hgolzar@uwaterloo.ca

Further reading:
http://hdl.handle.net/10012/19072

3D Printing and Electromagnetic Properties of Conductive Nanocarbon Based Composites

The research focus of this thesis was on the electrically conductive carbon nanocomposites with a low mass fraction of conductive component, allowing their production using digital light processing, and their potential use as electromagnetic wave absorbing materials in the microwave frequency range through dielectric losses. The approach comprised the development of novel transparent conductive acrylic resins based on graphene oxide and carbon nanotubes and tailoring the formulations and 3D printing process to achieve the required physical properties of resulting composites.

After a brief introduction, the text reviews relevant aspects of the 3D printing process and photosensitive resins for digital light processing, especially the electrically conductive nanocarbon-based composites. It highlights the properties of carbon nanotubes, graphene and graphene oxide and discusses the percolation influencing factors, including the geometry, orientation and dis-

Doctoral thesis – Summary

Author:
David Tilve Martínez

Speciality field:
*Physical Chemistry
of Condensed Matter*

Supervisor:
Philippe Poulin

Defended:
*2 November 2023,
University of Bordeaux,
CRPP – Paul Pascal Research Centre
Bordeaux, France*

Contact:
david.tilve@imdea.org

person state of the filler. Further, it provides an overview of recent studies on 3D-printed conductive nanocomposites and the 3D printing radar absorber materials by digital light processing, explaining the microwave absorption fundamentals and mechanisms of microwave performance. Then, three chapters present the key experimental steps. The first deals with transparent resins for accurate 3D printing of conductive materials based on neat graphene oxide with high monolayer content, reduced by thermal post-treatment after printing. The chapter describes the formulations, characterisation of their rheological and optical properties and the microstructural, mechanical and electrical properties of the 3D-printed nanocomposites. The next chapter is focused on electrical anisotropy in single-walled carbon-nanotube surfactant-assisted composites. The study revealed that the conductivity anisotropy of up to two orders of magnitude is mainly due to the large contact resistance between 3D-printed layers and probed that is not due to the orientation of the filler. It can be mitigated by a proper choice of process parameters. Finally, to further improve the electrical performance, both types of carbon nanoparticles were combined, with single-walled carbon nanotubes stabilised in an acrylic matrix by graphene oxide. The chapter also compares the dielectric properties of all three composites at microwave frequencies, showing the hybrid one as the most promising candidate for microwave absorbers.

Visualization, Analysis and Modeling of Fluid Dynamic Pattern Formation Phenomena in the Cylinder Gap Using Machine Learning

This thesis aimed to advance the understanding of fluid dynamic pattern formation phenomena in gravure printing to form a base for further improvement of process control in various industrial printing applications. The comprehensive research brought insight into key factors for achieving comparable results from laboratory and industrial printing machines, processes in the gravure nip, fluid splitting, applicability of machine-learning approaches and predictability of pattern formation.

The text provides an overview of the gravure printing process, areas of its application, and printing forms, inks and substrates used. Further, it describes the fluid splitting modes, pattern formation in the cylinder gap, viscosity and surface tension characterisation and methods for data-driven analysis, which included digital image data processing and feature extraction, fast Fourier transform for frequency analysis, singular value decomposition for modal analysis and machine learning, namely different classification algorithms and deep learning using convolutional neural networks. The experimental work is presented in four chapters, the first of which summarises the findings from the preliminary tests to optimise all the approaches applied in the main part of the work, detailed in the following chapters. As the first step, extensive test series of samples were printed on two industrial gravure presses for different combinations of printing speed, printing inks, viscosity, substrate, doctor blade angle, tone value, screen frequency, and electrostatic printing assist use. Also, a dedicated gravure research platform was developed to acquire high-speed video recordings of the temporal behaviour of printing ink in the gravure nip. The second step involved the classification into point splitting, transition regime and lamella splitting. This was complemented by frequency analysis and qualitative video data analysis, showing the influence of printing speed and screen frequency. The third step comprised the application-based modelling of cause–effect correlations between selected factors and fluid splitting class and the analysis of the finger patterns scaling behaviour. The dissertation also provides links to both raw and processed image datasets and other research data.

Events – J. Print Media Technol. Res. – Vol. 13 No. 2 (2024), 117–118

117

Events

NANOTEXNOLOGY 2024

Thessaloniki, Greece
29 June – 6 July 2024

This long-established international event keeps a scheme combining three conferences and an exhibition on nanotechnologies, organic electronics and nanomedicine, complemented by the business forum and matchmaking event and framed by three days of related summer schools. The 17th International Symposium on Flexible Organic Electronics includes several workshops organised in the scope of numerous EU-funded projects. Their programme offers keynotes, invited lectures and other contributions that share the advances in the areas ranging from organic and large-area electronics materials, organic and perovskite photovoltaics, novel manufacturing strategies of organic light-emitting diodes, organic thin-film transistors and sensor devices, smart textiles, wearables and the Internet of Things, to biosensors and bioelectronics, up to artificial intelligence, machine learning, intelligent manufacturing and automation, in-line and real-time metrology and quality control for nanomanufacturing, computational modelling of materials, devices and processes and open innovation and standardisation approaches.

FLEX 2024

San Francisco, California, USA
9–11 July 2024

The theme of this edition is additive innovation in flexible hybrid and printed electronics. The keynotes include 'A vision for next generation intelligent electric systems' by Ercan M. Dede, 'Microgravity: a new frontier for next-generation semiconductor materials & electronic fabrication' by Chyree Batton, 'Advanced packaging for sustainable additive manufacturing innovations' by C. P. Hung, and 'Responsible human/AI collaboration' by Lama Nachman.

SIGGRAPH 2024
The 51st International Conference & Exhibition on Computer Graphics & Interactive Techniques

Denver, Colorado, USA
28 July – 1 August 2024

The rich programme of this event continues to encompass the developments in production and animation, research and education, arts and design, gaming and interactivity and new technologies. The announced keynote speakers are Mark Sagar on the work towards the creation of autonomously animated virtual humans, Jensen Huang on artificial intelligence and graphics for the new computing revolution, Dava Newman on advanced space and climate computer graphics, and Manu Prakash on the insight into computing in biological matter. In addition, this year's edition of the High-Performance Graphics conference is co-hosted with SIGGRAPH from 26 to 28 July.

FLEPS 2024
6th IEEE International Conference on Flexible, Printable Sensors and Systems

Tampere, Finland
30 June – 3 July 2024

The schedule of this edition mostly runs in two tracks and combines technical sessions with tutorials and workshops. The plenary speakers are Aaron Thean, discussing low-thermal budget functional materials for enhancing flexible and semiconductor electronics, Jani Kivioja, presenting the solutions for atomic and molecular layer deposition in the flexible electronics industry, and Manos M. Tentzeris, introducing fully integrated printable broadband wireless modules for communication, energy harvesting and sensing.

FuturePrint 2024

São Paulo, Brazil
10–13 July 2024

The focus of this fair is on visual communication, screen printing and digital textile printing. Its forum covers colour management, outdoor media, personalised products, 3D printing, business management, and more. Also, training in print design and modelling can be joined,

I3S 2024
10th International Symposium on Sensor Science

Singapore
1–4 August 2024

This year, the symposium is joined with the 1st International Conference on AI Sensors. The event includes the invited talk 'Printed electronics and sensors for AI healthtech' and papers presenting other printed solutions.

ICFPE 2024
14th International Conference on Flexible and Printed Electronics

Taipei, Taiwan
28–30 August 2024

This year's programme offers each day three keynotes, including the one by Takao Someya on 'Recent progress of electronic skins', five tracks of technical sessions and workshops on applications, devices, processes and equipment, materials, and energy, with the additional session organised by OE-A on the first day.

PRINTING United Expo

Las Vegas, Nevada, USA
10–12 September 2024

This show offers the opportunity to explore the trends and developments in all kinds of printing, from commercial and publishing to apparel decoration up to functional and industrial printing, collect samples and other resources and meet industry leaders.

FESPA Events

The September events focused on printing and signage include this year's editions of FESPA Africa (11–13 September in Johannesburg, South Africa), co-located with Africa Print, Modern Marketing and Graphics, Print & Sign, FESPA Eurasia (11–14 September in Istanbul, Turkey), and FESPA Mexico taking place two weeks later (26–28 September in Mexico City).

The Print Show 2024

Birmingham, UK
17–19 September 2024

This UK event features talks on interesting topics, including printing for people with visual impairment and factors important for building print careers.

SPIE Optics & Photonics 2024

San Diego, California, USA
18– 22 August 2024

In 2024, this multidisciplinary event features several conferences on different types of organic and hybrid electronics, invited paper dealing with fast and edible transistors based on organic semiconductors towards applications in biomedicine and food quality monitoring, contributions presenting various applications of 3D printing, e.g. 3D-printed micro-optics and elastomer actuators, and more. The exhibition accompanies the conference for the last three days. A month later (16–19 September), the SPIE Sensors & Imaging event takes place in Edinburgh, UK, and also covers print-related topics.

Advances in Printing Technology 2024

Busan, South Korea
4–6 September 2024

This meeting comprises academic and business sessions and tutorials related to printing. It can also be accessed live online or later. The opening keynote by Toshitaka Uemura focuses on the benefits of digital printing technology beyond the printing process; the closing one by Gyoujin Cho presents the concept of the roll-to-roll gravure foundry for manufacturing flexible and inexpensive (bio)electronic devices. The focal talks cover sustainable and unattended print colour control, appearance reproduction and individual observer profiles, inkjet technology developments to increase sustainability, artificial intelligence patent trends, fully printed nanocomposite, and surface microstructure by additive manufacturing.

50th iarigai and 55th International Circle Conferences

Zurich, Switzerland
8–11 September 2024

Advances in Printing and Media Technology, the international research conference of iarigai, celebrates its 50th anniversary jointly with the International Circle of Educational Institutes for Graphic Media Technology and Management conference in its 55th year. The contributions deal with bio-based dyes, pigments and inks, additive manufacturing, augmented reality, generative artificial intelligence, model-based data-driven automation, and other topics.

22nd International Coating Science and Technology Symposium

Atlanta, Georgia, USA
8–11 September 2024

In 2024, this event features keynotes on sustainable coating materials by YuanQiao Rao, coating science for fuel cell and electrolyzer manufacturing by Scott Mauger, phase transformations in metal halide perovskites by Juan-Pablo Correa-Baena, coating, drying and post-drying in battery applications by Philip Scharfer and Wilhelm Schabel, and solution-processed perovskite films for scalable solar cells by Jangwon Seo.

Call for papers

The Journal of Print and Media Technology Research is a peer-reviewed periodical, published quarterly by iarigai, the International Association of Research Organizations for the Information, Media and Graphic Arts Industries.

JPMTR is listed in Emerging Sources Citation Index, Scopus, DOAJ – Directory of Open Access Journals, Index Copernicus International, NSD – Norwegian Register for Scientific Journals, Series and Publishers.

Authors are invited to prepare and submit complete, previously unpublished and original works, which are not under review in any other journals and/or conferences.

The journal will consider for publication papers on fundamental and applied aspects of at least, but not limited to, the following topics:

Printing technology and related processes
Conventional and special printing; Packaging; Fuel cells, batteries, sensors and other printed functionality; Printing on biomaterials; Textile and fabric printing; Printed decorations; 3D printing; Material science; Process control

Premedia technology and processes
Colour reproduction and colour management; Image and reproduction quality; Image carriers (physical and virtual); Workflow and management

Emerging media and future trends
Media industry developments; Developing media communications value systems; Online and mobile media development; Cross-media publishing

Social impact
Environmental issues and sustainability; Consumer perception and media use; Social trends and their impact on media

Submissions for the journal are accepted at any time. If meeting the general criteria and ethic standards of scientific publishing, they will be rapidly forwarded to peer-review by experts of relevant scientific competence, carefully evaluated, selected and edited. Once accepted and edited, the papers will be published as soon as possible.

There is no entry or publishing fee for authors. Authors of accepted contributions will be asked to sign a Licensing agreement (CC-BY-NC 4.0).

Authors are asked to strictly follow the guidelines for preparation of a paper (see the abbreviated version on inside back cover of the journal).

Complete guidelines can be downloaded from: <http://iarigai.com/publications/journals/guidelines-for-authors/> Papers not complying with the guidelines will be returned to authors for revision.

Submissions and queries should be directed to: journal@iarigai.org

Journal of
Print and Media Technology
A PEER-REVIEWED QUARTERLY   Research

Vol. 13, 2024
Prices and subscriptions

Since 2016, the journal is published in digital form; current and archive issues are available at:
<https://iarigai.com/publications/journals/>.

Since 2020, the journal is published as "open access" publication, available free of charge
for iarigai members, subscribers, authors, contributors and all other interested public users.

A print version is available on-demand. Please, find below the prices charged for the printed Journal,
for four issues per year as well as for a single issue

Regular prices

Four issues, print JPMTR (on-demand)	400 EUR
Single issue, print JPMTR (on-demand)	100 EUR

Subscription prices

Annual subscription, four issues, print JPMTR (on-demand)	400 EUR

Prices for iarigai members

Four issues, print JPMTR (on-demand)	400 EUR
Single issue, print JPMTR (on-demand)	100 EUR

Place your order online at: <http://www.iarigai.org/publications/subscriptions-orders/>
Or send an e-mail order to: office@iarigai.org

Guidelines for authors

Authors are encouraged to submit complete, original and previously un-published scientific or technical research works, which are not under reviews in any other journals and/or conferences. Significantly expand-ed and updated versions of conference presentations may also be con-sidered for publication. In addition, the Journal will publish reviews as well as opinions and reflections in a special section.

Submissions for the journal are accepted at any time. If meeting the gen-eral criteria and ethical standards of the scientific publication, they will be rapidly forwarded to peer-review by experts of high scientific compe-tence, carefully evaluated, and considered for selection. Once accepted by the Editorial Board, the papers will be edited and published as soon as possible.

When preparing a manuscript for JPMTR, please strictly comply with the journal guidelines. The Editorial Board retains the right to reject with-out comment or explanation manuscripts that are not prepared in ac-cordance with these guidelines and/or if the appropriate level required for scientific publishing cannot be attained.

A – General

The text should be cohesive, logically organized, and thus easy to fol-low by someone with common knowledge in the field. Do not include information that is not relevant to your research question(s) stated in the introduction.

Only contributions submitted in English will be considered for publica-tion. If English is not your native language, please arrange for the text to be reviewed by a technical editor with skills in English and scientif-ic communications. Maintain a consistent style with regard to spelling (either UK or US English, but never both), punctuation, nomenclature, symbols etc. Make sure that you are using proper English scientific terms. Literal translations are often wrong. Terms that do not have a commonly known English translation should be explicitly defined in the manuscript. Acronyms and abbreviations used must also be explicitly defined. Generally, sentences should not be very long and their structure should be relatively simple, with the subject located close to its verb. Do not overuse passive constructions.

Do not copy substantial parts of your previous publications and do not submit the same manuscript to more than one journal at a time. Clearly distinguish your original results and ideas from those of other authors and from your earlier publications – provide citations whenever relevant.

For more details on ethics in scientific publication consult Guidelines, published by the Committee on Publication Ethics (COPE):
<https://publicationethics.org/resources/guidelines>

If it is necessary to use an illustration, diagram, etc. from an earlier pub-lication, it is the author's responsibility to ensure that permission to reproduce such an illustration, diagram, etc. is obtained from the copy-right holder. If a figure is copied, adapted or redrawn, the original source must be acknowledged.

Submitting the contribution to the Journal, the author(s) confirm that it has not been published previously, that it is not under consideration for publication elsewhere and – once accepted and published – it will be disseminated and make available to the public in accordance to the Creative Commons Attribution-NonCommercial 4.0 International Public License (CC-BY-NC 4.0), in English or in any other language. The pub-lisher retains the right to publish the paper online and in print form, and to distribute and market the Journal containing the respective paper without any limitations.

B – Structure of the manuscript
Preliminary

Title: Should be concise and unambiguous, and must reflect the con-tents of the article. Information given in the title does not need to be repeated in the abstract (as they are always published jointly), although some overlap is unavoidable.

List of authors: I.e. all persons who contributed substantially to study planning, experimental work, data collection or interpretation of results and wrote or critically revised the manuscript and approved its final ver-sion. Enter full names (first and last), followed by the present address, as well as the E-mail addresses. Separately enter complete details of the corresponding author – full mailing address, telephone number, and E-mail. Editors will communicate only with the corresponding author.

Abstract: Should not exceed 500 words. Briefly explain why you con-ducted the research (background), what question(s) you answer (ob-jectives), how you performed the research (methods), what you found (results: major data, relationships), and your interpretation and main consequences of your findings (discussion, conclusions). The abstract must reflect the content of the article, including all keywords, as for most readers it will be the major source of information about your research. Make sure that all the information given in the abstract also appears in the main body of the article.

Keywords: Include three to five relevant scientific terms that are not mentioned in the title. Keep the keywords specific. Avoid more general and/or descriptive terms, unless your research has strong interdisci-plinary significance.

Scientific content

Introduction and background: Explain why it was necessary to carry out the research and the specific research question(s) you will answer. Start from more general issues and gradually focus on your research question(s). Describe relevant earlier research in the area and how your work is related to this.

Methods: Describe in detail how the research was carried out (e.g. study area, data collection, criteria, origin of analyzed material, sample size, number of measurements, equipment, data analysis, statistical methods and software used). All factors that could have affected the results need to be considered. Make sure that you comply with the ethical standards, with respect to the environmental protection, other authors and their published works, etc.

Results: Present the new results of your research (previously published data should not be included in this section). All tables and figures must be mentioned in the main body of the article, in the order in which they appear. Make sure that the statistical analysis is appropriate. Do not fab-ricate or distort any data, and do not exclude any important data; simi-larly, do not manipulate images to make a false impression on readers.

Discussion: Answer your research questions (stated at the end of the introduction) and compare your new results with published data, as ob-jectively as possible. Discuss their limitations and highlight your main findings. At the end of Discussion or in a separate section, emphasize your major conclusions, pointing out scientific contribution and the practical significance of your study.

Conclusions: The main conclusions emerging from the study should be briefly presented or listed in this section, with the reference to the aims of the research and/or questions mentioned in the Introduction and elaborated in the Discussion.

Note: Some papers might require different structure of the scientif-ic content. In such cases, however, it is necessary to clearly name and mark the appropriate sections, or to consult the editors. Sections from Introduction until the end of Conclusions must be numbered. Number the section titles consecutively as 1., 2., 3., ... while subsections should be hierarchically numbered as 2.1, 2.3, 3.4 etc. Only Arabic numerals will be accepted.

Acknowledgments: Place any acknowledgements at the end of your manuscript, after conclusions and before the list of literature references.

References: The list of sources referred to in the text should be collect-ed in alphabetical order on at the end of the paper. Make sure that you have provided sources for all important information extracted from oth-er publications. References should be given only to documents which any reader can reasonably be expected to be able to find in the open literature or on the web, and the reference should be complete, so that it is possible for the reader to locate the source without difficulty. The number of cited works should not be excessive – do not give many sim-ilar examples.

Responsibility for the accuracy of bibliographic citations lies entire-ly with the authors. Please use exclusively the Harvard Referencing System. For more information consult the fifth edition of the Guide to Referencing in the Harvard Style, used with consent of Anglia Ruskin University, released by ARU University Library, available at:
<https://library.aru.ac.uk/referencing/harvard.htm>

C – Technical requirements for text processing

For technical requirement related to your submission, i.e. page layout, formatting of the text, as well of graphic objects (images, charts, ta-bles etc.) please see detailed instructions at:
<http://iarigai.com/publications/journals/guidelines-for-authors/>

D – Submission of the paper and further procedure

Before sending your paper, check once again that it corresponds to the requirements explicated above, with special regard to the ethical issues, structure of the paper as well as formatting.

Once completed, send your paper as an attachment to:
journal@iarigai.org

If necessary, compress the file before sending it. You will be acknowl-edged on the receipt within 48 hours, along with the code under which your submission will be processed.

The editors will check the manuscript and inform you whether it has to be updated regarding the structure and formatting. The corrected man-uscript is expected within 15 days.

Your paper will be forwarded for anonymous evaluation by two experts of international reputation in your specific field. Their comments and remarks will be in due time disclosed to the author(s), with the request for changes, explanations or corrections (if any) as demanded by the referees.

After the updated version is approved by the reviewers, the Editorial Board will decide on the publishing of the paper. However, the Board retains the right to ask for a third independent opinion, or to definitely reject the contribution.

Printing and publishing of papers, once accepted by the Editorial Board, will be carried out at the earliest possible convenience.

The journal is publishing contributions
in the following fields of research

- ⊕ Printing technology and related processes
- ⊕ Premedia technology and processes
- ⊕ Emerging media and future trends
- ⊕ Social impacts

For details see the Mission statement inside

JPMTR is listed in

- ⊕ Emerging Sources Citation Index
- ⊕ Scopus
- ⊕ DOAJ – Directory of Open Access Journals
- ⊕ Index Copernicus International
- ⊕ NSD – Norwegian Register for
  Scientific Journals, Series and Publishers

Submissions and inquiries

journal@iarigai.org

Subscriptions

office@iarigai.org

More information at

www.iarigai.org/publications/journal